Pressure Tuned Magnetism in *d*- and *f*-Electron Materials

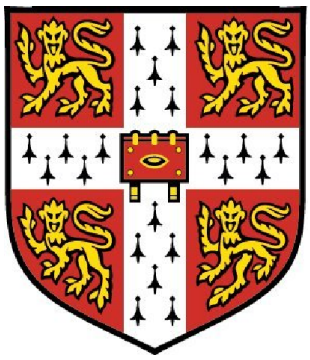

Charles Robert Sebastian Haines

College of Corpus Christi and the Blessed Virgin Mary

University of Cambridge

A thesis submitted for the degree of

Doctor of Philosophy Ph.D.

2011 July

Pressure Tuned Magnetism in *d*- and *f*-Electron Materials

Charles Robert Sebastian Haines

Quantum phase transitions (QPT) on the border of magnetism have provided a fertile hunting ground for the discovery of new states of matter, for example; the marginal Fermi Liquid and non Fermi Liquid states as well high T_C cuprate and magnetically mediated superconductivity. In this thesis I present work on three materials in which it may be possible to tune the system through a magnetic QPT with the application of hydrostatic pressure. Although the details of the underlying physics are different in each of the materials, they are linked by the possibility of finding new states on the border of magnetism.

Applying hydrostatic pressure, we have suppressed the ferromagnetic (FM) transition in metallic Fe_2P to very low temperature and to a potential QPT. Counter-intuitive broadening of the magnetic hysteresis leading up to the FM-AFM QPT may well be a crucial clue as to the nature of the model needed to understand this phase transition. A sharp increase in the quasi-particle scattering cross-section as well as the residual resistivity accompany a departure from the quadratic temperature dependence of the resistivity. This possible deviation from Fermi liquid behaviour is stable over a significant range of temperature.

The unexplained upturn in the resistivity of CeGe that accompanies the AFM transition was studied under pressure. Pressure increased the residual resistivity as well as decreasing the relative size of the upturn, but had a moderate effect on the Néel temperature. The insensitivity of the Néel temperature to pressure has been compared to its relative sensitivity to applied field. The existence of the upturn and its evolution with pressure and applied field can reasonably be argued to be due to the details of the electron band structure in the system.

By applying pressure we have drastically reduced the resistivity of the insulating antiferromagnet $NiPS_3$. Concurrent work on $FePS_3$ has shown metallisation under pressure. It seems reasonable to speculate that $NiPS_3$ may also metallise at higher pressure. The energy gap is narrowed in both materials as pressure is increased. Magnetisation measurements have revealed a low temperature upturn indicating some possible ferromagnetic component or proximity to another magnetic state. A peak in the magnetisation is also seen at 45K in zero-field cooled measurements. Both of these features point to a system with a complex magnetic ground state.

Declaration

This dissertation is the result of my own work and includes nothing which is the outcome of work done in collaboration except where specifically declared in the Acknowledgements and indicated in the text. It does not exceed the word limit and is not substantially the same as any work that has been, or is currently being, submitted to the University of Cambridge or any other university for any degree, diploma or any other similar qualification.

This dissertation does not exceed 60000 words.

Sebastian Haines April 2011

Acknowledgements

I must first of all say thank you to my mother, Gillian Haines. Throughout my entire time in education she has always supported me in the choices I have made. It is my mum who instilled in me the principle that science is worth doing for its own sake. That the expansion of knowledge doesn't necessarily have to lead to a new kind of table lamp to be worthwhile. I would also like to express my gratitude for the patience shown by my father, brother and sister during the last few years.

My time in Cambridge, studying for and then writing this thesis, would have been a great deal less fulfilling and a great deal less exciting without Hannah, my wife. The last few months would have been much more stressful and fraught.

I would like to show my appreciation for all the guidance, advice, direction and help given to me by my supervisor, Prof. Saxena. But most important I think is Montu's friendship and the faith he has always shown in me.

Learning all of the necessary techniques was a long and fascinating process. Setting up Bridgemann cells is difficult to enjoy but thanks to Anna Kusmartseva I at least got something out of them in return. Thanks to Rob Smith, Cheng Liu and Patricia Alireza for showing me how to run an ADR. Getting the most out of the limited time on the SQUID is due to advice and instruction from Noelia Marcano Aguado.

The work on CeGe was carried out in the most part in collaboration with Noelia. As were many of the SQUID measurements on Fe_2P.

For absolutely vital discussion on every aspect of physics, I would like to say thanks to: Leszek Spalek, Paul Nahai-Williamson, Noelia, Stephen Rowley and Montu.

Doing pressure work requires a lot of help from a good workshop. Thankfully, at the Cavendish we have an excellent workshop run by Peter Norman. Ray Flaxman, Dave Thompson and Nigel Palfrey have all helped a lot. However, there is one person without whose almost limitless knowledge of materials and machining the whole thing could not happen: Sam Brown.

Thanks go to all the friends that have made Cambridge such excellent fun: Ailsa and Dave, Leszek, Paul and Rosie, Jules and Sarah, Kevin and Kirsten, Alex and Carol, Cheng, Jim and Sarah, Isla and Ewan, Mark, Diarmuid and Julie, Nick, Montu and Prajakti, Catherine and Chris, Liz and James and also to those friends from outside Cambridge: Olly and Rosa, Becky and Alex, Lara, Harriet, Spol, Colin and Hannah, Ed, Doug,

Also, thanks to my cat, Betty, for never asking me how the thesis was going.

I would like to acknowledge the thousands of individuals who have coded for the LaTeX project for free.

Contents

List of Figures

1

Motivation

A second order phase transition, occurring at sufficiently low temperature that the population distribution of the fluctuations is quantum mechanical, is termed a quantum phase transition (QPT). At absolute zero a continuous phase transition terminates in a quantum critical point where the only fluctuations are those caused by zero-point motion. The number and variety of systems in which new states of matter have been observed in the vicinity of a quantum phase transition is so great that it would be impossible to list them all here. To give an idea of the breadth of the field, here are some of the most diverse and high profile systems; high T_C cuprate superconductivity, Helium-3, ferroelectrics and multiferroics.

Within the field of QPTs is that of the magnetic QPTs. This is itself a broad field, encompassing pnictide superconductivity, magnetically mediated superconductivity in the antiferromagnetic heavy fermion systems, the non-Fermi Liquid state and the marginal Fermi Liquid as well as other states. Studies on three materials in which it may be possible to tune the system through a magnetic QPT with the application of hydrostatic pressure are presented in this thesis. One is a d-metal ferromagnet, one an anti-ferromagnetic f-electron system and one a semi-conductor. They all present an exciting prospect for observing new states on the border of magnetism.

1.1 Fe_2P

Fe_2P is a d-metal ferromagnet (FM). The search for superconductivity (SC) near an FM QPT was the initial motivation for investigating this system. Evidence for an FM QPT was indeed found. The number of confirmed FM QPTs is relatively small and superconductivity has only been discovered at very low temperatures in a handful of systems. It would appear that it is generally favourable for a FM system to avoid a QCP and, in most systems where FM is suppressed to near absolute zero, there are other structural or magnetic phase transitions that appear.

Magnetisation measurements are presented which agree with previous data and show an expanding hysteresis under pressure. This behaviour is not fully understood, but may well provide a clue to the nature of the QPT. Resistivity data is presented showing a clear deviation from Fermi Liquid (FL) behaviour above the critical pressure as well as evidence for the FM phase transition at much lower temperatures than previously seen, $\sim 7K$.

1.2 CeGe

As an antiferromagnetic (AFM) heavy fermion (HF) system, CeGe would appear to fit into a well studied physical framework; that of the competition between the Kondo interaction and the RKKY exchange as demonstrated in the famous Doniach phase diagram. It is, however, relatively understudied, due mainly to difficulties in sample preparation. CeGe displays unexplained features in the temperature dependence of its resistivity. Below the Néel temperature there is a significant upturn in the resistivity followed by a peak a few Kelvin lower. A desire to account for these features has led to the proposal of some exotic magnetic states. Resistivity under pressure in this system is discussed in terms of the interplay of magnetic interactions present in the heavy fermion systems. More specifically the possibility of magnetic super zones in the material and their effect on the pressure and field dependence is considered.

1.3 $NiPS_3$

$NiPS_3$ is discussed in the context of some preliminary resistivity data under applied pressure and its promise for future work. $NiPS_3$ is a semiconductor that orders antiferromagnetically at $\sim 150K$. The application of pressure causes the resistivity at room temperature to reduce drastically, possibly indicating a metal insulator transition that can be tuned with pressure. Similarities in this system with the layered iron pnictides as well as with the parent compounds of the high-T_C cuprate superconductors add an extra level of interest to this material. The fact that sulphur is in the same group as oxygen means that there are many possible analogies and comparisons to be drawn with the transition metal oxides. This potential is largely untapped in the field of QPTs and offers both a new direction as well as an interesting comparison to the oxide compounds that have been more thoroughly investigated both experimentally and theoretically.

2

Theoretical Concepts

2.1 Fermi Liquid Theory

The simplest quantum mechanical model for the electrons in condensed matter considers the electrons as free particles confined in a box the size of the system. This model is known as the Fermi gas. It gets this name due to the fact that no inter electron interactions are taken into consideration. The only physical concepts taken into account are the Pauli exclusion principle and the boundary conditions of the box. Extending the electron gas picture to include the effects of the lattice, involves treating the electron-ion interactions in various approximation schemes. This leads to the concept of an electron band structure, the form of which, is dependent on the nature of the lattice. In these approximations the electron-electron interactions are often neglected. In fact, in many materials the electron-electron interactions may be very strong and comparable with their kinetic energies. Fermi liquid theory is an attempt to include the effects of the electron-electron interactions in metals.

Landau imagined turning on the electron-electron interactions slowly and observing the evolution of the eigenstates. Landau supposed that it would be possible to label the eigenstates of the interacting electrons with the same quantum numbers as are used in the Fermi gas. This is called adiabatic continuity, and can be seen to work in trivial problems. The labels do not apply to electrons now but to 'quasiparticles'. This distinction is important as the quasiparticles will

have a different energy, mass and wavefunction to the electrons associated with the same labels in the non-interacting case. One important feature of the Fermi gas that is retained in the Fermi liquid is the Fermi surface.

To check the consistency of this procedure we calculate the lifetime of a quasi-particle state. Fermi liquid theory includes the coulomb interactions between the electrons. So first of all we write down the coulomb term in the Hamiltonian:

$$H_C = \sum_{\sigma\tau} \int d\mathbf{r} \int d\mathbf{r}' \Psi^\dagger_\sigma(\mathbf{r}') \Psi^\dagger_\tau(\mathbf{r}) \frac{e^2}{4\pi\epsilon_0 |\mathbf{r} - \mathbf{r}'|} \Psi_\tau(\mathbf{r}) \mathbf{\Psi}_\sigma(\mathbf{r}'). \tag{2.1}$$

Where σ and τ represent the spin states and Ψ is the Fourier transform of the momentum space field operator c:

$$\Psi_\sigma(r) = \frac{1}{\sqrt{V}} \sum_k e^{i\mathbf{k}\cdot\mathbf{r}} c_{k\sigma} \tag{2.2}$$

This interaction can then be written in the form:

$$H_C = \sum_{\sigma\tau\mathbf{qkp}} V_{\mathbf{qkp}} c^\dagger_{\mathbf{q}\sigma} c^\dagger_{\mathbf{k}\tau} c_{\mathbf{p}\tau} c_{\mathbf{q}+\mathbf{k}-\mathbf{p}\sigma}. \tag{2.3}$$

The scattering event that this describes is one quasiparticle lying just above the Fermi scattering into a lower energy state. The final state is one in which there are two particles and a hole all closer to the Fermi energy than the first quasiparticle. The energy dependence of the lifetime of these quasi-particle states gives information on the stable states of the system. By Fermi's golden rule, the lifetime T is given by:

$$T_{i\to f} = \frac{2\pi}{\hbar} |\langle i|H_C|f\rangle|^2 \rho \tag{2.4}$$

and taking V_{qkp} to be constant we can see that the density of final states (ρ) is the important factor. This is quadratic in the energy of the first electron. What this implies is that the quasi-particles at low temperature, i.e. with low energy

are very long lived. Therefore, the non-interacting Fermi gas is a good qualitative approximation of the electrons in a metal at low temperatures if the different mass is taken account. Fermi liquid theory allows us to calculate properties that are in good quantitative agreement with experiment. The resistivity is proportional to the scattering rate shown above. Therefore, it is quadratic in temperature and gives the Fermi liquid result:

$$\rho(T) = \rho_0 + AT^2 \tag{2.5}$$

ρ_0 is the residual resistivity and A is a constant. The reason we can get away with treating the scattering matrix as constant is to do with the fact that it is the coulomb scattering that has been considered, and in a metal this can be shown to be screened. It is therefore a short range, repulsive interaction. As we shall see this is important in determining the effect of a given scattering process on the transport properties.

The specific heat and susceptibility predictions are qualitatively the same as the non-interacting case but with the quasi-particle mass and a term related to the Landau f-function. This f-function contains what we don't know about the distribution of quasi-particles and can be measured by experiment. The fact that there are more pertinent experiments than f-factors is important to the success of this picture. The f-function includes information about quasiparticle interactions that have not been fully accounted for. In many cases these interactions are weak, but in some cases they may be strong. Near a quantum phase transition these interactions can be tuned to be strong.

2.1.1 Quantum Phase Transitions

There are many systems which are not paramagnetic metals. The Fermi liquid can undergo a transition into another state in a number of ways. The coulomb interaction can be turned up very high and the lattice sites taken to be far apart. This leads to localisation of electrons and a number of insulating magnetic states described by the Hubbard model and termed Mott insulators.

However, the particular case of interest in this report is what happens near a magnetic quantum critical point. In this area of phase space the fluctuations that drive the phase transition are spin fluctuations. Near a classical second order phase transition it is well known that the fluctuations slow down and the length scale of the thermally excited fluctuations in the order parameter diverges. They are then in a position to scatter the quasi-particles in the system. A quantum critical point occurs at absolute zero. This has important consequences. Firstly, the fluctuations are quantum mechanical, driven by zero point motion, rather than classical and thermally driven. Secondly, as Nernst's theorem tells us that at zero temperature the entropy is zero, then the transition cannot be from a more to less ordered state, it must be from order to order.

Mean Field Theory (MFT) provides a tractable way to predict the behaviour of a strongly correlated system. If we take as the starting point a Landau free energy, for a ferromagnetic system, of the form:

$$F = \frac{a}{2}M^2 + \frac{b}{4}M^4 - \frac{c}{2}(\nabla M)^2 - HM \tag{2.6}$$

and minimise with respect to the order parameter M, then we have a magnetic equation of state:

$$H[M] = aM + bM^3 - c(\nabla^2 M) \tag{2.7}$$

from which we can, to leading order in M, identify the enhanced linear susceptibility in the paramagnetic phase, a. a is enhanced over the Pauli susceptibility by a linear in M exchange field term added to the non-interacting equation of state.

$$\frac{M}{H} = \chi = a^{-1} \tag{2.8}$$

This describes a system close to a ferromagnetic transition in equilibrium. To understand the role of critical fluctuations it is necessary to consider the spatial

and temporal dependence of the average magnetisation in an applied field that is also varying in space and time. Introducing a random small exchange field, H becomes $H + h$ and M, $M + m$. After taking the ensemble averages and retaining the lowest order, non-zero terms, we find that a has been modified to $a + 3b\bar{m^2}$.

Further modifications are the result of generalising this method to vector fields. These modifications are also functions of the average squared fluctuations as well as terms involving the time derivative of m. The time derivative of M and m are determined by the damping in the system as well as, in the vector field, a precession term. The form of the fluctuations and the damping can be discussed in analogy to the harmonic oscillator for which the response function or susceptibility is given by:

$$\alpha_{\omega}^{-1} = \alpha^{-1}\left(1 - \frac{i\omega}{\Gamma} - \frac{\omega^2}{\Omega^2}\right). \tag{2.9}$$

Using the fluctuation dissipation theory (Nyquist's) we can write down the following relation for the variance of the fluctuation amplitude:

$$\bar{m^2} = \frac{2}{\pi}\int_0^{\infty} d\omega \left(\frac{1}{2} + n_{\omega}\right) Im\alpha_{\omega}, \tag{2.10}$$

where n_{ω} is the Bose function. It is through this function that the thermal population of the excitations or fluctuations and therefore the temperature dependence of the calculated susceptibility enter.

The above integral can be split into the zero point motion component and the thermal component.

$$\bar{m^2}_T = \sum\nolimits_q \bar{m^2}_q, \tag{2.11}$$

and

$$\bar{m^2}_q = \frac{2\hbar\gamma_q}{\pi}\int_0^\infty d\omega \frac{\omega n_\omega}{\omega^2+\Gamma^2}. \tag{2.12}$$

Drawing further analogies with a damped harmonic oscillator, and using Nyquist's theorem to calculate the potential and kinetic energy of the modes via a generalised damped harmonic oscillator entropy, the heat capacity of these modes can be calculated (see Ref. (1) and references therein):

$$\Delta C = \frac{3}{2}\sum\nolimits_q \chi_q^{-1}\frac{\delta\bar{m^2}_q}{\delta T}. \tag{2.13}$$

The resistivity is the quantity of most importance in this work. To calculate the resistivity due to the fluctuations, first the scattering rate of the quasi-particles with the exchange field is calculated in perturbation theory. The result can be written as:

$$\Delta\rho = \eta\sum\nolimits_q q^2\frac{T}{\hbar\gamma_q}\left(\frac{\delta\bar{m^2}_q}{\delta T}\right)_\Gamma, \tag{2.14}$$

where η depends on the strength of the coupling between the quasi-particles and the field and is temperature independent.

The result for the susceptibility is:

$$\Delta\chi^{-1} = \Delta a = a + 5b\bar{m^2}_q. \tag{2.15}$$

Another feature of materials tuned close to a quantum critical point is that the inclusion of the dynamics of the order-parameter field leads to an increase in the number of effective dimensions in the problem. This comes about when the order parameter is generalized to be quantum mechanically compatible by putting time dependence on an equal footing with the spacial dependence. The dimensionality is integral to the applicability of MFT to the system (see eg. Ref. (**?**)). The purely fluctuation terms that are neglected in MFT become more

System	χ	C	ρ
2-D FM	1	2/3	4/3
3-D FM	4/3	$Tln(T^*/T)$	5/3
3-D AFM	3/2	1	3/2

Table 2.1: The results shown are the thermal exponents except for the form of the correction to the specific heat in the 3-D FM case which is given explicitly with T^* a constant.

important in lower dimensions. This therefore leads to the constraint that MFT is valid when the effective dimensionality of the system is greater than 4:

$$d_{eff} = d + z > 4 \tag{2.16}$$

where d represents the spatial dimensions and z is the dynamical exponent. z is so-called as it is representative of the dynamics or time-dependent properties of the system. Experimentally, z is determined from the dispersion relation of the relevant excitations, in this case over-damped modes called paramagnons. Therefore, QCPs are a rich source of test problems for statistical mechanics, in particular the area of universality classes and the Renormalisation Group (RG) theories.

The predictions that this spin fluctuation theory (SFT) make for the critical exponents of measurable quantities is then determined by the dimensionality of the system, the fluctuation spectrum and the dispersion relation. The predictions are summarised in Table 2.1.

As is implied in Fig.2.1, it is often necessary to access very specific regions of phase space in order to observe the new phenomena arising from QPTs. Low temperature is necessary to reduce the effects of classical thermal excitation that usually dominate observable properties. It is also a common part of studying QPTs; that a tuning parameter be used to suppress a transition to near absolute zero. The tuning parameters are chosen to alter the dominant physics of the problem. In the case of a magnetic QPT the usual choices are: applied magnetic field, pressure and chemical doping. An applied magnetic field will obviously

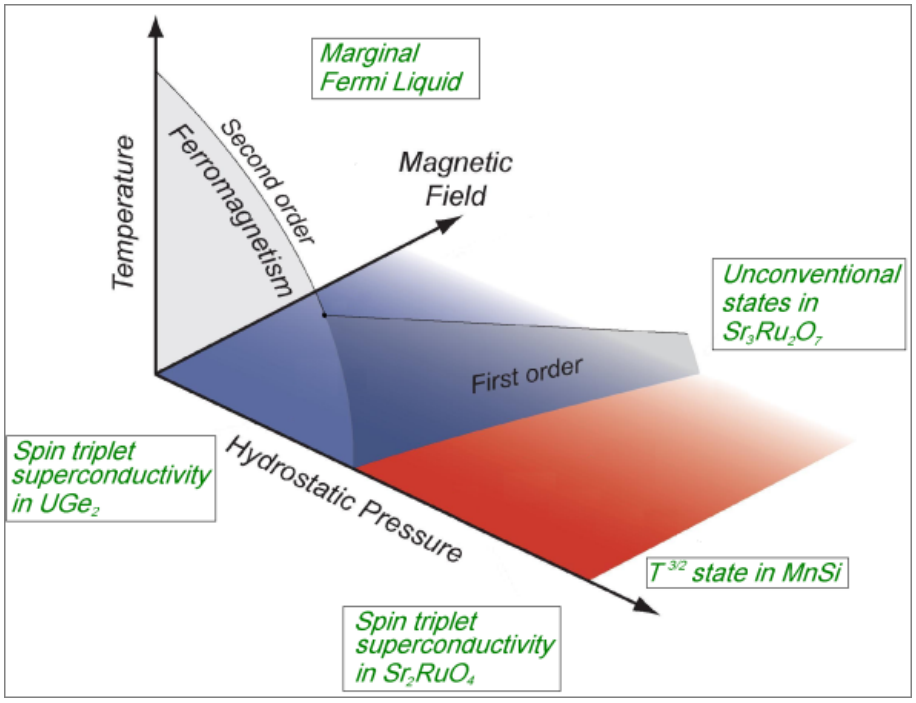

Figure 2.1: The temperature of a phase transition is tuned by hydrostatic pressure until at some critical value the transition temperature is zero Kelvin. The application of field may also be a tuning parameter in some systems. This phase diagram shows a number of systems that SFT has had some success in describing and where they fit into the overall picture developed with this framework.

favour specific configurations over others giving us the ability to tune the system from one state to another. Doping and pressure can both be used to change the inter-atomic spacing therefore altering the exchange integrals in the system, once again allowing a system to be tuned from one phase to another. Pressure has the advantage over doping of avoiding the introduction of disorder into the system. A further consideration is the quality of the sample. In some ways the disorder in a system could also be seen as a tuning parameter, however, it is less accurately tunable and it may have the disadvantage of masking the very states that are being sought. For example, spin triplet superconductivity is predicted to be very sensitive to disorder (1) (2). Small impurity levels can, in this way, mask the underlying physics being studied. The degree of purity required to observe the characteristic critical phenomena can be very high, e.g. samples with residual resistivities much less than $1\mu\Omega cm$. The physics of disordered systems is interesting in its own right, but in this case one has to limit the number of effects in the problem to make it tractable.

2.1.2 Breakdown of the Fermi Liquid Near to a QCP

The interaction mediated by long-ranged fluctuations is active at very short wave vectors. In this case the scattering matrix can no longer be taken as constant. To calculate the scattering rate we may write Fermi's golden rule as: (see Ref. (3))

$$\frac{1}{\tau_\epsilon} = \frac{2\hbar}{\pi}\int_0^\epsilon g_F \omega d\omega \int_{\omega/\hbar v_F}^{2k_F} \frac{q^{d-1}dq}{(2\pi/L)^d}\frac{|D(q,\omega)|^2}{(\hbar v_F q)^2} \tag{2.17}$$

If $D(q,\omega)$, the matrix element of the scattering element, is independent of q and ω then the result for the Fermi liquid is obtained. The dependence of $D(q,\omega)$ on q will determine the exponent for the energy dependence of the scattering rate. With different forms for the scattering matrix elements one obtains different exponents for the temperature dependence of observables. This Spin Fluctuation Theory (SFT) (see (4), (1) and references therein) can be calculated for the various effective dimensions and types of fluctuations that are present in itinerant metallic magnets. These calculations are involved and only the results will be

discussed in this thesis. Ferromagnetic fluctuations lead to a linear dependence of the scattering rate. To get to the dependence of the resistivity one must also take into account the fact that only high angle scattering effectively reduces conductance. With this correction the result for the resistivity close to a quantum critical point with $d = 3$ is that $\rho \sim T^{5/3}$. Anti-ferromagnetic fluctuations give rise to a state in which the resistivity goes as: $\rho \sim T^{3/2}$.

The case for anti-ferromagnetic SFT has been made increasingly strong with experimental evidence (5),(6), (7), where a marginal Fermi Liquid (mFL) is predicted. The idea of magnetically mediated superconductivity, in which the pairing mechanism is related to the spin fluctuations rather than to the lattice fluctuations of conventional superconductivity has also been well supported experimentally (8). It has even been possible using this theory to predict and observe a large increase in SC transition temperature when reducing the number of effective dimensions in a system from 3 to 2 (Ref. (9)).

The case of ferromagnetism is not as strong. There are indeed cases in which the theory and observations match (10) (11) (12). However, the agreement is rarely complete, for example in MnSi the region of resistivity that follows the SFT prediction appears to be far too large to be accounted for by the theory. Another factor that clouds the issue is that the ferromagnetic transition is often seen to become first order. The superconductivity predicted to be mediated by ferromagnetic fluctuations near a QCP has not been unambiguously discovered. There are good reasons within the model of magnetically mediated superconductivity why this is the case (see eg. Ref. (8)).

Pressure is one of the possible external fields that can be used to tune the system through a QCP. Resistivity is possibly the most accurately measurable quantity under very high pressure.

2.2 The Doniach Phase Diagram

In a system containing both localised moments due to f-electrons and itinerant charge carriers from other bands, the interaction between the two populations will, in general, have a profound effect on the properties of the material. In the limit that the localised moments are a perturbation to the Fermi liquid state, i.e.

they are well dispersed in a metal, the conduction electrons will screen out the spins of the moments entirely below a certain temperature. This is the Kondo effect. If the moments can not really be considered dilute, they will interact indirectly through the polarisation of the conduction electrons. This indirect exchange is the Ruderman-Kittel-Kasuya-Yosida (RKKY) interaction.

The conduction electrons are polarised in the vicinity of the magnetic ion. The form of the magnetisation in a Fermi gas is that of an exponentially decaying sinusoid. The distance from the point moment determines whether the magnetisation is parallel or anti-parallel. If a second local moment is placed within the magnetised electron cloud it will feel the induced magnetisation and will therefore be indirectly coupled to the first moment. This RKKY interaction tends to be antiferromagnetic in the cerium (Ce) based systems. The distance dependence of the strength of the interaction, J(r), is given by:

$$J(r) \propto \frac{2k_F r\cos(2k_F r) - \sin(2k_F r)}{(2k_F r)^4} \tag{2.18}$$

k_F is the Fermi wave number and r the distance between 2 moments. It is therefore possible, by compressing the system, to alter the magnitude of the exchange interaction. The magnetisation of the conduction band electrons has an associated energy which is proportional to the square of the exchange stiffness, J, and the density of states at the Fermi energy, $N(E_F)$:

$$K_B T_{RKKY} \propto J^2 N(E_F) \tag{2.19}$$

The exchange coupling between the local moments and the conduction band could be either ferromagnetic or antiferromagnetic. Only AFM coupling produces contributions to the resistivity and it can be shown that AFM coupling will exist when 4f electrons hybridise with the conduction electrons (13). The process that leads to the extra resistivity that characterises the Kondo effect is a spin flip process and gives rise to a peak in the density of states at the Fermi energy below a characteristic temperature, T_K:

$$K_B T_K \propto \exp\left(\frac{-1}{|J|N(E_F)}\right) \tag{2.20}$$

It is therefore the density of states and the exchange interaction energy that determine whether a system will be dominated by long range magnetism or the Kondo effect. It is this competition that is represented in the well known Doniach phase diagram, see Fig. 2.2.

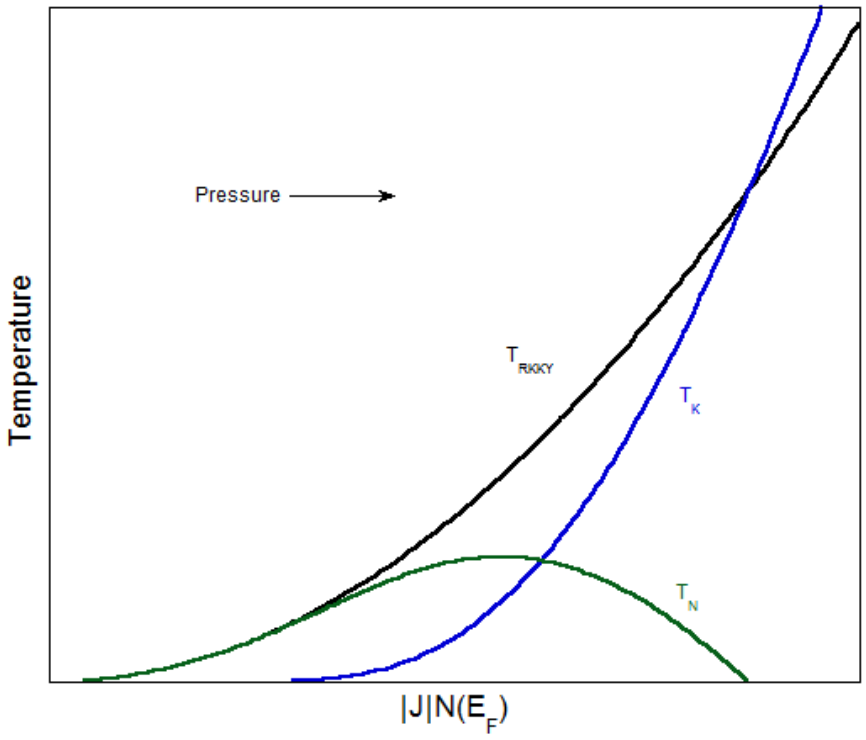

Figure 2.2: Application of pressure can drive a magnetic Ce compound to be non-magnetic with a resulting QPT.

The point in the Doniach phase diagram at which the Néel temperature is at zero Kelvin was discovered to be a good candidate for a QCP. The balance of the RKKY and Kondo interactions - in other words, the position on the Doniach diagram - can be altered with pressure. It is therefore possible to use pressure to tune a system from left to right (in the case of many Ce based compounds) or

right to left (in some Yb based compounds). This physical picture has been used to great effect and there are now many HF compounds that have been studied in the context of a QCP, e.g. (5) (7).

Another insightful way to think about the effect of pressure in the Ce systems is to consider its effect on the formation of f-electron bands. As a rule of thumb, when the Ce atoms are brought within 3.4Å, it is considered that the f-states overlap sufficiently for a band to have formed. This is important, as it allows the system to reduce energy by delocalising the 4f electrons and so avoid having a single 4f state occupied. This change eliminates the magnetic moment associated with the Ce ion.

2.3 QCPs in Diverse Systems

As well as the QCP seen on the Doniach phase diagram and those investigated on the border of itinerant magnetism, the same physics has been suggested in a dizzying array of systems: from the high temperature cuprate superconductors (eg. Ref. (14)) to organic superconductors, from superfluid ^3He to ferroelectric systems (Ref. (15)). The cuprate superconductors have been studied at greater length than possibly any other class of materials, and the diversity of physics discovered there has been very exciting. Certainly, they seem to fit in with the principal that reduced dimensions are conducive to the survival of quantum behaviour at higher temperatures. The planar structure of these materials has inspired many related research fields. Sr_2RuO_4 and other perovskites are one fascinating example. A schematic of the phase diagram for the cuprates, Fig.2.3 shows why the QCP explanation has remained popular. The features are strongly reminiscent of the 'classic' QCP diagram.

The role of the Oxygen p-orbitals in the conduction mechanisms of the perovskites is crucial. Sulphur sits underneath Oxygen in the periodic table. However, planar sulphur based systems are much less well studied in this field than their Oxygen based cousins.

The exciting new iron pnictide materials based on Iron-Arsenic show superconductivity when appropriately electron-doped, see for a review eg (16). A generic phase diagram is shown in Fig.2.4. These materials all have in common

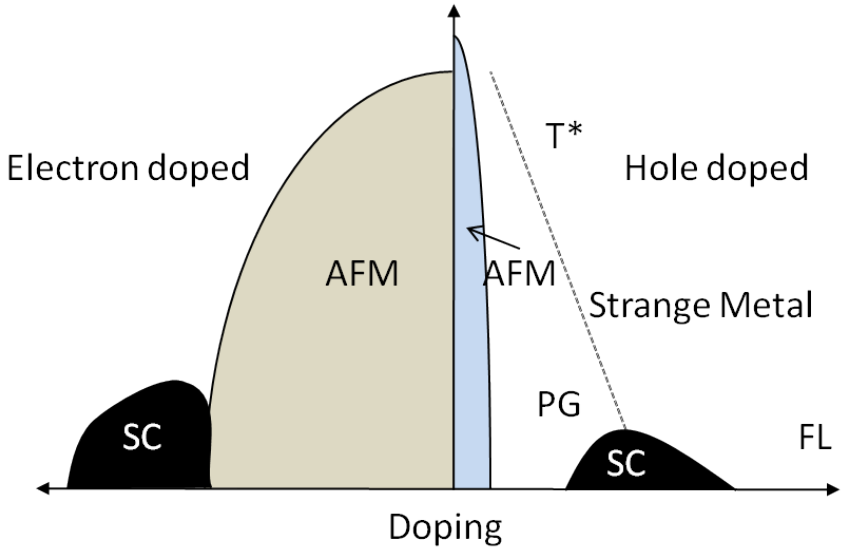

Figure 2.3: Schematic high T_C cuprate phase diagram showing the antiferromagnetic insulator (AFM), pseudo-gap (PG), superconducting (SC) and unconventional metallic (Strange Metal) states.

a layered structure including a layer of FeAs. This has inspired comparison with the ruthenates as well as the cuprate superconductors. As well as doping, pressure has been used as the tuning parameter to induce superconductivity, (17). However, the pressure phase diagram is still being debated in most cases.

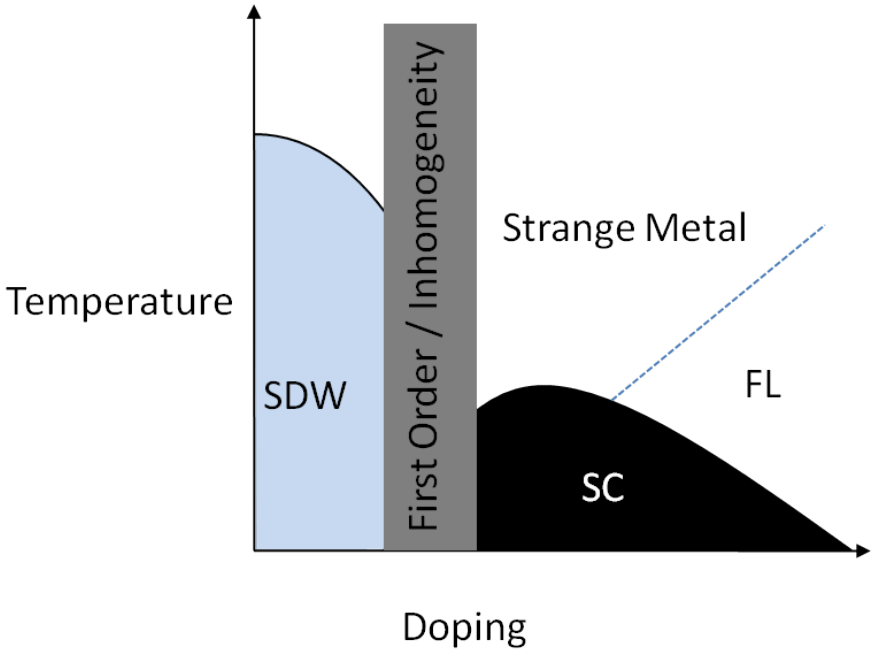

Figure 2.4: Schematic pnictide phase transition based on the diagram made from the data on $LaFeAsO_{1-x}F_x$ and $SmFeAsO_{1-x}F_x$ found in Ref.(18).

3

Experimental Technique

As has been discussed, magnetic systems tend to be sensitive to changes in applied pressure. In order to drive the system through a QPT and measure the temperature dependence of the magnetic susceptibility, χ and the resistivity, ρ, it is vital to achieve very low temperatures simultaneously with high pressure. In this section the various experiments carried out will be described.

3.1 Sample Preparation

The piston cylinder cells have a reasonably large sample space, around 5×5×20mm in dimension. This allows one to be exacting in the requirements for a well suited sample shape. A long rod is probably the best shape to use, based on the fact that extracting the resistivity from the resistance is relatively straightforward. The Bridgmann cells have a much smaller sample space. Samples are typically planar in shape, with a thickness of $100\mu m$ and edges of $\sim 1mm$.

Samples are rarely in the ideal configuration straight from the growth process, therefore it is usually necessary to polish or cut down the samples. Several processes were used to obtain suitable samples for the various experiments.

3.1.1 Cutting Techniques

The simplest cutting technique is to use a scalpel or razor blade to cleave the sample directly into the shape required. This technique was used in the prepara-

tion of the $NiPS_3$ samples. The samples cleave very easily along the planes and can be cut through the planes with care. As the surface is highly reflective it is easy to see any cracks that occur during the cutting process.

CeGe and Fe_2P are too hard to cut with a scalpel or razor blade. The main tool used to cut these materials was a wire saw. When used carefully the wire saw is capable of high precision as well as being very gentle on the sample. The sample is mounted on a piece of cork or balsa wood and held in place with some crystallography wax which is clear and easily melted. The sample plus mount is then stuck to the goniometer stage used in an x-ray diffractometer. This allows the precise alignment of the sample under the cutting wire. The wire used is made from tungsten and is $50\mu m$ in diameter. This precise alignment is very important for the Fe_2P samples as they are highly anisotropic single crystals. The CeGe samples are polycrystals and it is therefore impossible to cut along any given direction. The sample is then coated periodically with a mix of glycerin and a powder of a hard material whilst the wire is run back and forth across the surface. This cuts the sample quite slowly but very accurately; typically it would take twenty minutes to cut thorough a two millimetre piece of Fe_2P.

The only disadvantage to the wire saw is the amount of time taken to cut the larger pieces of sample. The Fe_2P sample was originally in the form of one large ingot, about 7mm on a side and irregularly shaped. It was clear from observing the sample that there were portions that had crystallised in a particular orientation. The ingot was cut along these directions, as much as possible, using a spark cutter. The spark cutter uses a high voltage across a wire and the sample to melt through metallic samples. The wire and sample are immersed in oil which takes away the heat and insulates the rest of the apparatus from the current. The removal of heat is important as it stops the sample from being too badly damaged at the cutting surface. The roughly aligned pieces were then oriented by the use of a SQUID magnetometer and then cut into more useful shapes on the wire cutter.

3.1.2 Cleaning and Polishing Techniques

In order to obtain good electrical contact on the sample surface it is important to make sure the surface is clean and flat. After spark cutting there is inevitably some damage to the sample surface. In order to remove the damaged layer the initial polishing technique used on the Fe_2P samples was that of electro polishing. The sample is placed in a bath of acid solution which is cooled by dry ice (solid $C0_2$) at 195K. The solution used was 1% perchloric acid ($HCl0_4$) in methanol. Cooling the solution reduces the acid action on the surface and stops the methanol from evaporating too quickly. The acid acts as an electrolyte and oxidising agent. The sample is anodised and a cathode is placed in the solution. The metal oxide is dissolved in the solution removing the material from the surface. The electric field is strongest at the tip of any peak and weakest in any trough. It is this property that allows the surface to be polished rather than uniformly removed. Electro-polishing typically removes about 50-100μm of the surface as well as smoothing it out.

Electro-polishing is good at removing any damaged surfaces or significant oxide layers, but in order to achieve a planar surface onto which it is best to attach wires, the samples were mechanically polished. This technique uses a similar principle as the wire saw cutting. The sample is held in place on a stainless steel jig with crystallography wax. The jig is then placed sample side down on a piece of glass that has a mix of glycerin and an abrasive small grain powder. The powder is typically of a material such as silicon carbide, boron carbide, alumina or diamond. The jig is then gently moved in circles on the glass to cut a flat surface onto the sample. The jig is designed to take most of the weight away from the sample so it is only gently pressing on the cutting fluid and glass. This technique can also be used to make very thin samples when it would be impossible to cut such a small sample without destroying it. It is possible to polish a sample down to 100μm thickness and with good precision (in the tens of micrometres).

Finally, before any electrical contacts are made it is important to clean the surface of any dirt or grease from the air or from one's fingers or other tools used to manipulate the sample. This is done first with acetone and then with ethanol.

Used together these two solvents will remove most organic compounds that may be present.

3.1.3 Contacts

Because the metallic samples (Fe_2P, CeGe) are relatively large it is possible to spot-weld gold wires to them. Spot-welding is only applicable to conducting samples as it relies on passing a current through the wire to be attached and the sample. The equipment needed for spot-welding is shown in Fig.3.1 and a description in Ref.(19). The sample is placed on the bottom electrode. The gold wire is rested on the sample in the position it is to be connected and the top needle electrode is positioned to be right on top of it and in contact. A current of several Amps at a voltage of about 6V is then passed through the electrodes, wire and sample for a short time. This melts the gold wire, welding it to the sample. The wires are welded in a line on one face of the samples. The main advantages of spot-welding are a reasonable joint strength (although this depends on the material being spot-welded to) and a very low contact resistance. The contact resistance is typically less then one Ohm. When measuring resistance it is favourable to have a four point measurement. This allows the resistance of the leads and contacts to be automatically removed. Two point measurements can be used if it is not possible to reliably make four contacts to a sample, however it becomes more difficult to make accurate quantitative measurements in this case.

Contact resistance has a number of contributing factors. Primarily, it is determined by the presence and thickness of any oxide layers on the wire and sample as well as by the mismatch of the Fermi energy within the two materials. Spot welding all but eliminates any oxide layers at the point of contact. A high contact resistance can cause problems in a measurement due to the heat produced. The heating power of a flowing current is proportional to the resistance. The metallic samples measured will typically have room temperature resistances of $\sim 10 - 50m\Omega$ and residual resistivities ratios of 1-30. This means that a contact resistance of one Ohm is the dominant source of heating.

Making contacts to semiconductors, poor metals and insulators requires the use of different contact methods. The CeGe was very difficult to spot weld to as

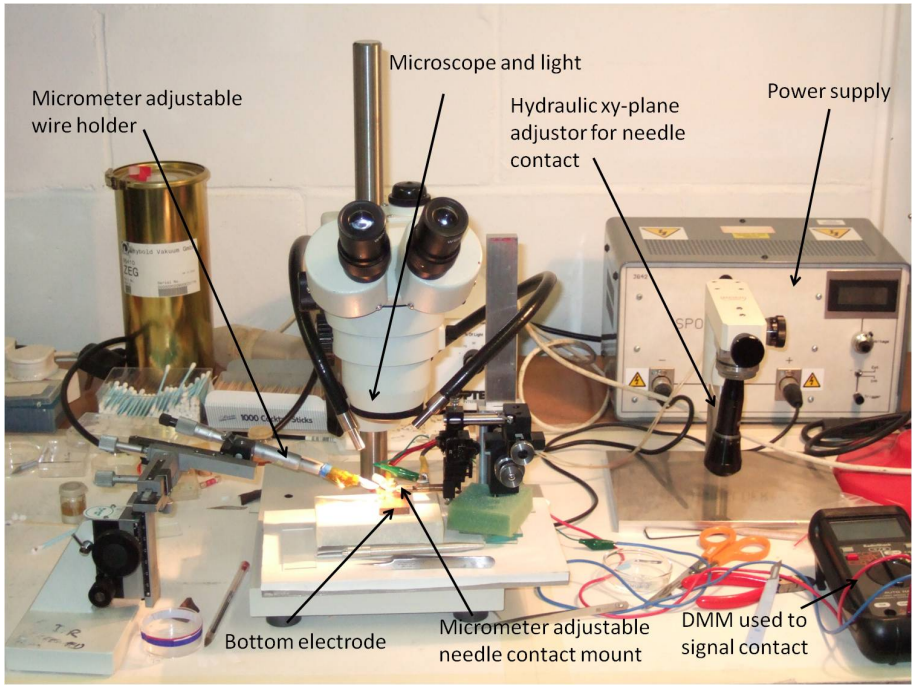

Figure 3.1: Apparatus used to spot weld the contacts onto the metallic samples

it is not a very good conductor compared to copper or even Fe_2P. For the $NiPS_3$ the contacts had to be very small as the sample was going in the Bridgmann cell. The most common way to make a contact is the use of a silver glue or epoxy. However, these pastes have an unfortunate tendency to smear out over the sample when put under pressure in a Bridgmann cell, leading to shorts. Therefore, the contacts used were pressure contacts: the wire, which is either gold or platinum, is placed directly onto the sample and then the contact is made when the cell is sealed under pressure. These contacts are difficult to set up in the first place but generally make very good electrical connection to the sample once under high pressure.

3.2 Cell Preparation

3.2.1 Piston Cylinder Cells

In the piston cylinder cells used, the experiment (the sample plus any wiring and the pressure gauge) is placed in a Teflon cap. This cap is then inserted into the cell body. The piston is in contact with the closed end. The open end is then either closed with a stopper, if the experiment to be done requires no contacts (Fig. 3.2), or a feedthrough (Fig. 3.3), if it is to be a transport measurement.

If the measurement to be done is a magnetisation measurement then a miniature clamp cell, or SQUID cell is used. The SQUID cell shown in Fig. 3.2 is small enough to be used in the Quantum Design MPMS or SQUID. It allows high precision DC magnetisation measurements to be made under pressures of up to about 12Kbar. The sample is loaded into the Teflon cap after a lead pressure gauge. The sample and lead used are long and thin as this reduces demagnetisation effects, which would complicate both the magnetic measurements of the sample and the superconducting transition measurement on the lead. The entire cell is made from a Beryllium Copper (BeCu) alloy apart from a copper washer and the Teflon cap. BeCu is used for its strength and very low magnetisation over a wide range of temperature and applied magnetic field.

The system used comprises of the Quantum Design Sample Property Measurement System cryostat with the 1822 MPMS Controller electronics. The SQUID

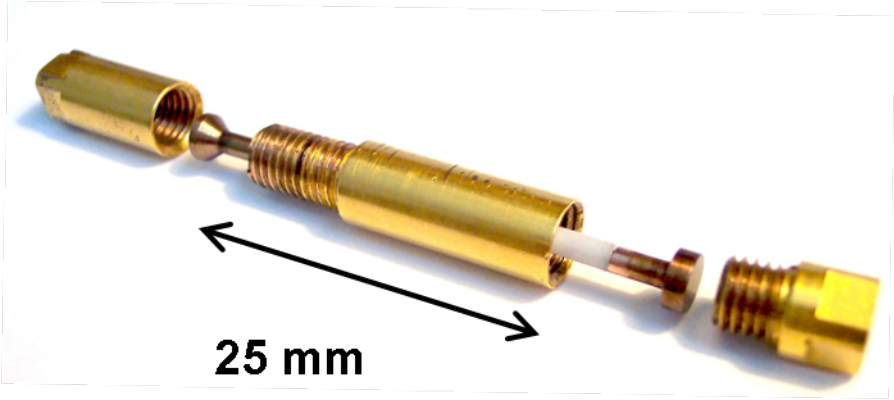

Figure 3.2: Miniature BeCu used for SQUID magnetometer magnetisation measurements

is referred to as such because it employs a Superconducting QUauntum Interference Device to measure magnetisation to a very high accuracy; 1×10^{-8}emu at 2500Oe. The measurements done are DC magnetisation and susceptibility as a function of field, up to 5T, and temperature, from 5K - 300K.

The clamp cells used in the resistivity measurements differ from the miniature BeCu cells in two main ways. Firstly, the cells can be larger and the magnetic background signal is not so important, so a second alloy is used to strengthen the cell and allow it to reach higher pressures. This second alloy is called MP35N and is used to make an inner cell body, see Fig.3.3. MP35N is a non-magnetic nickel-cobalt-chromium-molybdenum alloy with a very high tensile strength. Although non-magnetic MP35N has a significantly higher magnetic background than BeCu. Secondly, in order to measure the resistivity of a sample one must be able to accommodate access to the sample space for wires. To do this a feedthrough is used. A detailed description of how to set this up may be found in Ref. (20). The feedthrough is shown in Fig. 3.3. The wires that pass through the centre of the feedthrough are sealed in place there by an epoxy resin. This resin is sucked down through the feedthrough until it fills the cavity. The epoxy is then cured to form a tight seal.

The samples can then be mounted onto a printed circuit board which is soldered onto the wires coming through the feedthrough. A strip of high purity tin

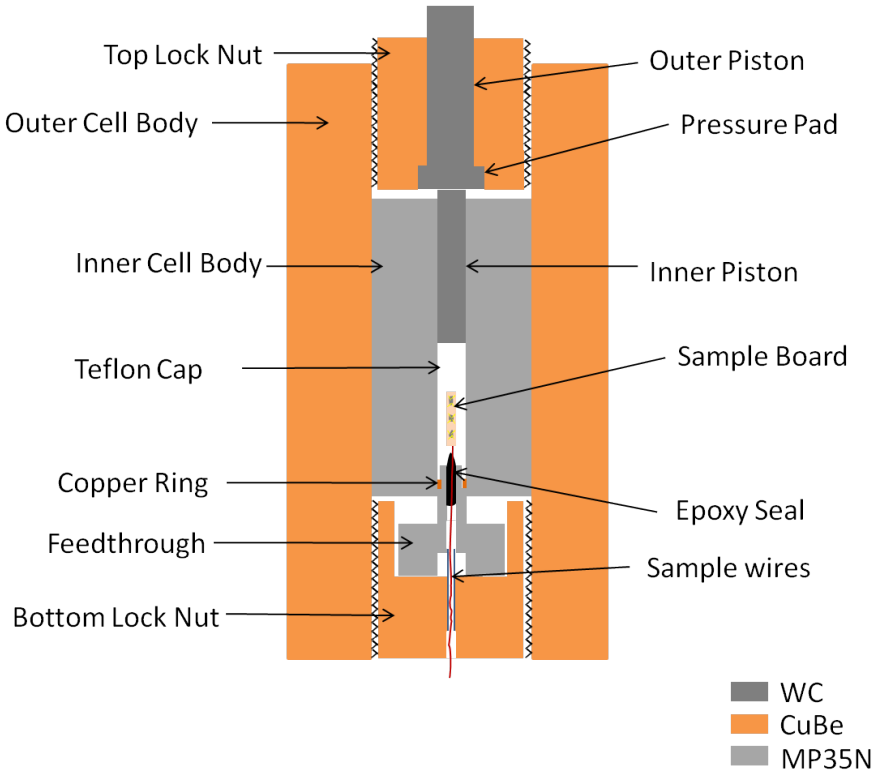

Figure 3.3: Cross-section of the cylindrical piston cylinder cell with inserted feedthrough

foil is then soldered onto the back of the board to save space. The tin is used as the pressure gauge both at room temperature, by measuring the change in resistivity, and at low temperature, using the superconducting transition temperature. This whole setup is forced into the Teflon cap which is full of hydrolic oil. The pressure cell is then assembled and pressurised up to around 6Kbar. This pressure is maintained for quarter of an hour before the cell is depressurised. The purpose of this initial pressurisation is to seal any very small gaps in the system with the large molecule hydrolic oil, before the smaller molecules of the pressure medium are introduced. The pressure media used were Daphne Oil 7373 or an isopentane - n-pentane mix.

3.2.2 Bridgmann Anvil Cells

By placing the experiment, with or without pressure medium, directly on one of two opposed anvils, very high pressures can be achieved. The down side is the loss of hydrostaticity when using a solid pressure medium. The culet size and strength of the anvils are the factors determining the maximum value of the achievable pressures. Using a reasonably sized culet (of order 3mm diameter) and tungsten carbide (WC) anvils, the maximum pressure is about 100Kbar. This culet size and maximum pressure corresponds to the Bridgmann Anvil Cells (BACs) used in the $NiPS_3$ measurements. Using very small culets and diamond anvils, pressures into the megabar regime have been reported (see Ref. (21) and references therein).

Access to the sample can be achieved for the introduction of wires by the use of a pyrophyllite gasket and steatite pressure medium. Slits are cut in the gasket into which the wires are forced before the slits are filled with pyrophyllite powder. The wires are platinum and flattened at one end. They are then placed on the sample and lead gauge. A second steatite disk is then placed on top of the experiment. The upper anvil is gently locked in place with a second lock nut.

The cell is then pressurised using a load calculated to give the desired pressure. This is only an educated guess however, as to the pressure exerted on the sample at low temperature. Experience gives a feel for the pressure range that is expected for a given load. After pressurisation the cell is checked for the most common

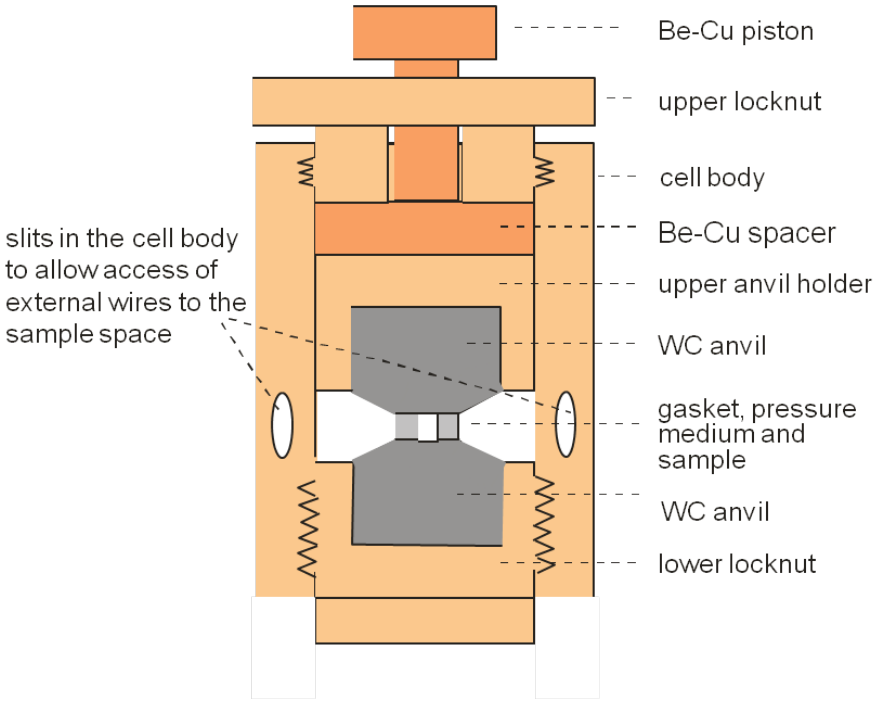

Figure 3.4: Schematic of a Bridgmann anvil cell (BAC)

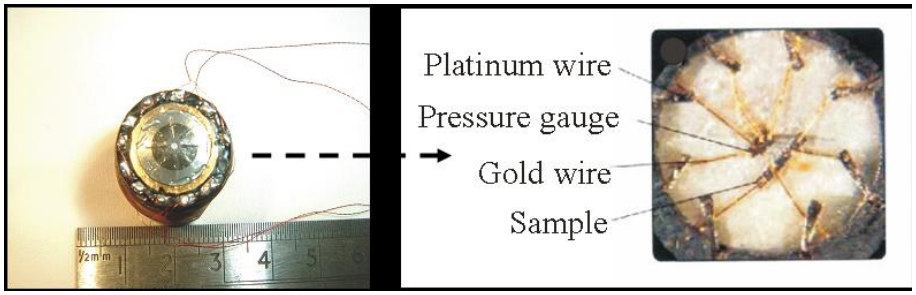

Figure 3.5: Resistivity set-up in the WC BAC. The photograph shows a sample and lead pressure gauge sitting on the lower steatite disk. The Au wires spot-welded to the sample and gauge are overlapping with the flattened ends of Pt wires leading out through the gasket.

failures: shorts to the cell body and broken wires. When measuring insulators it is not easy to check for broken wires as most voltmeters will not have the impedance necessary to give an accurate reading whether or not the wire is broken. This has to be done using an electrometer capable of detecting very small currents. Even then it is not 100% certain.

3.3 Cooling and Measurement Electronics

As well as high pressure, low temperatures and accurate measurement systems are vital to determining the exponents of the resistivity and, therefore, distinguishing between different states. Once the sample is cut, polished, has electrical contacts and the cell is assembled and pressurised, it is then mounted on a cryostat for a temperature sweep of the resistivity.

3.3.1 Adiabatic Demagnetisation Refrigerator

The Adiabatic Demagnetisation Refrigerator (ADR) was used for the temperature sweeps of CeGe and Fe_2P (see Fig.3.6). A 1K pot is used to cool the system to about 1.8K. At this point a large magnetic field of up to 6T is applied to a salt pill attached to the sample stage. This salt pill contains a paramagnetic material, usually chromic potassium alum, ferric ammonium alum or cerium magnesium nitrate, although there are many others. The spins are all aligned and the 1K pot is used to draw away the heat generated in this process. The sample stage and salt pill are then thermally isolated from the rest of the system and the salt pill demagnetised adiabatically. The moments in the salt pill then disorder. As the total entropy of this state is the same and the system is isolated, thermal entropy transfers into magnetic entropy and the salt pill lowers the temperature of the sample stage (22). Temperatures of around 50mK can be achieved and held for about half an hour. The system will then warm up. The rate of warming can be controlled with a heater. Measurements of the four-point resistivity of the sample and pressure gauge are then made as the system warms up. The optimal heating rate is the fastest rate at which there is no thermal hysteresis; that is to say that when heating or cooling at this rate the measurements are identical.

This rate is different for different systems. When using the clamp cells, which have a considerable mass, a heating rate of less than $1Kmin^{-1}$ is used above 2K and is found to allow for good thermal equilibration. Below this point the heating is significantly slower: typically $100 - 200mKmin^{-1}$.

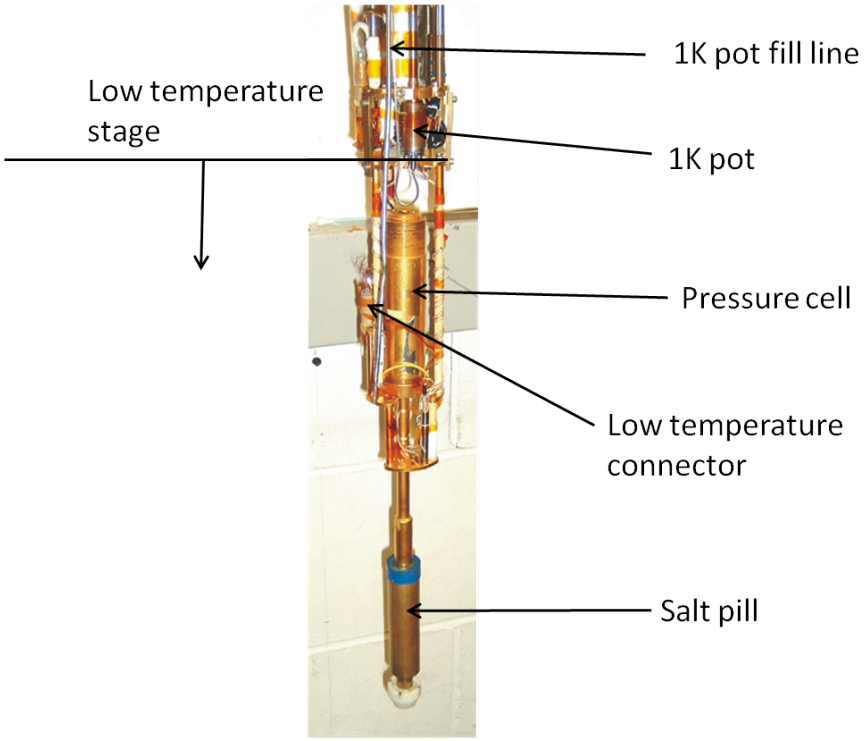

Figure 3.6: ADR used in the Quantum Matter (QM) group

There are three low temperature and three room temperature transformers connected by superconducting $NbSn_3$ wire to the room temperature stage. These transformers are used for the voltage measurements. Six other room temperature transformers are connected to the sample by CuBe wires. These are used for current measurements. The use of the transformers in this way allows both the low and high temperature behaviour of the resistivity to be measured very accurately. This sensitivity is needed when measuring the resistivity of metals. For a given applied current the voltage drop, from V=IR, is very small owing to the low resistivity. At low temperatures the resistivity can be below $1\mu\Omega cm$ which would correspond to less than a nanovolt for an applied current in the hundreds

of microamps. The low temperature transformers provide an amplification to the signal of about a factor of thirty. Crucially, they are at 4.2K, so the thermally induced noise that is also stepped up is very low.

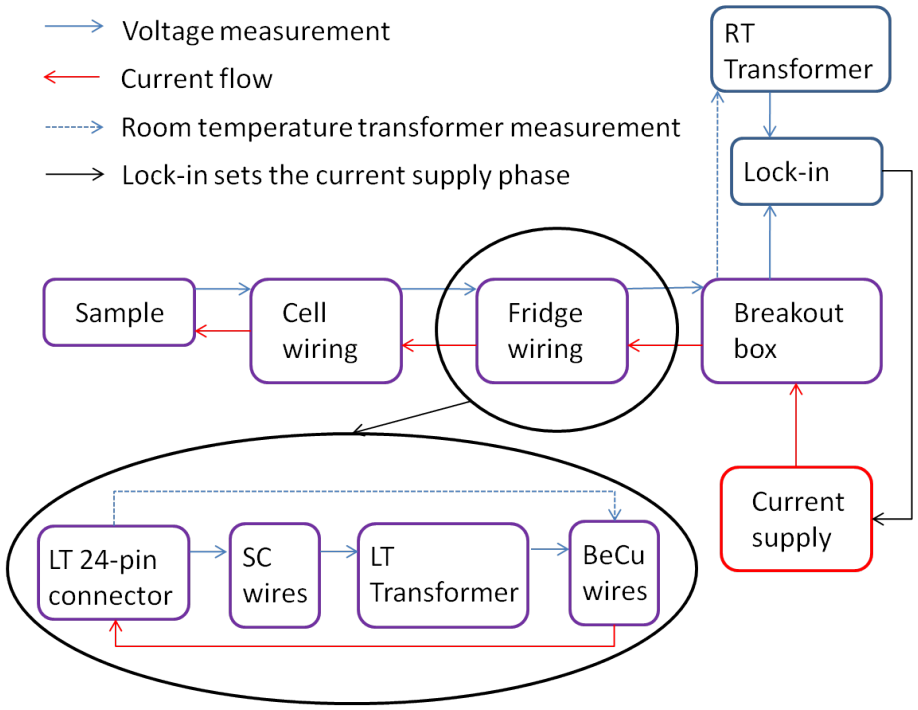

Figure 3.7: The four point measurement set-up used to measure metallic samples

Figure 3.7 shows a schematic of the equipment used in the resistivity measurements performed on the metallic samples, CeGe and Fe_2P. The lock-in used is a Signal Recovery 7265. The 24-Pin CMR Low Temperature Connector is a gold plated connector. The cell wires are soldered onto the female connector and the male is fixed to the cryostat with the cryostat wiring soldered to that side.

3.3.2 Heliox

The measurement of resistivity of a good insulator requires a different approach to that of a metal. The difficulty has changed from trying to detect small voltage drops to picking up very small currents. It is this feature that imposes one of the most important constraints on the measurement system. The impedance of

the measurement device must be several orders of magnitude larger than that of the sample. This includes the wiring. It is therefore not possible to use the lock-in measurement technique. Instead, a simple digital multimeter (DMM) and a Lakeshore 340 resistance bridge were used. The piece of apparatus with the highest internal resistance is an electrometer. The electrometer is now being used to carry out further measurement on the MPS_3 family of compounds. The other major consideration in terms of measurement apparatus is that the wiring be well enough shielded to prevent cross-talk, from parasitic capacitance or induction. This is more of a problem the longer the wires are. Therefore, the fact that the wiring on the Heliox is several metres long compared to tens of centimetres for the room temperature measurements, is likely to be the reason why the temperature sweeps were less successful then the room temperature measurements.

The resistance measured on the lock-in has in-phase and out-of-phase components. The out-of-phase component is very close to zero for a purely resistive sample. When the out-of-phase component becomes appreciable, the measurement becomes harder to interpret as there is now some indication or capacitance or inductance. Therefore, the out-of-phase component can be used as a guide to the reliability of the measurement. Fig. 3.8 shows that above 100K the measurement is entirely resistive. However, as seen in Fig.3.9, the out-of-phase component grows in magnitude slowly below 50K and then quickly below 15K.

The lock-in and the resistance bridge agree at high temperatures, see Fig.3.10, but as the temperature is reduced and the resistivity increases the results follow a different evolution. It is likely that this is due to the difference in the way the two systems respond to a capacitive sample, combined with the less than ideal heating profile in the case of the Lakeshore measurement. Fig. 3.11 shows the temperature profiles for the two measurements. It is clear that the measurements on the Lakeshore are unreliable between 10K and 250K due to the very fast heating rate. However, at room temperature the measurement is reliable and agrees with the lock-in. Both give a room temperature resistance of $\sim 120\Omega$. The difference between the measurements at low temperatures is troubling and makes it clear that the measurement apparatus is currently unable to cope with the large resistances encountered. 2-point resistances of the order of MegaOhms were recorded at low temperatures.

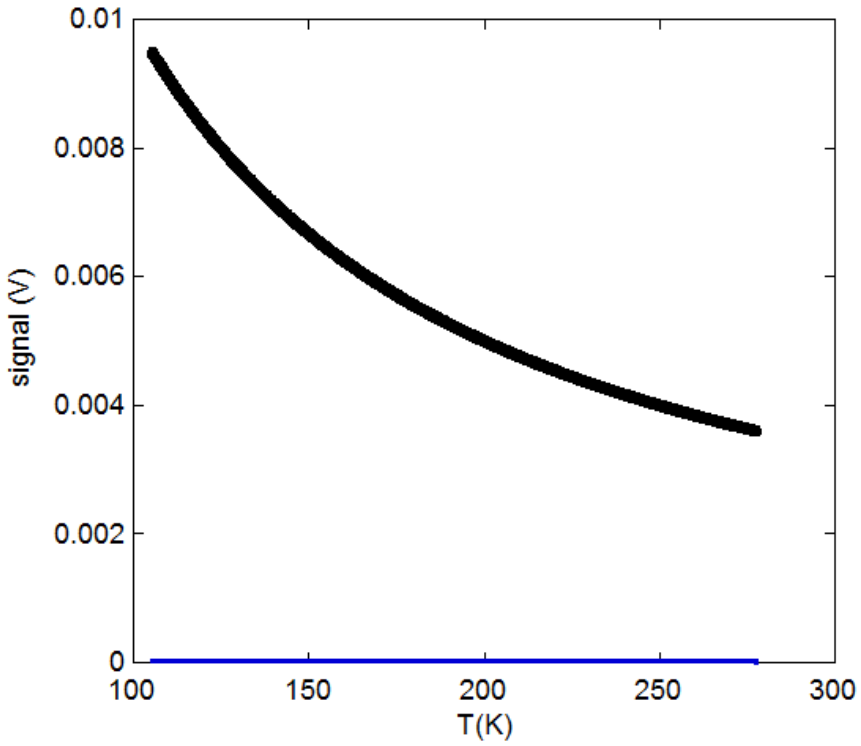

Figure 3.8: Measurement of a semi-conducting or high resistance sample on a lock-in amplifier. At high temperatures (T>20K) the voltage signal on the lock-in amplifier is almost entirely made up of the in-phase component (black). The out-of-phase signal (blue), which represents loss in the system, is very small, indicating that the system is resistive rather than capacitative or inductive.

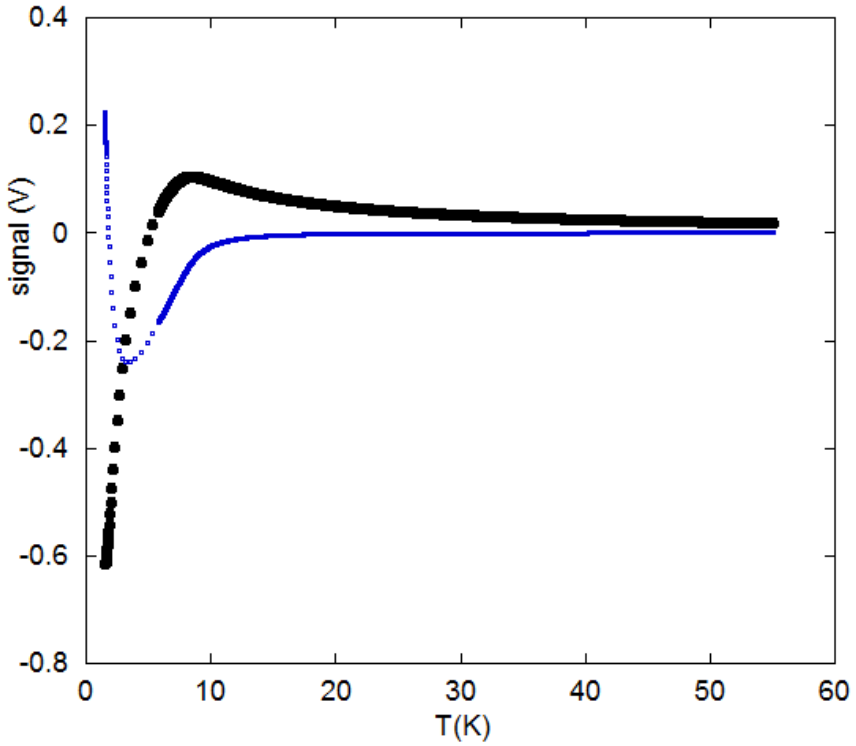

Figure 3.9: Measurement of a semi-conducting or high resistance sample on a lock-in amplifier. At low temperatures (T<20K) the voltage signal on the lock-in amplifier has an appreciable element out-of-phase (blue) with the reference signal.

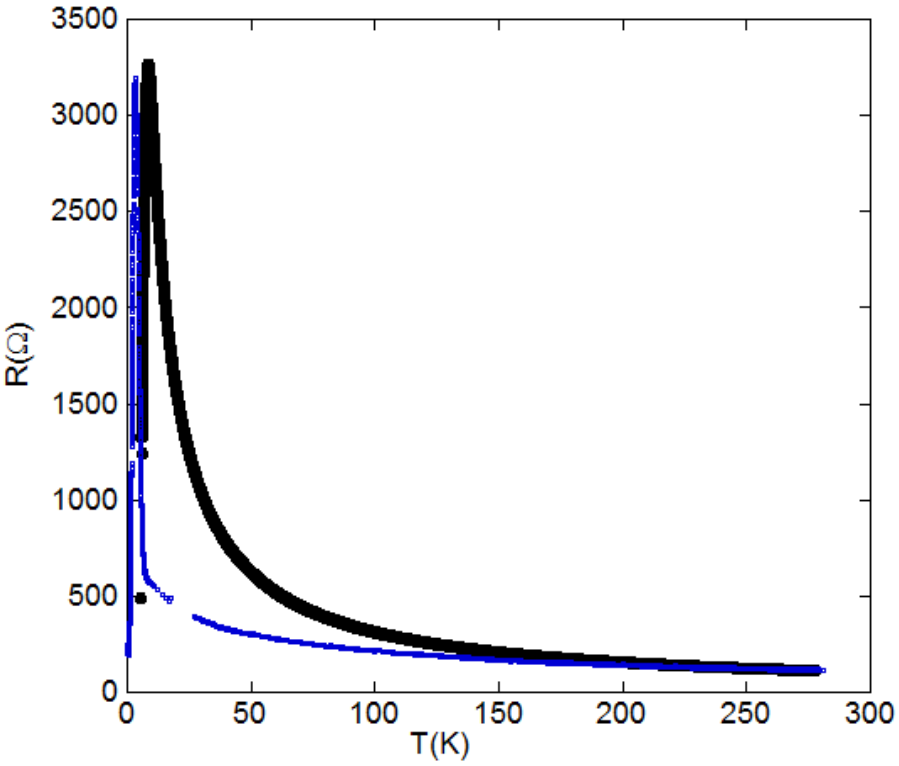

Figure 3.10: At room temperature the two measurement techniques (Lakeshore - blue and lock-in - black) agree. However after that only a general agreement is seen. The measurement becomes unreliable (characterised by a 'peak' in the measured resistance) at different temperatures but at the same value of the resistance.

The huge discrepancy between the values of the 2-point and 4-point measurements is related to the conduction processes involved. To measure resistance a current must be passed through a sample. In a metal this is easy and with care the contact area will pose a very small obstacle to the current. However, for current to pass from a metal into an insulator it is necessary for the electrons to tunnel into an empty state, of which there are very few and the number decreases with temperature. This makes the contact resistance rise sharply with decreasing temperature. So for example the 2-point measurement at 80Kbar and room temperature is of the order of 1KΩ and the 4-point of the order of 100Ω, one order of magnitude difference rather than the 2 or three seen at low temperature.

The fact that the resistance vanishes from the same peak value suggests that the potential weak link is not the measurement device itself but the wiring used.

The Heliox is an evaporative ^{3}He cryostat; it generates the cooling power by first pumping on the ^{4}He bath and then on the sealed ^{3}He reservoir once it has been liquefied. The Heliox has the advantage of being used previously for capacitance measurements and is therefore fitted with 2 shielded coaxial wires. These wires will help to reduce the cross-talk problem in the future.

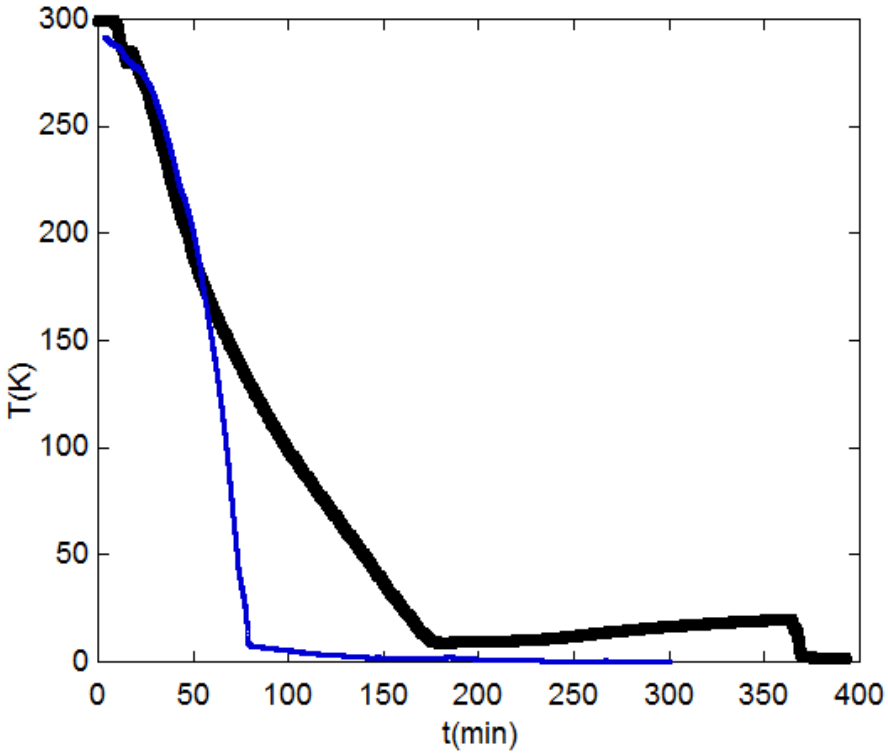

Figure 3.11: The measurement was taken as the system was cooled in the case of the lock-in (black) and during heating for the Lakeshore (blue). The heating profile of the Lakeshore measurement has been plotted in reverse time order to allow more direct comparison. The cooling rate during the measurement using the lock-in is much more stable and therefore reliable.

4

Fe_2P

4.1 Introduction

The ambient pressure magnetic properties of Fe_2P were characterised in the 1960's. Fe_2P was found to be a ferromagnet with a Curie temperature (T_C) significantly lower than elemental iron(23). However, differences in sample quality meant that it took until the 1970's to accurately determine the T_C to be $\sim 215K$. In 1980 Fujiwara et al.(24) applied pressure and found the system could be tuned through a transition to an AFM state at a relatively low applied pressure ($\sim 5kbar$). Since then, more pressure studies have suggested a very rich magnetic phase diagram with up to 3 AFM states as well as the FM and paramagnetic (PM) states seen at ambient pressure. A consideration of the magnetic structures allowed by the symmetry of the system was done by Yablonskii and Medvedeva in 1990(25). This revealed a large number of permissible magnetic structures. It provides a reasonable explanation for the number of claimed order-order transitions in this material, it does not, however, predict when these may be stable.

Its properties as a magneto-caloric have also been investigated to a significant degree ((26) and references therein). The FM transition was found to be weakly first order (27) (28) and accompanied by a 0.05% volume change. By 'weakly' it is meant that the discontinuity in the order parameter, i.e. magnetisation, is only partial. That is, as the temperature is lowered through the transition, the mag-

netisation varies continously on either side of a moderate discontinuity. Another feature of the weak first order transition is that it is washed out by the application of a modest field of about 100Oe. Upon alloying with manganese the transition temperature can be tuned between 200-350K and therefore covers a very useful temperature range for the potential application of magnetic refrigeration.

Fe_2P has received a lot of attention recently due to its potential in the field of Li-ion batteries (29). It is, however, the pressure dependence of the magnetic properties that interested me; specifically the suppression of 2-D ferromagnetism giving way to antiferromagnetism. Pressure studies by Fujiwara et al(24) and Chen et al(30), show that the T_C is rapidly suppressed with the application of hydrostatic pressure. Therefore, despite its relatively high T_C under ambient pressure, it was conceivable that the T_C may be tuned down to absolute zero and, therefore, into the region of a quantum phase transition. The first order nature of the transition is of some importance in the discussion of a QCP. It is only for a second order transition that the term applies. The concept of a QPT is of course more general. If the transition can be tuned to the proximity of absolute zero, then the question of the nature of an order-order transition stands.

The properties of d-metal ferromagnetic compounds are not much explored in the context of QC Phenomena. There are now a good few AFM materials that have been driven to superconduct as the magnetism is suppressed by applied pressure (e.g. (6; 7)). There are only a very few cases of FM materials in which this is the case(2; 31; 32), and in most of these cases there are other relevant underlying energy scales confusing the picture. Usually, either a metamagnetic transition or a structural phase transition. The main examples are UGe_2 and Fe ((2; 32)).

In the case of Fe the superconductivity is observed only once the system has undergone a structural phase transition and is no longer FM. In UGe_2 there is the presence of another magnetic transition that appears to have more direct consequence for the QCP and superconductivity, see Fig.4.1 (Ref. (33)).

Apart from the very small volume expansion at the ferromagnetic transition Fe_2P has no known structural phase transition under the pressures and temperatures explored in this thesis. Fe_2P is a FM with a Curie temperature, $T_c \sim 215K$ and saturation magnetisation, $M_s \sim 2.9\mu_B$. Its hexagonal 2-D structure, shown

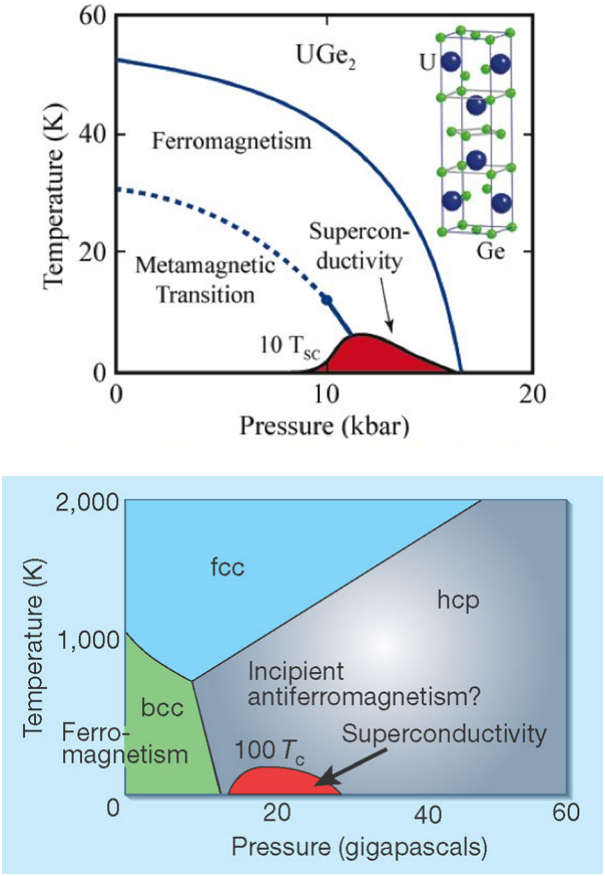

Figure 4.1: UGe_2 (top) and Fe (bottom) are two of a very few FM materials in which the case has been made for magnetically mediated superconductivity on the border of magnetism. (Taken from (32**?**))

in Fig.4.2, is significant for two main reasons: the superconductivity seen in Fe is observed only once the system has undergone a transition from a cubic to hexagonal structure, therefore, parallels between the two systems are easy to draw. Secondly, lower dimensionality of the magnetic state has been suggested to enhance the magnetic fluctuations around the QPT.

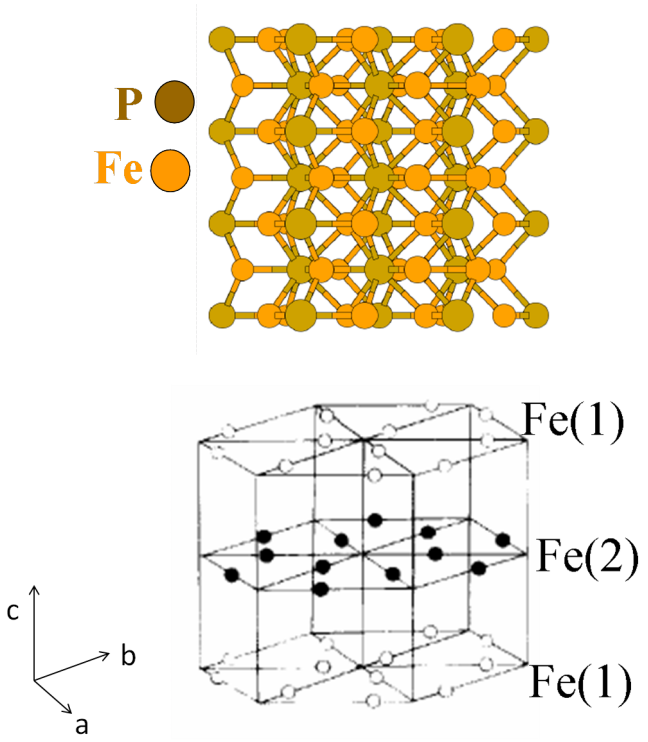

Figure 4.2: Fe(l) is surrounded with four P atoms forming a distorted tetrahedron and eight Fe atoms Fe(2) atom is surrounded with five P atoms located at the corners of a distorted pyramid.

The Pressure-Temperature magnetic phase diagram of Fe_2P investigated by measurements of the weak field ac susceptibility and the resistivity by Fujii et al (24) shows two separate magnetic phase transitions (T_C, T_N) that can be tuned with pressure. The ferromagnetic transition appears to be suppressed by pressures achievable in a piston cylinder cell. From Fig.4.3 the critical pressure (P_C) for suppressing T_C would appear to be around 15kbar. In the later study of Chen (30), in which the T_C is followed down to lower temperatures (25K rather

than 50K) a $P_C \sim 20kbar$ seems more likely. This work also makes measurements at much higher pressures (up to 80kbar) and shows that the T_N changes only very slowly with applied pressure.

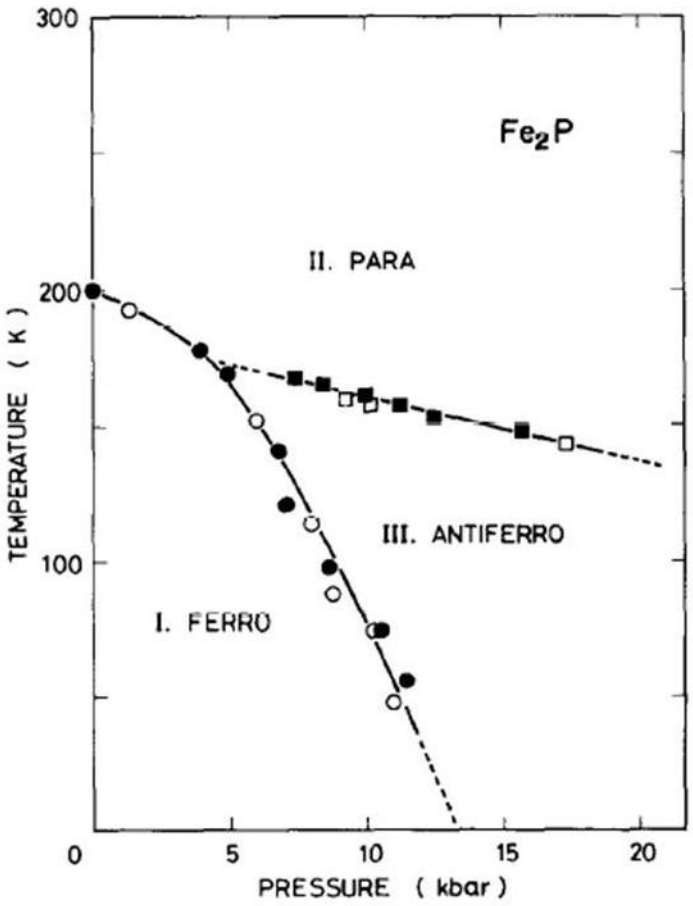

Figure 4.3: Both magnetic transition temperatures are observed to fall with increasing pressure. They are observed in resistivity (filled shapes) and susceptibility (open shapes). From Ref.(24)

Some interesting magnetic properties have been reported in Fe_2P. Metamagnetism was investigated by E. A. Zavadskii, L. I. Medvedeva and A. E. Filippov (34). Kadomatsu et.al. (35) measured the magnetisation under pressure and observed widening hysteresis loops with increasing pressure. They also reported that the saturation moment was insensitive to the increasing pressure in contrast

to the rapidly suppressed transition temperature. In a bid to explain these observations they used a Landau expansion of the free energy for two competing order parameters: One each for the ferromagnetic and antiferromagnetic orders. An approach which seems even more promising when viewed in light of neutron diffraction data on single crystal samples presented by Fujii et. al. (36) which would appear to suggest some competition between different magnetic ground states. At low temperatures, below 130K, the system appears to be a simple c-axis ferromagnet, albeit one with two inequivalent moments, however, in a large temperature range above 130K and below the transition temperature the system shows coexistence of ferromagnetism with a staggered component within the plane. As there has been no neutron diffraction measurements made under pressure, it is impossible to know for sure, but it seems likely that the staggered moment component seen in the metamagnetic region is related to the antiferromagnetic ground state observed at high pressure.

4.2 Results

Before any magnetic or transport measurements were carried out the crystallinity of the sample was determined. The easy-axis of magnetization is the c-axis and the hexagonal anisotropy is very large (see Fig. 4.4). The saturation magnetic moment is 2.9 μ_B/f. unit, in agreement with previous work (37) on single crystals.

4.2.1 Magnetic Data

The results presented were obtained using a Quantum Design MPMS or SQUID and a squid cell (see Fig. 3.2). Fig. 4.5 shows the DC susceptibility of the sample and lead gauge around its superconducting transition temperature, which is known to be pressure dependent in a reliable and well known way (38). A clear jump is visible in each. The narrowness of the transition is a good measure of the homogeneity of the pressure in the cap. If the pressure varied throughout the pressurised volume, then there would be pressure gradients across the lead gauge and one would therefore expect a spread of transition temperatures which would lead to a broad transition.

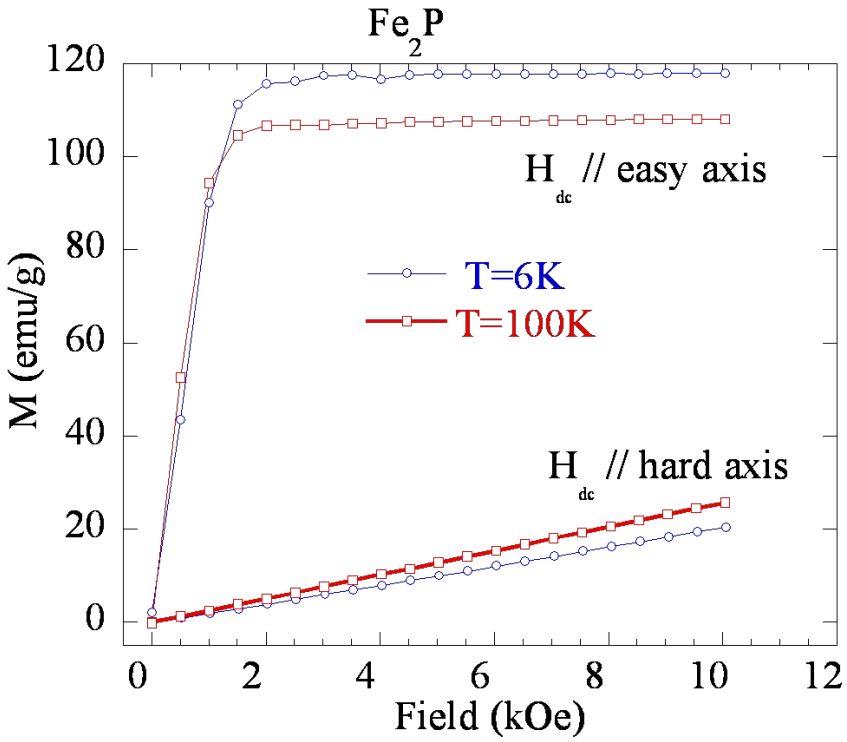

Figure 4.4: Field dependence of the magnetization parallel and perpendicular to the c-axis

Figures 4.6, 4.7 and 4.8 show the ferromagnetic and anti-ferromagnetic transitions. The Curie temperature, T_C, is defined as the inflexion point of the magnetisation versus temperature curve. The Neél temperature, T_N, is taken to be the temperature of the shoulder in the magnetisation versus temperature curve. Both are shown in Fig.4.6. They also show the effect of both pressure and field on the magnetisation measurements. Pressure is seen to suppress the ferromagnetic transition whereas the application of a stronger field increases T_C and widens the transition. The hysteresis curves shown in Figs. 4.9 and 4.10 reveal a counter-intuitive widening as the Curie temperature is suppressed. The P-T phase diagram shown in Fig. 4.11 is a collection of data from several samples cut from the same ingot. They all have the same transition temperatures. The saturation moment was higher in the smaller pieces indicating a better orientation of the crystal. The transition temperatures up to 12kbar are taken from the magnetic data. The point included at 19kbar represents the transition as seen in the resistivity data.

4.2.2 Resistivity

The temperature dependence of the resistivity of a sample under atmospheric pressure (Fig.4.12) show a reasonably robust quadratic temperature dependence at low temperatures. This is good evidence that the atmospheric pressure state of Fe_2P is that of the Fermi Liquid. As pressure is applied to the system the resistivity changes as a function of temperature, see Fig.4.13. The effect of increasing hydrostatic pressure is subtle up to 15kbar. The changes after this point happen are marked and sensitive to relatively small increases in pressure. At pressures below 15kbar, see Fig.4.14, the resistivity follows the T^2 behaviour of the Fermi-Liquid. This can be seen as a straight line in the data when plotted against T^2. The straight line persists up to slightly different temperatures for the different pressures, but is around 12-15K for all of them. As can be seen in this figure there are changes with applied pressure, most notably, the 11kbar data has a steeper gradient. At pressures above 15kbar (Fig.4.15) the changes are significant: firstly, the value of ρ_0 is seen to sharply increase. Secondly, the data no longer form a straight line when plotted against T^2.

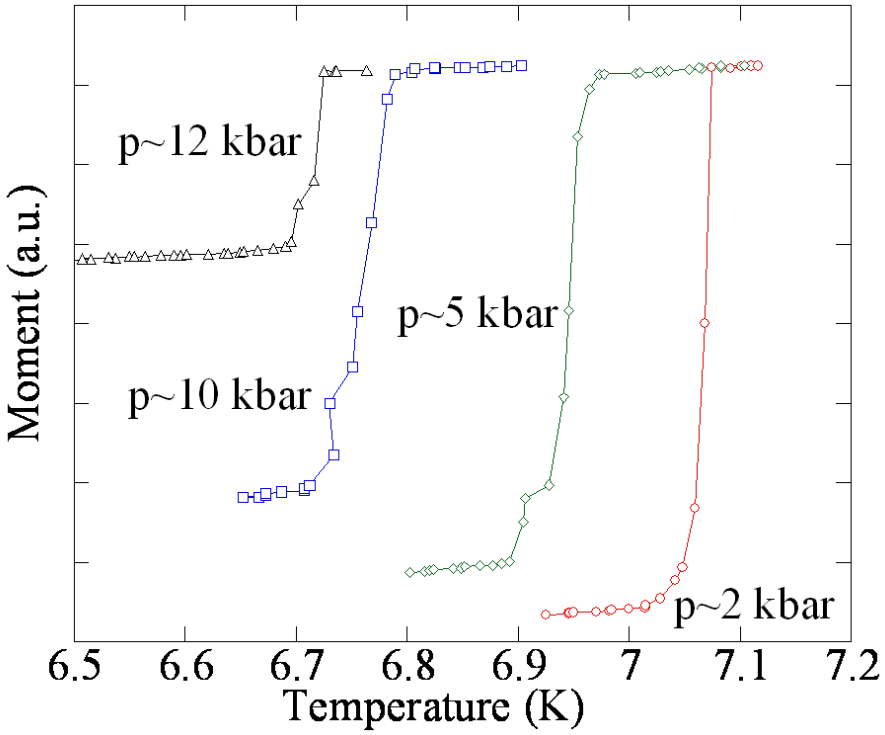

Figure 4.5: Typical lead superconducting transitions measured in a 20Oe field used to estimate the pressure in the cell.

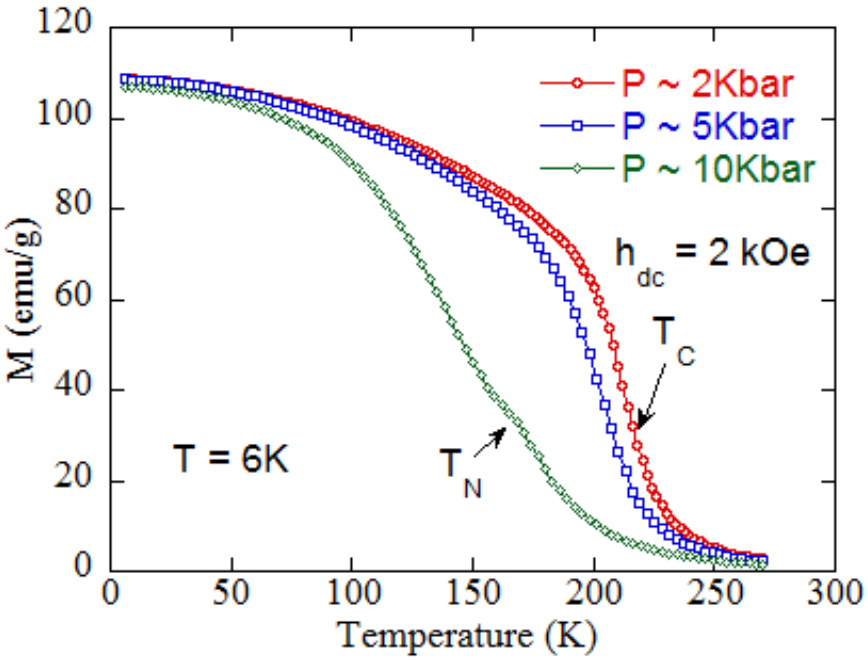

Figure 4.6: Temperature dependence of the magnetisation at H=2KOe under 2,5 and 10 Kbar in Fe_2P. The Curie and proposed Neél temperature are both seen.

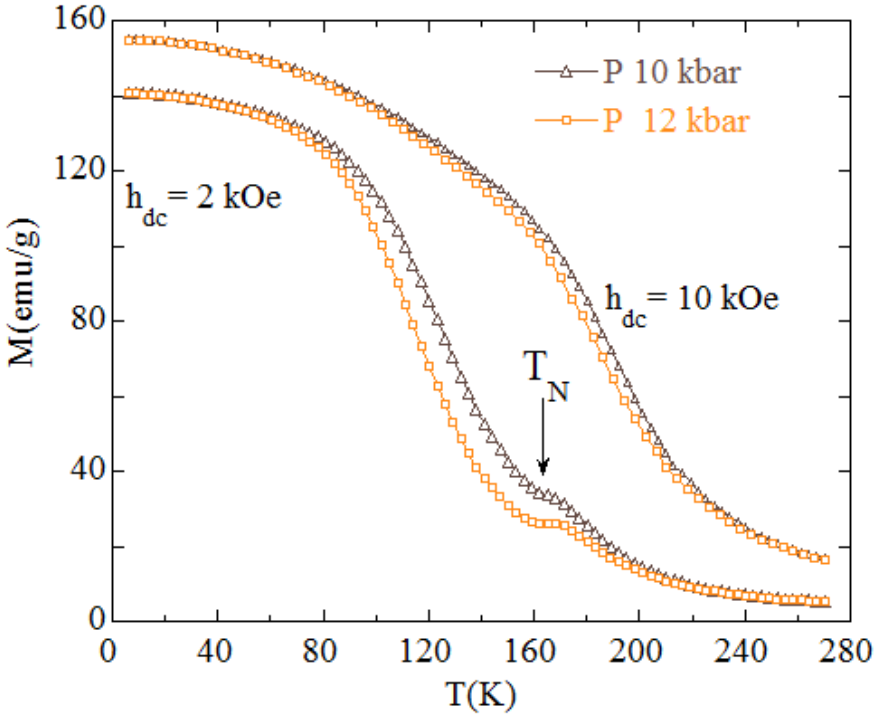

Figure 4.7: Temperature dependence of the magnetisation at H=2 and 10 KOe under 10 and 12 Kbar in Fe_2P. The proposed Neél temperature is seen more clearly as a peak in the susceptibility.

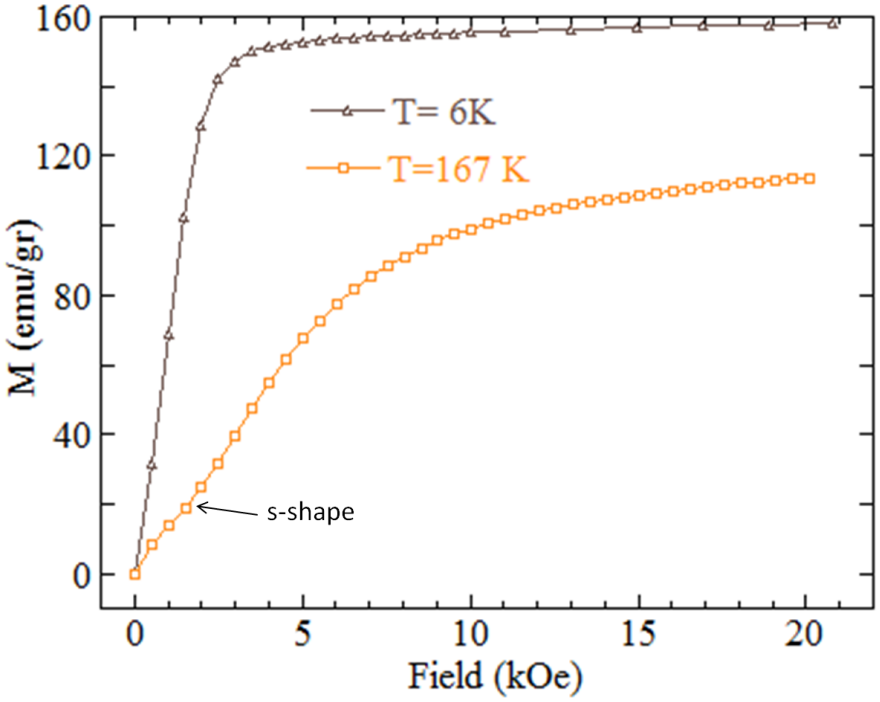

Figure 4.8: Isothermal magnetisation curves along the c-axis in Fe_2P under 12 Kbar. An s-shape, indicating a tendency towards a meta-magnetic transition, can be seen in the MvH data at 12kbar and 167K.

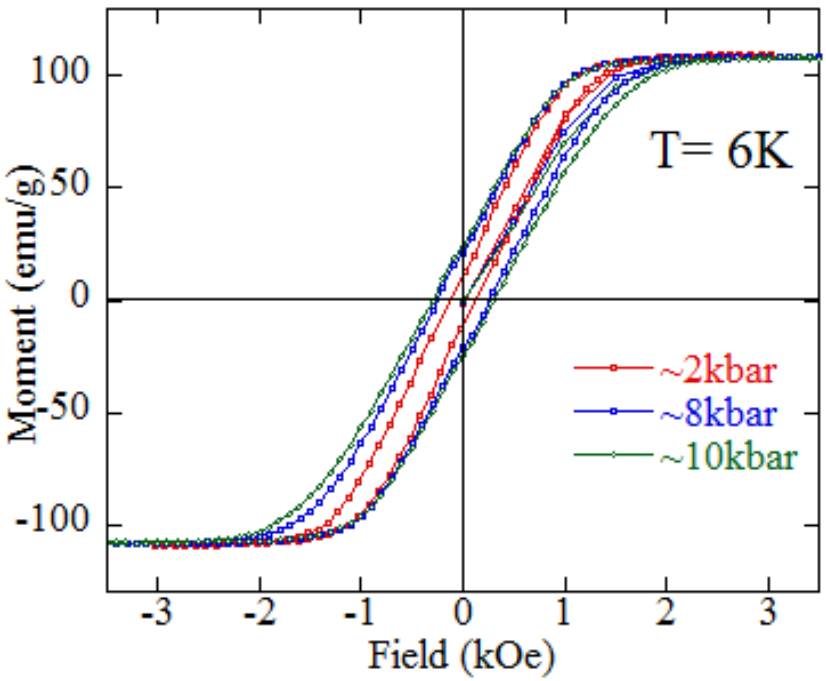

Figure 4.9: Hysteresis loops obtained for Fe_2P at 6K at selected pressures. The area of the hysteresis curves increases with pressure.

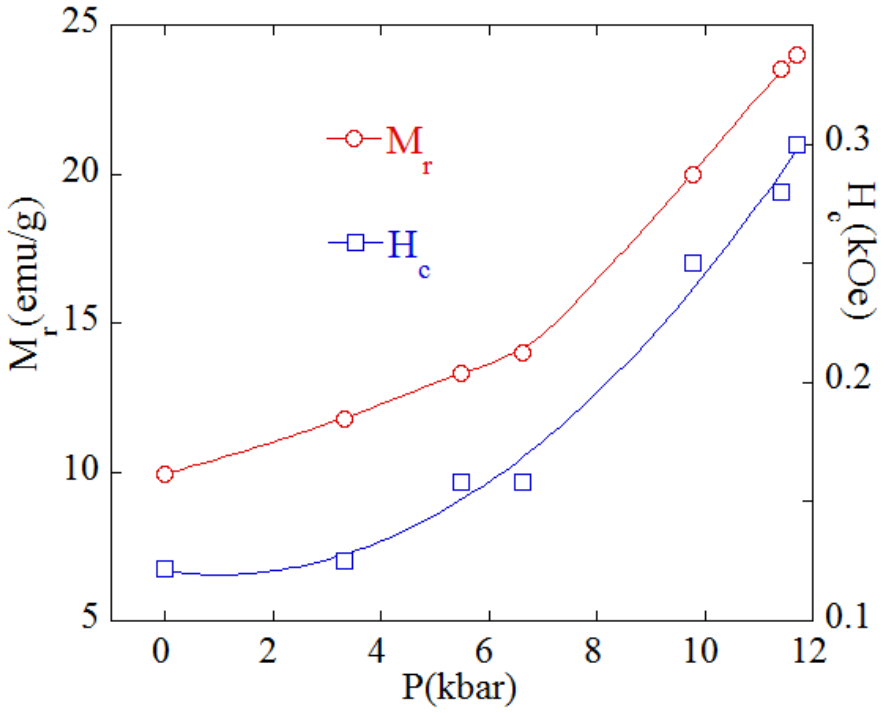

Figure 4.10: The coercive field, H_c, and remnant magnetisation, M_r, obtained at 6K, increase with pressure.

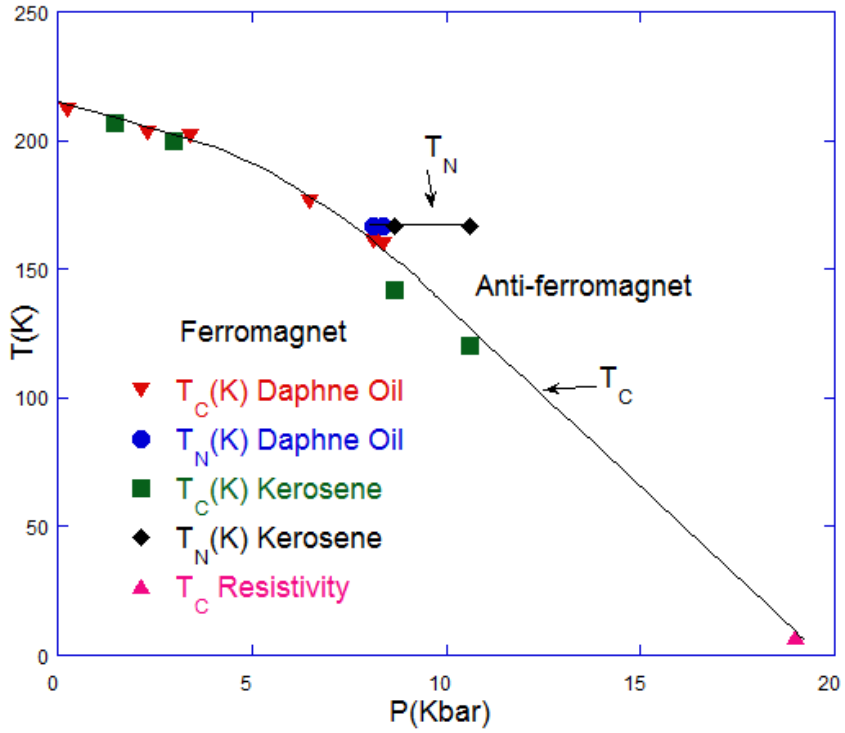

Figure 4.11: Phase diagram acquired using the labelled pressure medium. The lines are just a guide.

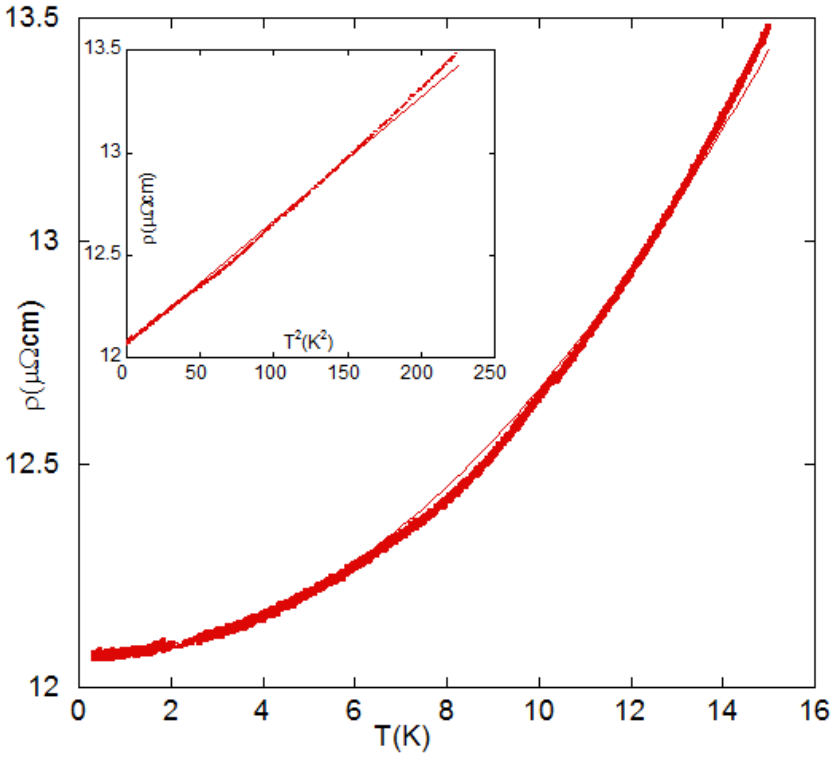

Figure 4.12: Resistivity of Fe_2P under atmospheric pressure. The red points are data. The black line is a quadratic fit: $\rho(T) = \rho_0 + bT^2$ where $\rho_0 = 12.063 \mu\Omega cm$ and $b = 6.06 \times 10^{-3} \mu\Omega cm K^{-2}$

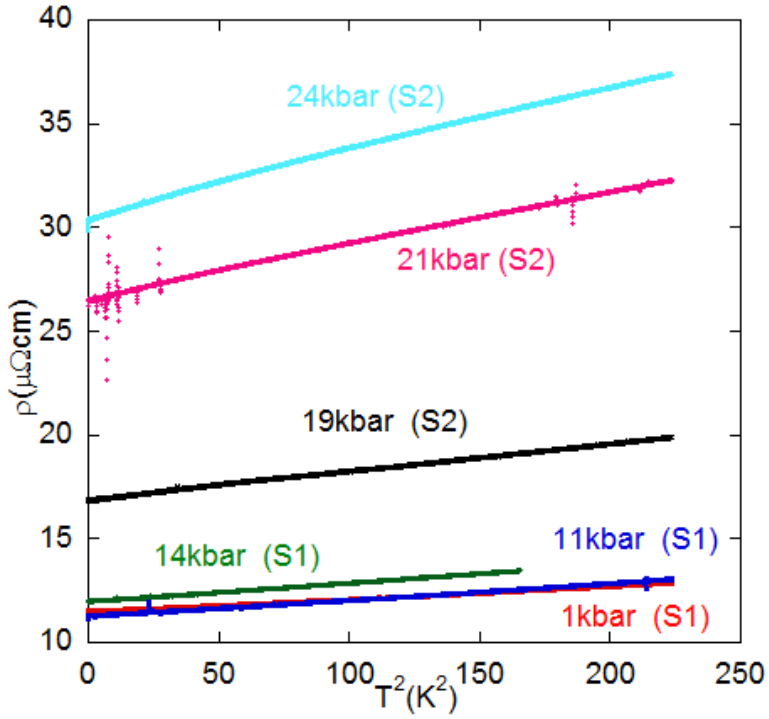

Figure 4.13: The resistivity of Fe_2P as a function of the temperature squared. The shape and offset of the curve starts to change significantly at approximately P=15kbar. S1 and S2 refer to two samples, cut from the same initial piece, in different cells.

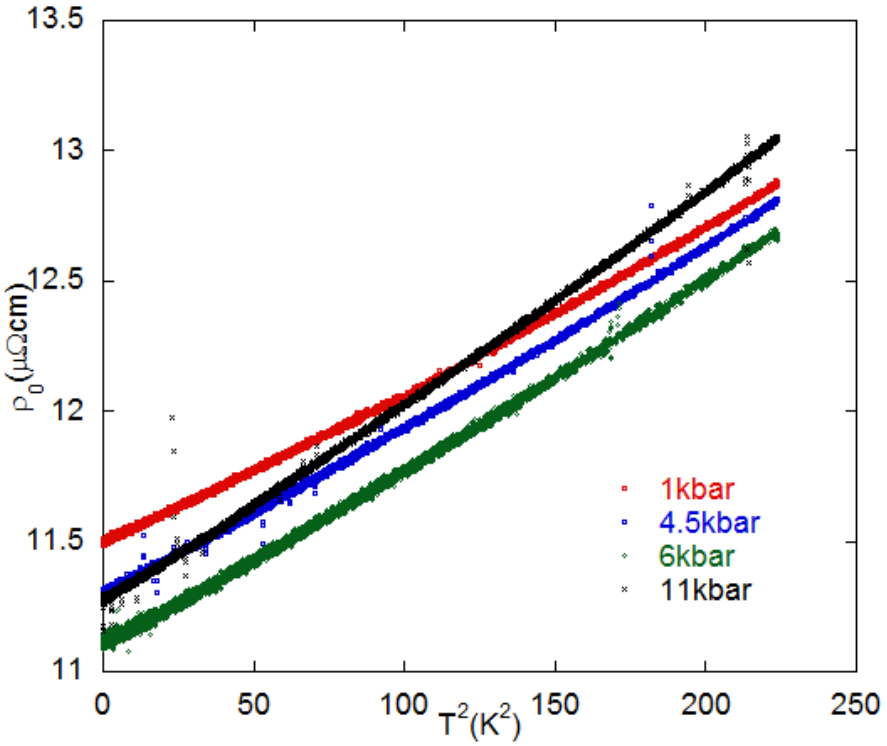

Figure 4.14: Measured resistivity of Fe_2P at several applied pressures below 15kbar plotted against T^2. At low pressures (<15kbar) the fermi-liquid prediction that $\rho \sim AT^2$ holds well at low temperatures. At temperatures above 12K the exponent increases.

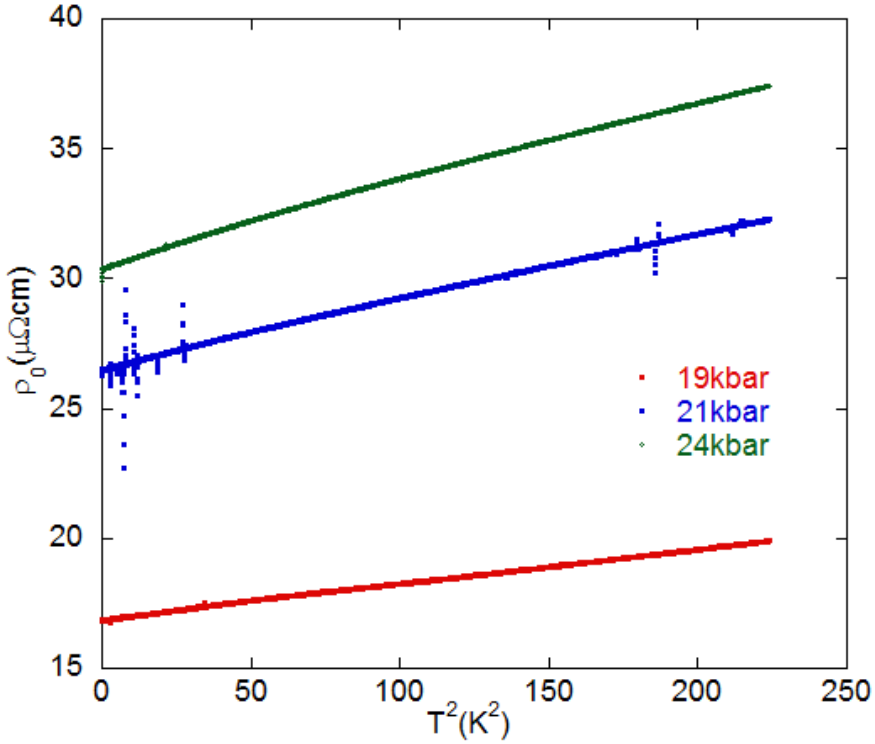

Figure 4.15: Measured resistivity of Fe_2P at several applied pressures above 15kbar plotted against T^2. At higher pressures ($> 15kbar$) the fermi-liquid prediction that $\rho \sim AT^2$ holds less well. It is clear that the exponent is significantly different from 2 over a large temperature range.

Some selected data is shown in more detail and plotted against various powers of temperature in order to see more clearly the evolution of the temperature dependence of the resistivity as pressure is increased, see Figs.4.16,4.17,4.18. What these figures show is that the exponent of the temperature that best describes the data changes as the pressure is increased through 19kbar. At 6kbar, the exponent appears to be above a little above 2. At 19kbar, the exponent is around 2 or slightly higher. Above 19kbar, the exponent is more like 1.8. The other obvious feature is that what looked like a deviation from the FL $\rho \sim T^2$ behaviour at 19kbar is actually due to a kink or shoulder in the data at approximately 7K. Due to the proximity, in terms of pressure and temperature, to the predictions made by other studies and, indeed, my own magnetic data, there is a strong possibility that this 'kink' is attributable to the ferromagnetic transition.

4.3 Discussion

By measuring the DC magnetisation as a function of temperature from 5K to 300K, see Figs. 4.7 and 4.6, at every pressure attained it is possible to observe the evolution of the magnetic transition temperatures (T_N and T_C) with pressure. With this information one can plot a phase diagram (see Fig. 4.11), and compare to previous results (see Fig. 4.3). My phase diagram matches up qualitatively with that plotted by Fujiwara in 1980. There is a difference quantitatively; higher pressures are required to induce the AFM state and to suppress the FM state, therefore the results obtained in this study agree more strongly with those of Chen et al.

It was not possible to achieve high enough pressures in the squid cell to follow the suppression of T_C all the way until it either terminated in an end point or reached 0K. The transition would be expected to be evident in the resistivity data, and a kink in the data has been observed previously (24). As the resistivity data was taken primarily at low temperatures (in the range 0-15K) and the T_C is expected to fall quickly with applied pressure, it is not surprising that this signal was only seen at one pressure. The data taken at 19kbar, when plotted against T^2, shows a very clear kink at a $T_C \sim 7K$, see Fig. 4.17. This is the lowest temperature that T_C has been observed. Given the rate of suppression of

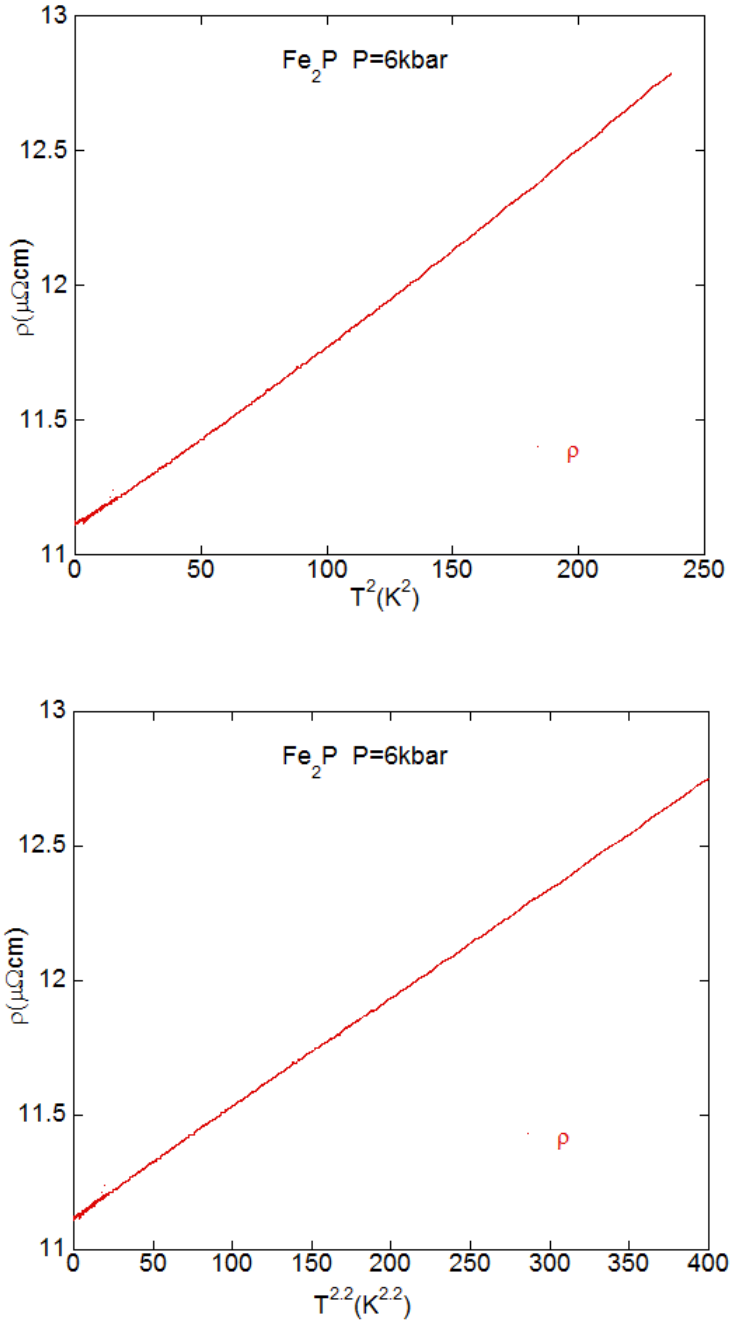

Figure 4.16: A bowing of the 6kbar data below a straight line when plotted against T^2 and above the line when plotted against $T^{2.2}$ show that the exponent is within these two values.

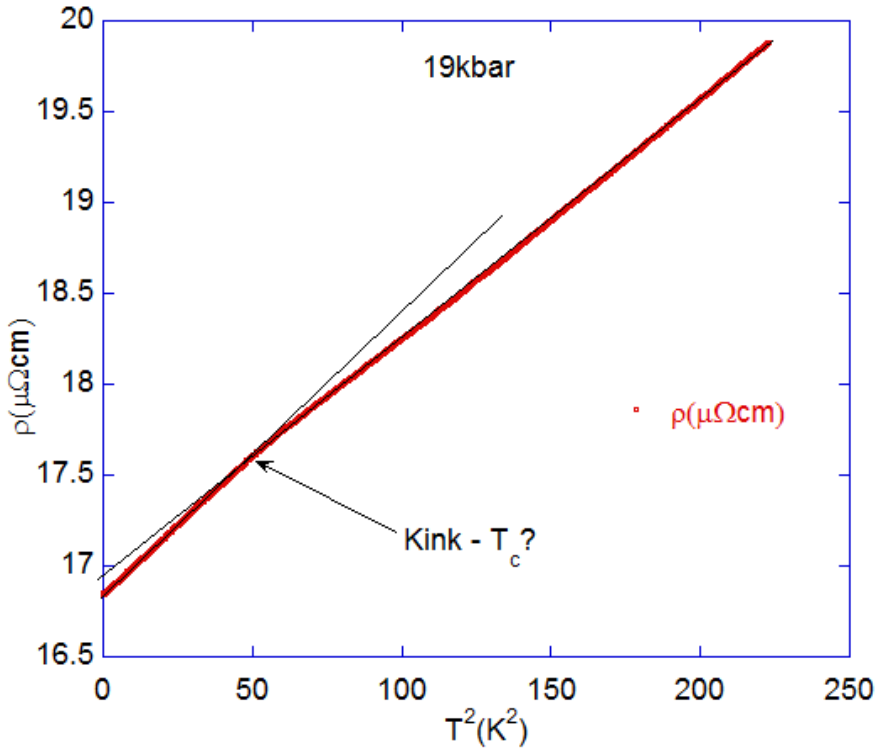

Figure 4.17: The 19kbar resistivity data follows a straight line above and below a change of gradient at T_C $7K$

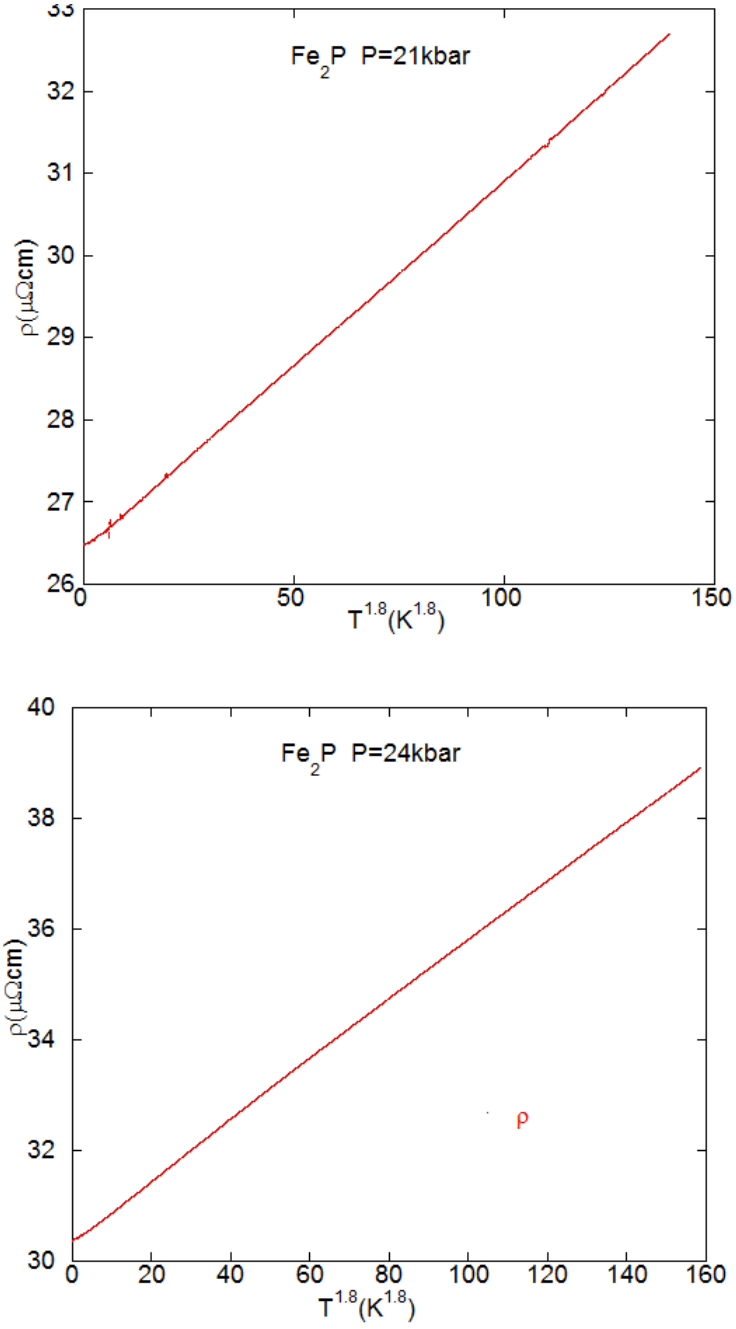

Figure 4.18: At 21kbar and 24kbar the resistivity is linear when plotted against $T^{1.8}$ rather than T^2

T_C, and the fact that no such kink is seen at 21kbar, a $P_C \sim 20kbar$ is proposed. This value is in reasonable agreement with previous estimates in the literature and fits well into the phase diagram drawn using the magnetic data acquired by the author.

The hysteresis curves shown in Fig. 4.9 were measured at 6K and the system was in its FM state. They do not behave as one would expect with the application of pressure. The FM state is suppressed by applied pressure, yet the hysteresis curves get larger. The remanence and coercive field both increase by a factor of ~ 3. It would therefore appear that the magnetic ground state here is not that of a simple FM. A Landau model similar to the one used in the discussion of Kadomatsu et. al.(35) has been used to recreate the phase diagram of the system. It does not, however, predict the behavior of the hysteresis. There is one obvious problem with the approach - it is only strictly valid in the case of a second order transition. Perhaps interestingly, the way to produce a system in which the hysteresis curve expands before presumably disappearing at the antiferromagnetic transition, is to manipulate the pressure dependence of the coefficients. The Landau model does not include any details of the microscopics of the magnetism involved. Therefore, there is no justification for this. It seems that it may be helpful to formulate a microscopic model of the system to be able to explain the observed behaviour. This would then also suggest the kind of fluctuations that might be expected at the quantum phase transition.

It is, however, possible to analyse resistivity data taken up to 25kbar for signs of the approach to a QPT. In the Fermi Liquid (FL) theory the resistivity is predicted to depend on the temperature squared:

$$\rho(T) = \rho_0 + AT^2 \tag{4.1}$$

ρ_0 is the resistivity due to the impurity scattering in the sample. A is related to the scattering cross-section of the quasi-particles. The power of 2 is specific to FL theory. Deviations from this value of the exponent are good indicators that there are important interactions not accounted for in the FL picture. Increases in A and ρ_0 are also associated with the introduction of new scattering processes.

The ambient pressure resistivity shown in Fig.4.12 demonstrates that with no applied pressure this system is well described by the FL theory. As can be seen in Figs. 4.14 and 4.15, the resistivity as a function of temperature only gradually changes with pressure up to 15kbar. The difference between the form of the resistivity under 15kbar and 19kbar is quite large. To give an accurate quantitative representation of these changes the resistivity data was analysed for deviations from FL predictions. The data is plotted against T^x where x is raised by 0.01 from 1 to 3. The quality of a straight line fit is then calculated using a least-squares method. The best straight line gives the best fit value of x. Using this and again the least squares method, the A-coefficient and residual resistivity can be calculated along with the statistical error. The error in the exponent, x, was estimated by comparing the least squares fit of the line with the two coefficients modified to be on the edge of a 95% confidence interval with that of the next value of x with best fit parameters. For all three parameters the statistical error was found to be negligible when the fitting was performed over a temperature range of 5K or more. These values are plotted in Figs.4.19 and 4.20. In all 3 cases it is clear that there is a sharp change around 19kbar. This we attribute to the presence of spin fluctuations leading to extra scattering. As mentioned in the introduction, the A-coefficient is proportional to the scattering cross-section of the quasi-particles. Therefore, its increase by a factor of 15 leads to the conclusion that some extra scattering mechanism has become important.

The similar increase in ρ_0 must also be attributed to the fluctuations. The residual resistivity is a measure of the impurity scattering in the system as it is independent of temperature. However, the number of physical impurities is not changing. An explanation is that the fluctuations in the magnetisation are frozen into the system at low temperatures, effectively creating new impurities. The effect is greater the closer to the QCP the system is driven.

The term quantum critical point refers to a transition second order with the tuning field being suppressed to absolute zero. It is, however, conceivable for a transition to be or become first order as it is suppressed. In this case one may see a critical end point. If this were to be located at a very low temperature, it would be reasonable to consider a quantum critical end point. It is possible to fit the data for the exponent and coefficients over varying temperature ranges, therefore,

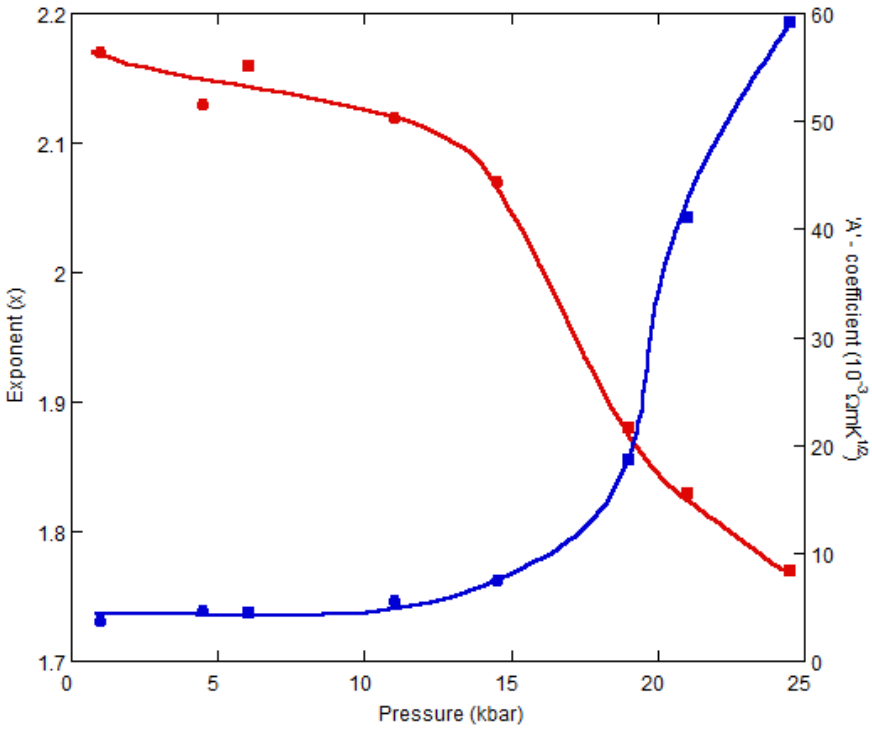

Figure 4.19: When fitted over the temperature range T=0-15K it is clear that the exponent (red) drops below 2 at pressures above 15kbar. The enhancement in the 'A-coefficient' (blue) of around a factor of 15 bears a strong resemblance to that seen in the heavy-fermion systems as they approach a QCP.

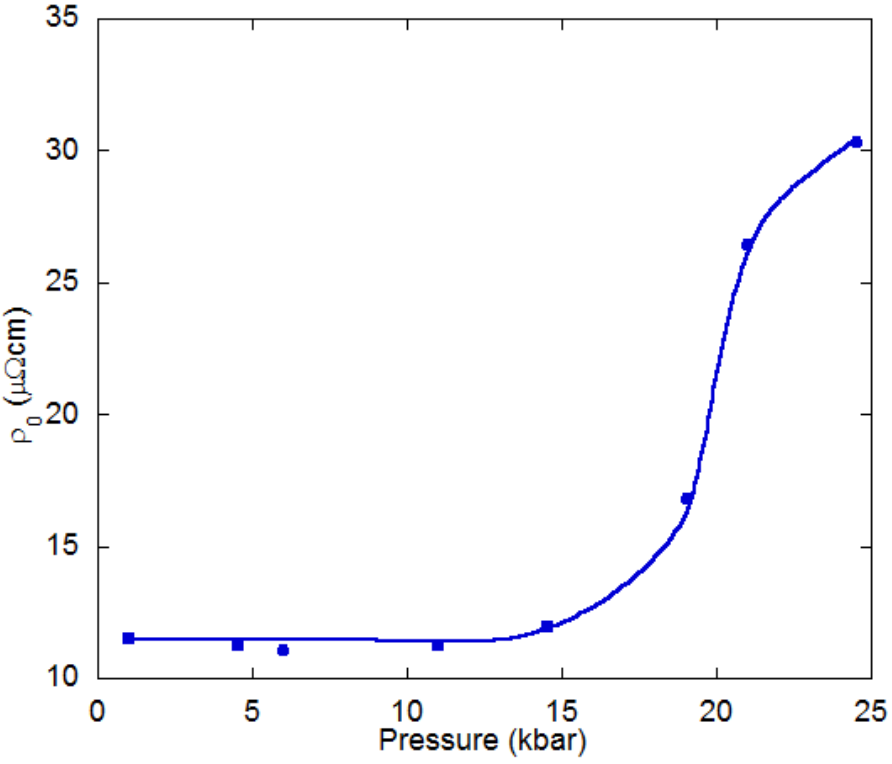

Figure 4.20: The value of ρ_0 increases sharply at around 19kbar.

hoping to see the boundaries in temperature of any effects due to quantum critical fluctuations.

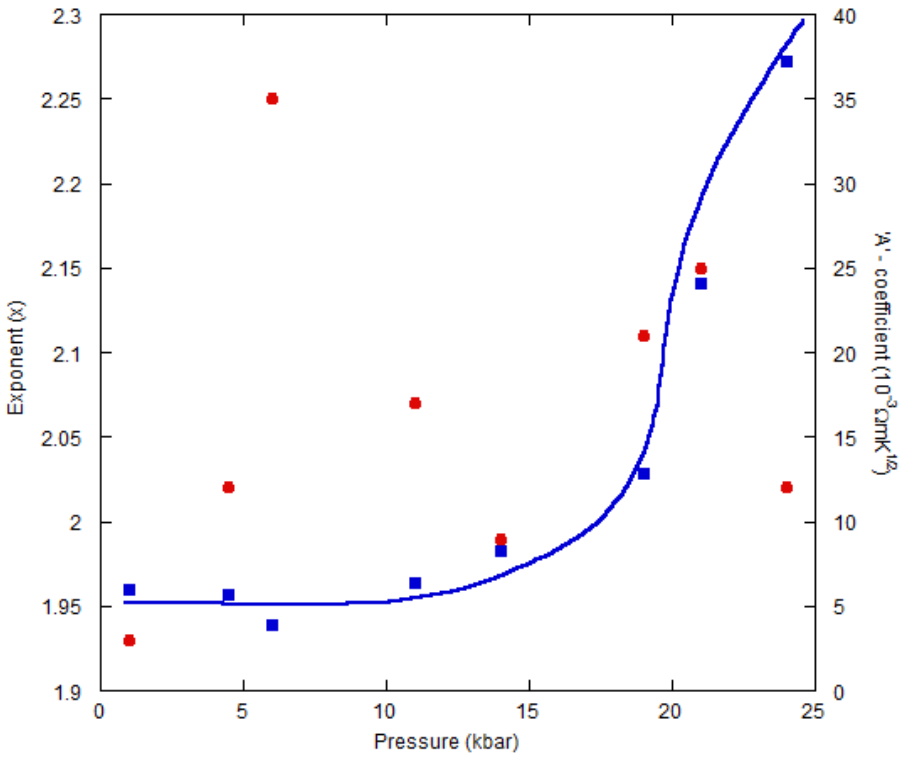

Figure 4.21: At the lowest temperatures, 0-5K, the fitting exponents (red) are dominated by the residual resistivity. The Enhancement in the 'A-coefficient' (blue) is clearly visible.

There are two very noticeable things to be seen in these plots (Figs.4.214.224.23). There appears to be little pressure sensitivity in the exponent at temperatures below 5K. The residual resistivity is dominant here, although the 'A-coefficient' does show the same order of enhancement as over the full temperature range (0-15K). When the data is analysed in the range 5-10K, the most significant deviations from 2 are seen in the exponents at every pressure. At 19kbar there is a very strong deviation: x=1.5, corresponding to the suppressed transition temperature. In the range 10-15K the same general features are observed as over the full range and at 5-10K. This shows that the pressure-induced changes are stable over a reasonable temperature range, and not just the result of some artifact.

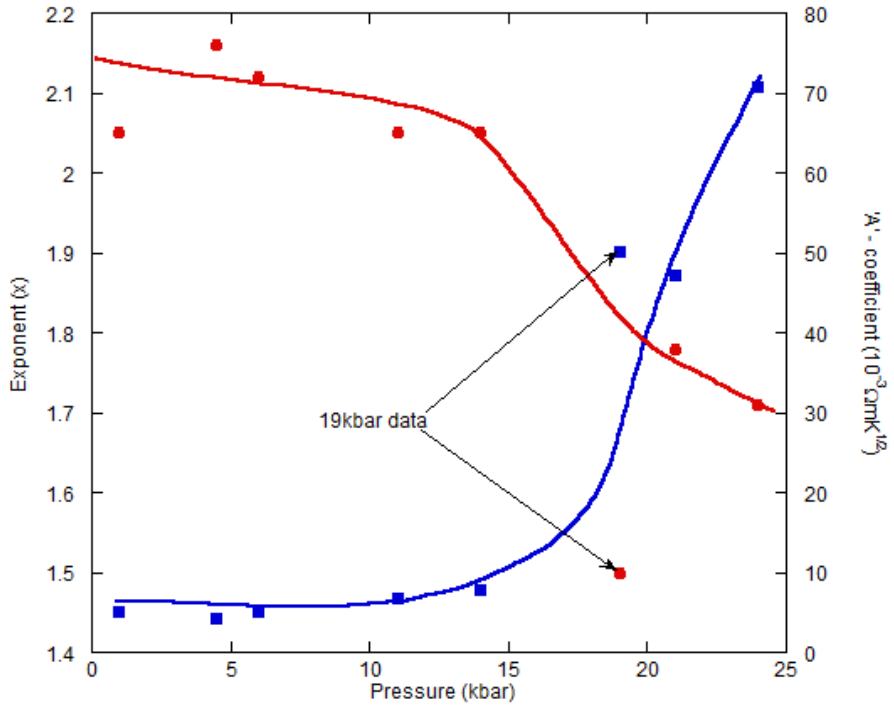

Figure 4.22: Possibly the most reliable evolution of the resistivity exponent (red) and 'A-coefficient' (blue) is in the temperature range 5-10K.This is above the influence of the impurity scattering but below any thermal fluctuations. The value of 1.5 for the exponent at 19kbar is an effect of the kink at about 7K.

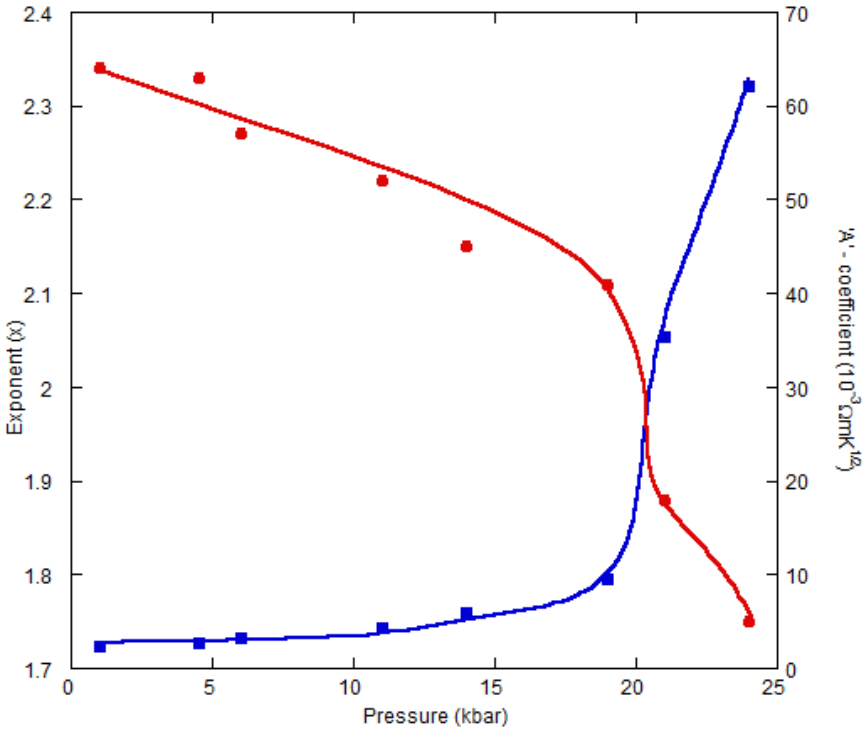

Figure 4.23: The pressure dependence of resistivity exponent (red) and 'A-coefficient' (blue) in the temperature range in which thermal fluctuations begin to play an important part in the transport properties, 10-15K. However, the data is still dominated by the electron-electron and electron-magnon interactions.

In order to check the results arrived at by the least squares analysis described above it is desirable to analyse the data in other ways as well. Firstly, the data can be plotted against T^x. This has been done and provides an important visual check that the exponents given are representative of the system over a range of temperature, as it is entirely possible that x should be a smoothly varying function of T and that the analysis done has little meaning. It is clear that this is not the case though. This method also allows one to check that the results are not being effected by physics that is not being taken into account, for example the phase transition seen in the 19kbar data.

The next method of analysis relies on taking natural logs in order that the data may be plotted as a straight line.

$$\rho(T) = \rho_0 + AT^x \tag{4.2}$$

$$\ln(\rho(T) - \rho_0) = \ln(A) + x\ln(T) \tag{4.3}$$

By plotting the data on a log-log scale it is possible to extract the exponent as the gradient of the line. Furthermore, this gives the exponent as a function of temperature, providing another way of checking the assertion that the exponent is really representative.

Figs.4.24 4.25 4.26 show that the logarithmically determined exponents as a function of temperature are in agreement with previous conclusions. Below 19kbar the exponent is stable at a value somewhat above 2. At 19kbar there are two distinct regions of T^2 behaviour with a transition in between. Above 19kbar the exponent is stable over a temperature range of about 10K at a value somewhat below 2.

4.4 Conclusions

We have found strong evidence for the pressure induced onset, at 15-19kbar, of a quantum critical regime, see Fig.4.27. The transition was observed at 7K under a pressure of 19kbar. Whilst it was not possible to reach high enough pressures to be sure how far this region extends, the enhancement of the residual resistivity

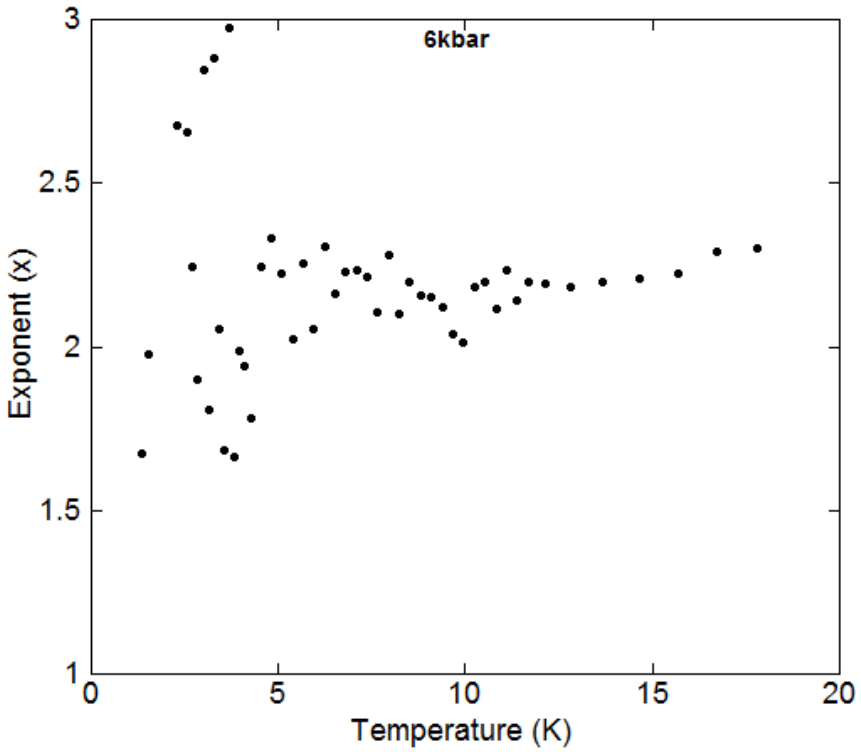

Figure 4.24: The exponent settles out at roughly 2 as expected for a Fermi liquid.

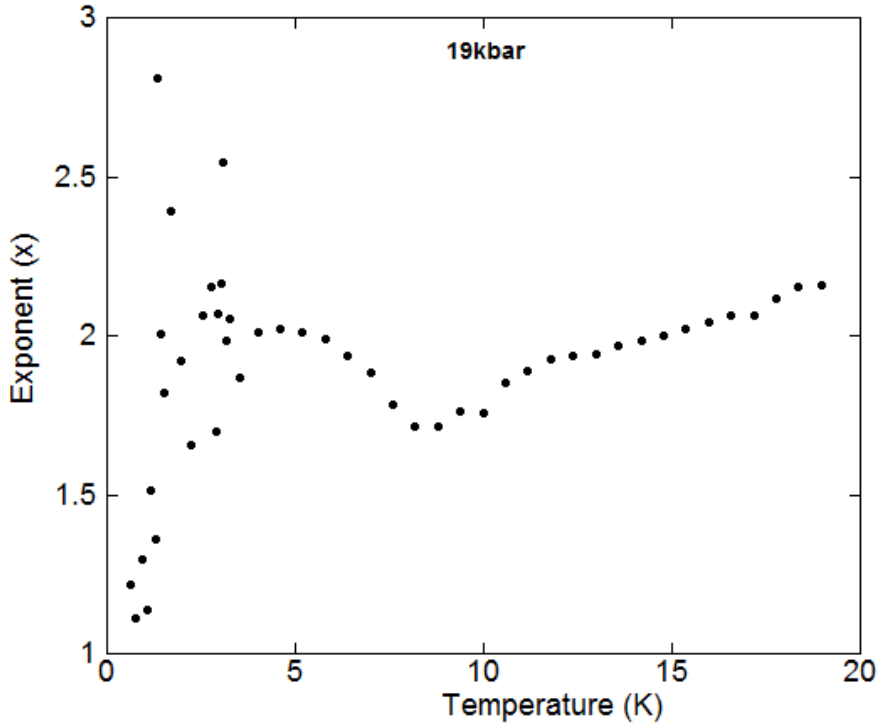

Figure 4.25: The exponent is roughly 2 either side of a dip coinciding with the proposed transition.

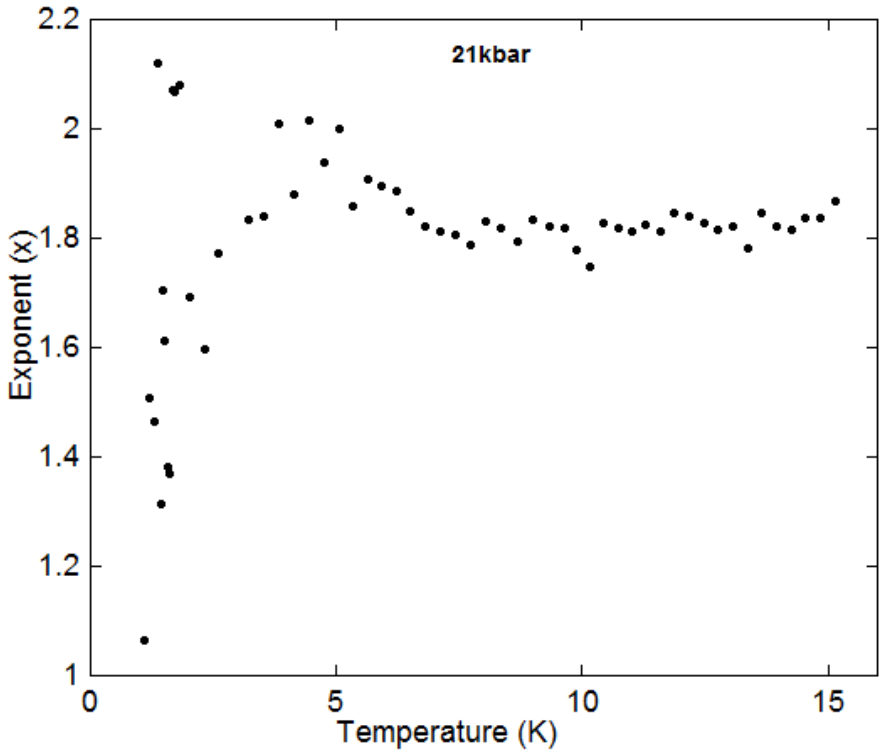

Figure 4.26: The exponent is stable over a large temperature range at a value significantly below 2. The exponent is roughly 1.8.

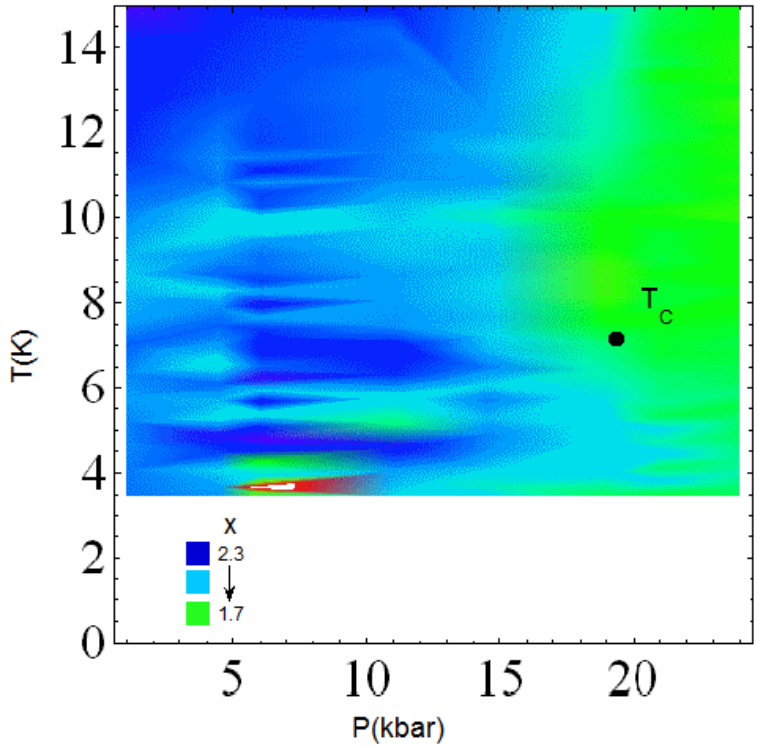

Figure 4.27: The exponent is seen to undergo a transition coincident with the proposed curie temperature. The system shows two distinct phases in pressure-temperature space. This kind of evolution is evocative of a QPT.

and A-coefficient and the lowering of the exponent appeared to be tailing off by 25kbar.

The as yet unexplained behaviour of the hysteresis under pressure may offer clues as to the exact nature of the magnetic ground state and of the nature of the quantum phase transition.

5

CeGe

5.1 Introduction

The binary alloy, CeGe, has not received a great deal of attention. It was characterised as a simple antiferromagnet by Buschow in 1966 (39). The reported Néel temperature was around 10K and the system was found to follow closely the Curie-Weiss law yielding a moment close to that of the free ion, $2.14\mu_B$. CeGe crystallises in the FeB-type structure, which is of the space group Pnma.

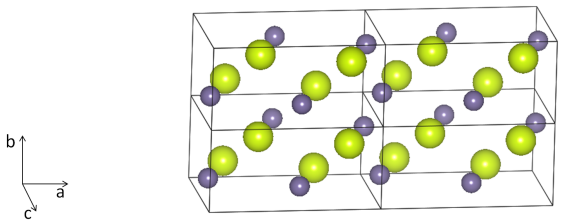

Figure 5.1: The structure is viewed down the c-axis. Green spheres are cerium and purple are germanium.

More recent studies have suggested that there is more to this material (40).

In two publications (40)(41) N. Marcano et. al. present results from a number of experiments: magnetisation up to 90kOe, DC-susceptibility, specific heat, muon spin relaxation and resistivity in an applied field. The data as a whole points to a system with an exotic low temperature magnetically ordered state. Perhaps the most obvious signature is seen in the resistivity which shows an upturn at T_N as the temperature is reduced. There is then a peak approximately 2K lower. This peak is suppressed by the application of magnetic fields in excess of 7T, although a kink is still visible up to 9T. This is reminiscent of a number of the elemental rare earths (42) and uranium compounds (43), in which the upturn is attributed to the formation of magnetic super zone gaps. In many of these materials the crystal is hexagonal and the magnetic order takes on a variety of configurations, many of which are of a lower symmetry than the crystal. These give rise to Fermi surface deforming extra zone boundaries within the first Brillouin zone. There is no evidence for a similar symmetry mismatch in CeGe.

The DC-susceptibility data shows the expected peak at $\sim$10.5K but at temperatures below this there is a wide discrepancy between the field cooled (FC) and zero field cooled (ZFC) data. This is evident in a wide range of applied fields and indicates the existence of a small ferromagnetic component. Isothermal magnetisation measurements up to 9T show what appears to be a metamagnetic transition below 8.3K, although it is widely extended in field and saturation is not obtained even up to 9T. This implies a strong magnetic anisotropy. This is another similarity of CeGe with the rare earths with super zones. The sample studied was polycrystalline. An aligned single crystal may well show a much sharper transition with applied field. The muon spin relaxation spectra were analysed and revealed 3 distinct precession frequencies and therefore 3 distinct magnetic environments for the Ce moments. This is strong evidence that the magnetic ordering is more complex than previously reported (44).

Magnetic contributions to the specific heat and entropy show a lambda peak and kink respectively at the Néel temperature. Estimates of the Kondo temperature from these data are $T_K \sim 8.1$K and 7.1K. The jump in specific heat due to the magnetic ordering can be used to estimate the magnetic moment and yields a value of $1.1\mu_B$ in agreement with neutron data (44). Compared to the free ion value for Ce^3+ of $2.14\mu_B$ this also suggests a very substantial Kondo effect.

5.2 Sample Preparation

The measurements presented in the following section were carried out on the same polycrystalline CeGe samples used in the work by Marcano et. al. discussed earlier. Stoichiometric quantities of pure cerium and germanium were melted together in an arc furnace with provision made for the loss of the more volatile germanium. Flipping and remelting the CeGe ensures good homogeneity. More details of the sample preparation and results of X-ray diffraction can be found in Ref. (40).

5.3 Results

The application of hydrostatic pressure should affect the strength of the RKKY interaction by modifying the interatomic distances. The balance between the magnetically ordered state and the Kondo lattice will be shifted. The comparison between the effect of hydrostatic pressure and applied magnetic field will provide information on the nature of the relevant physics.

It is clear from Fig. 5.2 that applied pressure and field are not equivalent as tuning parameters. Although both reduce the peak height due to the magnetic super zones, the behaviour of the resistivity is quite different in each case. The application of field reduces the resistivity everywhere below T_N and has the most effect on the peak itself. The application of pressure increases the resistivity over a wide range of temperatures and has the largest effect at T_N thereby appearing to suppress the peak.

Fig. 5.3 shows that whilst applied field suppresses the peak associated with the magnetic super zones and also suppresses the Néel temperature, the application of pressure actually slightly enhances T_N as well as reducing the height of the peak. The enhancement is small, at $\sim$20mK.Kbar^{-1}. T_N is taken to be the point at which the gradient of $\rho(T)$ becomes negative as the temperature is reduced.

The low temperature resistivity with applied field and pressure are shown in Fig. 5.4 with ρ_0 subtracted, and it is clear that the pressure increases the curvature whereas the applied field reduces it to the point where it is very nearly linear.

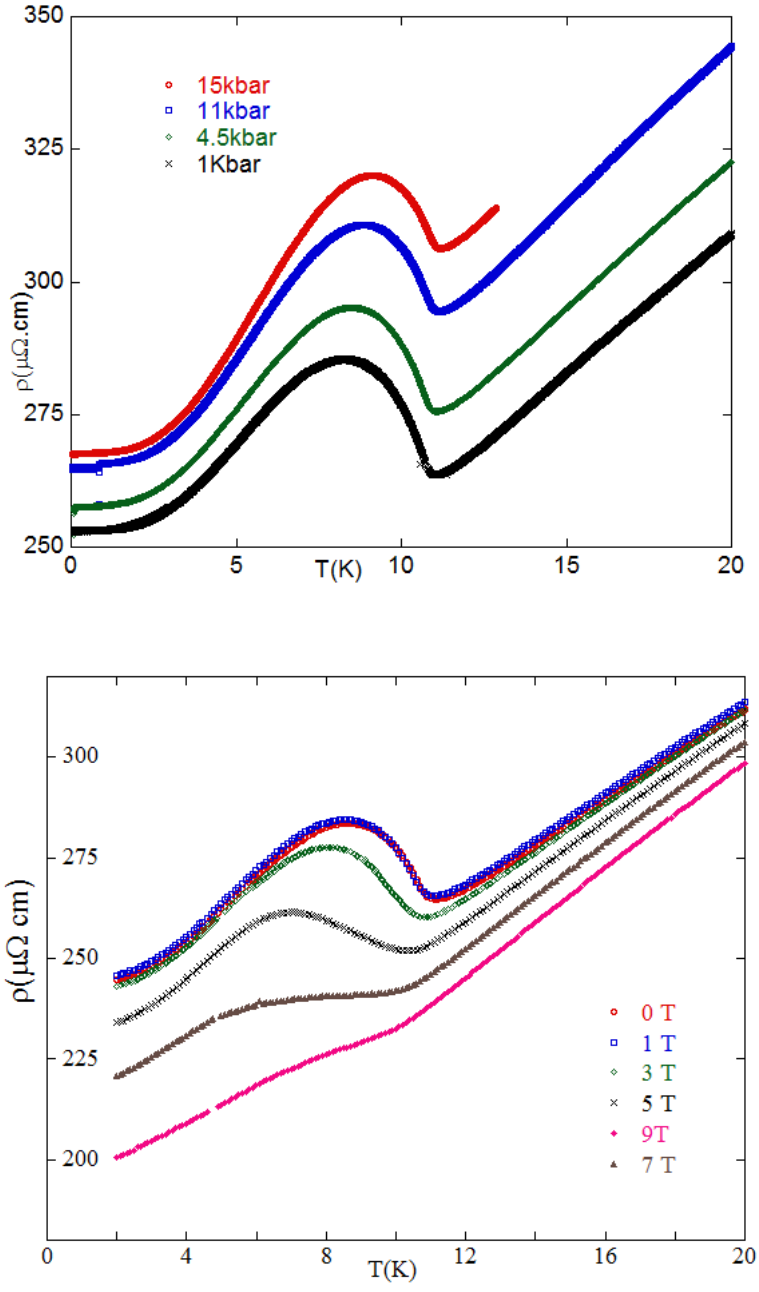

Figure 5.2: The application of pressure (top) can be seen to affect the resistivity in a number of ways: the residual resistivity is raised, the peak height above the curve is suppressed, and the Néel temperature is slightly enhanced. The effect of field is different (from (40)). The peak is suppressed and the residual resistivity is reduced.

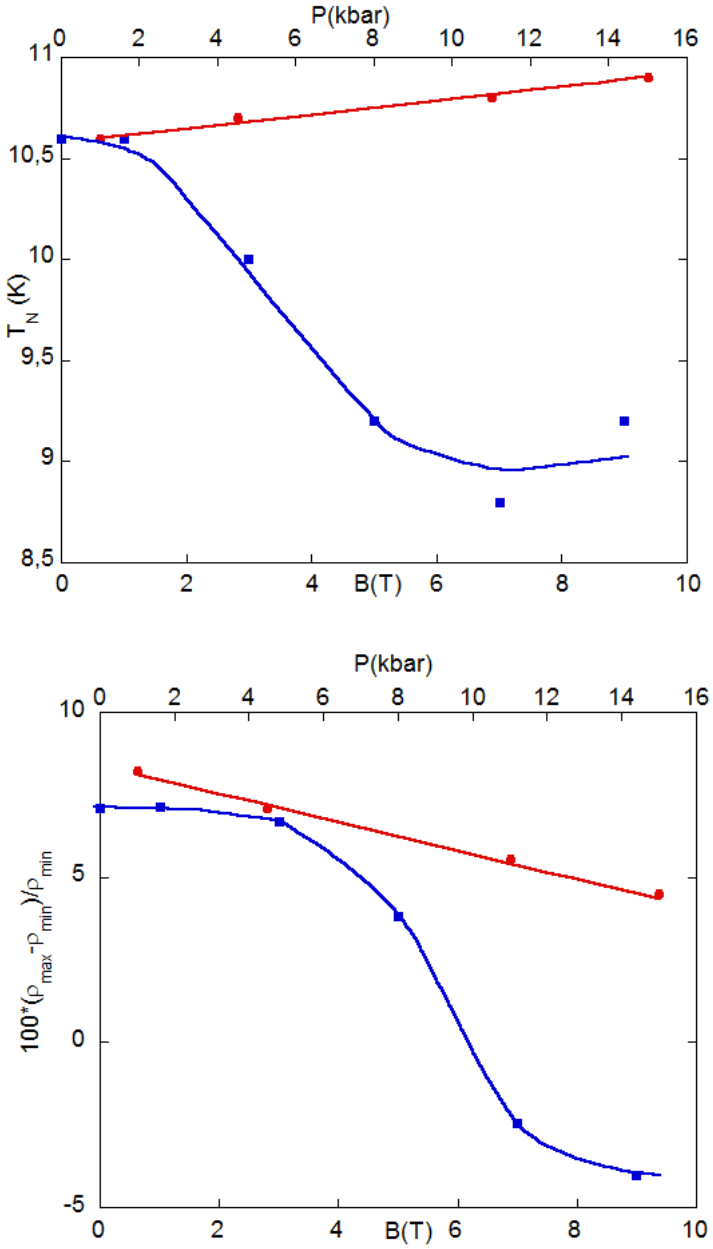

Figure 5.3: The effects of applied field and pressure on the Néel temperature (top) and peak height (bottom). In both plots the red circles correspond to the pressure axis and the blue squares to the applied field.

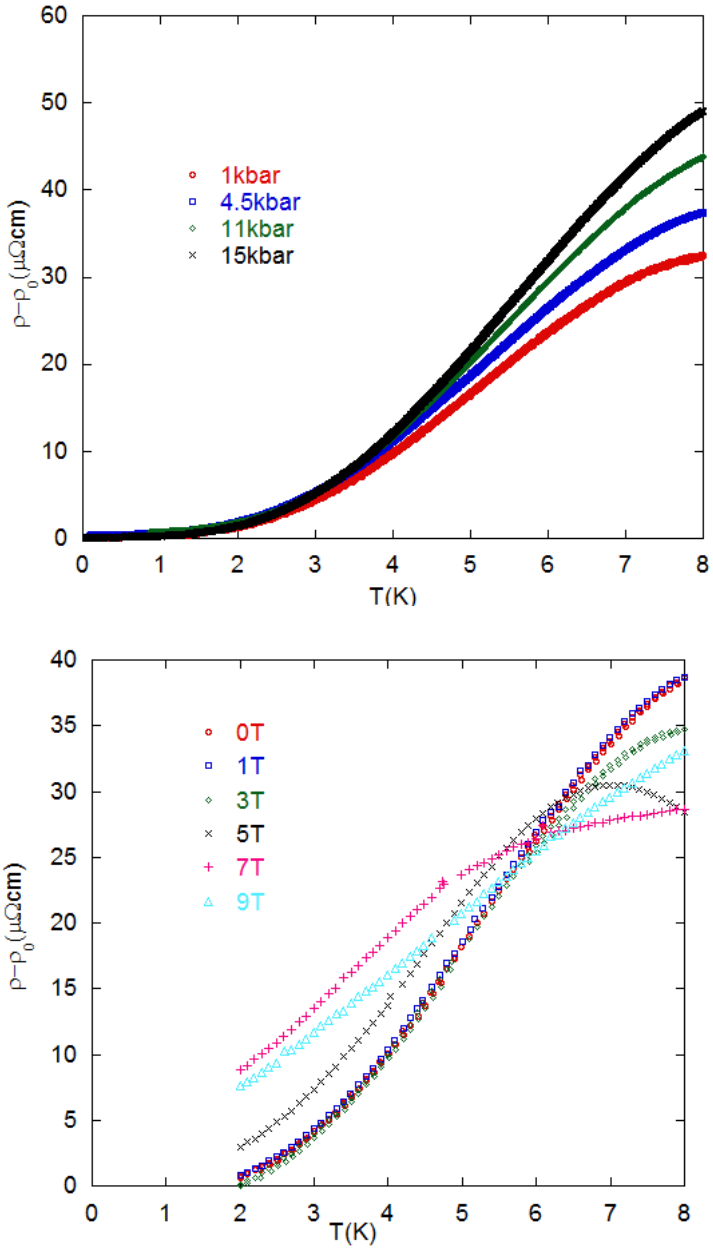

Figure 5.4: By subtracting the residual resistivity it is easier to see that whilst the application of pressure increases the curvature, applied field changes the behaviour of the resistivity more drastically.

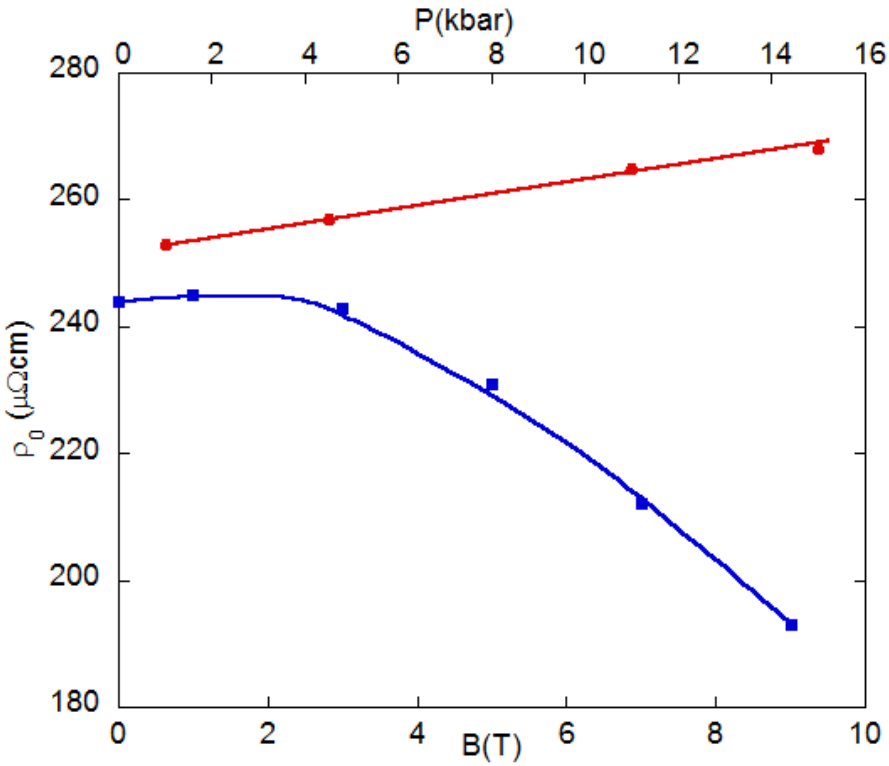

Figure 5.5: Effect of pressure and field on ρ_0. The red circles correspond to the pressure axis and the blue squares to the applied field.

The residual resistivity is enhanced by the application of pressure and reduced with the applcation of magnetic field (Fig.5.5).

5.4 Discussion

The resistivity of a metal is determined by the number of available charge carriers and the total scattering rate of the carriers. The overall scattering rate is a sum of the scattering rates associated with a number of different processes that will in general have different dependencies on temperature, pressure, applied magnetic field, etc.

$$\rho(T) \sim \frac{\tau^{-1}}{n} \tag{5.1}$$

$$\frac{1}{\tau_{Tot}} = \frac{1}{\tau_{Imp}} + \frac{1}{\tau_{ep}} + \frac{1}{\tau_{em}} + \frac{1}{\tau_{Kon}} \tag{5.2}$$

The first of the above scattering rates, τ_{Imp}, is that attributed to impurities and crystal imperfections. This rate is assumed to be a constant in temperature. The extrapolated ρ_0 value is entirely due to this scattering mechanism as all other scattering mechanisms will eventually vanish at absolute zero. The second term, τ_{ep}, represents the scattering rate associated with electron-phonon interaction. This is the transfer of momentum to the crystal lattice by the absorption and creation of phonons by the conduction electrons. Within this there are two distinct processes: normal scattering where an electron is scattered a small angle from one part of the Fermi surface to another, and Umklapp scattering, when an electron is scattered across the Brillouin zone boundary to a state equivalent to that on the other side of the Fermi surface from where it started. Therefore, Umklapp processes are large angle scattering events that make a large contribution to the resistivity.

τ_{em} is the scattering of conduction electrons with the absorption and emission of magnetic excitations. Again these scattering events can be normal or Umklapp

processes.

Finally, τ_{Kon} gives the rate of scattering from the partially screened local moments. These local moments are antiferromagnetically coupled to the electron cloud surrounding them and screening the moment by a substantial fraction. This screening gets more complete as the temperature is lowered, leading to resistivity that increases with lowering temperature. Neutron diffraction and specific heat studies have confirmed that the Kondo effect is non-negligible in CeGe. The observed moment is half that of the free cerium ion, suggesting that the moment has been substantially screened by the conduction electrons. The Kondo Lattice (KL) model as presented by Coqblin et. al. in ref. (45) suggests that the KL state must be in competition with long range magnetic order (LRO) but may coexist with short range order (SRO).

This fine balance of energy scales is one of the fundamental reasons for the interest in the heavy fermion systems. It would be expected that in this situation some relatively small change in any tuning parameter could lead to large changes in the systems properties. Indeed, the application of field does appear to affect a large change in the resistivity of the system. It is possible, in a very simple way, to compare the energy introduced into the system via an increase in temperature, magnetic field and hydrostatic pressure. In useful units, and very approximately, the thermal energy is given by Boltzmann's constant: $k_B \sim 9 \times 10^{-5} eVK^{-1}$. This compares with the Bohr magneton: $\mu_B \sim 6 \times 10^{-5} eVT^{-1}$. The energy equivalent of applied pressure is slightly less trivial to estimate, however, the work done on a test cube with realistic modulus of compression gives the energy as $\sim 9 \times 10^{-5} eVkbar^{-1}$. The fact that the effect of pressure is markedly less than that of field suggests, therefore, that this approximation is lacking. This is not surprising as this very simple comparison neglects any effects arising from the strongly correlated electrons in the system. A more telling comparison would require a calculation of the lattice spacing dependence of the exchange interaction. Neutron scattering may well be able to reveal this relationship and shed light on the seeming stability of the magnetic state under pressure.

The discussion of the effect of pressure on the resistivity and what this can tell us about the balance of the energy scales in the system falls naturally into two parts: namely above and below the magnetic ordering temperature, T_N. Above

this temperature the system has a unit cell and therefore Brillouin zone that corresponds to the primitive unit cell of the crystal. Once the system orders antiferromagnetically, the real space unit cell is doubled, and the Fermi Surface is reduced and its shape changed.

5.4.1 $T > T_N$

To understand the effect of pressure on the resistivity of CeGe it is necessary to consider how the applied pressure changes the magnetic interactions in the system. There are two mechanisms to consider: the Kondo screening and the RKKY interaction. The competition between these two energy scales is usually discussed in the terms of the Doniach phase diagram (see Fig. 2.2), where J is the magnetic exchange between the localised f-electrons and the conduction electrons. In cerium based compounds the pressure effectively squeezes the one f-electron out of the localised f-orbital and into the conduction band, reducing the contribution that can be made to the local moment to zero eventually. In the intermediate regime, the application of pressure is serving to increase the hybridisation between the f-electrons and the charge carriers. This enhances the strength of the Kondo scattering interaction leading to an increased resistivity. This can also provide an explanation for the rising Néel temperature; the enhanced scattering is increasing the entropy of the system making it more favourable for the magnetic ordering to which the system is already prone. It would therefore be reasonable to look for an enhanced magnetic susceptibility. However, this is not observed. The effect of the depletion of the f-orbital may well be dominant.

The ratio of $\frac{T_K}{T_N} \sim 0.75$ means that we can place CeGe, under atmospheric pressure, on the Doniach phase diagram somewhere near the apex of T_N. This may well explain why T_N is relatively insensitive to applied pressure and actually increases slightly. This does not mean that the applied pressure is having no effect on the system in general - it just so happens that the effects on the Néel temperature are cancelled out for the most part in this pressure range. There are many cerium based heavy fermion compounds that have been studied under pressure. It is reasonably common for the Néel temperature to start at around 10K and increase slightly with applied pressure before being suppressed strongly.

One of the possible indicators of how close to the tipping point at which the Kondo lattice suppresses the antiferromagnetism is the electronic specific heat factor γ. In general those materials on the left of the Doniach diagram display low values of γ; in other words, the heavy fermions are quite light and the Kondo effect is negligible. Usually, the materials with a very large γ do not order magnetically and are dominated by the Kondo interaction. In CeGe, specific heat measurements have shown $\gamma \sim 260 mJK^2mol$. This is somewhere in the middle of the range that has been observed. Work on $CeSi_{1-x}Ge_x$ (44) has shown that the introduction of the larger germanium atom into the lattice leads to a volume expansion of the unit cell that is smaller than the extra volume taken up by the germanium, leading to an effective increase of pressure. As x is increased the Néel temperature is increased from $\sim 6K - 10.5K$ as would be expected if the system was following the standard Doniach picture. It is therefore reasonable to suggest that a moderate further application of pressure may achieve the QPT that was initially sought in this work.

5.4.2 $T < T_N$

As the temperature is reduced towards T_N and the system is nearing the second order transition to the antiferromagnetic state, the magnetic fluctuations will become increasingly long-lived and long-ranged. When the system orders antiferromagnetically the magnetic fluctuations present above the transition are frozen out. This means a reduction in scattering rates which, if this was the dominant effect, would lead to a reduction in resistivity (see Ref. (10)). However, as has been mentioned, this is often not the case and the resistivity increases just below the transition. The Fermi surface is fundamentally changed by the magnetic ordering. The unit cell is doubled in the case of a simple antiferromagnet. This can either be viewed as a reduced Brillouin zone or left in the original Brillouin zone but with gaps. Either way, it is clear that the carrier concentration is reduced. The details of the Fermi surface then become the crucial parameters determining the behaviour of the system at the transition. Unfortunately, theoretical calculations based on detailed Fermi surfaces are in short supply. For example, it is not known what effect the application of magnetic field will have on the shape of the Fermi

surface of a band antiferromagnet with regard to the reduction in carriers and the effects that will then have on the exchange interaction and electron-electron scattering. Likewise, the exact effects of pressure on the lattice parameters and thence on the band structure and the exchange, density of states and scattering rates are not known for a realistic antiferromagnetic Fermi surface.

In a paper published in 2005 (46) Monthoux and Lonzarich considered a tight binding band appropriate for Sr_2RuO_4. The effective interaction, assumed to be magnetic, was then studied at different band filling factors. They showed that even within the relatively simple model explained, the effective interaction could have attractive regions in k-space. If a Cooper pair can exist which principally samples these regions, then an instability to superconductivity may exist. In this single band it was found that the interaction may be attractive and of different symmetries, depending sensitively on the filling of the band. This calculation should make us aware that the intricacies of the electronic band structure may very well contain the necessary physics to account for many features seen in the transport and susceptibility properties of strongly correlated systems.

5.4.3 Magnetic Superzones?

The account of the resistivity anomalies in the heavy rare earths (Gd-Tm) given by Elliott and Wedgwood (47) in 1963 is based on the magnetic ordering having a spiral spin structure. This kind of ordering has a lower symmetry than the hexagonal structure of these rare earths and leads to new boundaries in the Brillouin zone which distort the Fermi surface. The form of the Fermi surface and the symmetry of the crystal play an important role in determining, within this theory, the effect of the magnetic ordering on the electron scattering and hence the resistivity. Calculations done by Ellerby et al. in Ref. (42) based on the theory of Elliott and Wedgwood, are successful at explaining the effect of applied magnetic field on the resistivity anomaly in thulium. The form of the resistivity of Tm is very similar to that seen for CeGe. There are, however, important differences. Neutron diffraction measurements in Tm have confirmed that the magnetic structure is of the necessary type to make magnetic superzones very important in descriptions of transport, i.e. of a lower symmetry than the crystal.

Thulium has an hexagonal crystal structure and a ferrimagnetic ordering at low temperatures. These are also generally to be found in the rare earths that show magnetic super zones. CeGe is neither hexagonal, nor has neutron diffraction shown any ferromagnetic component to the magnetisation. Furthermore, cerium is not a heavy rare earth.

Accounting for the pressure and field dependence of the resistivity is a key test for the applicability of these two models to this system. If it is found that only the magnetic superzone model can account for the observed data then the magnetic ground state of this system would warrant further neutron study to determine.

5.5 Conclusions

The pressure-magnetic field phase diagram is plotted in Fig.5.6.

The changes in the form of the resistivity are explained in terms of the various scattering rates and changes to the carrier concentration that are present in a system caught in a fine balancing act between two states with comparable energy scales. Magnetic superzones are not supported or disproved by the pressure work so far performed. Analysis of the effect of the extra zone boundaries and how this can be distinguished from commensurate AFM is needed to settle this point.

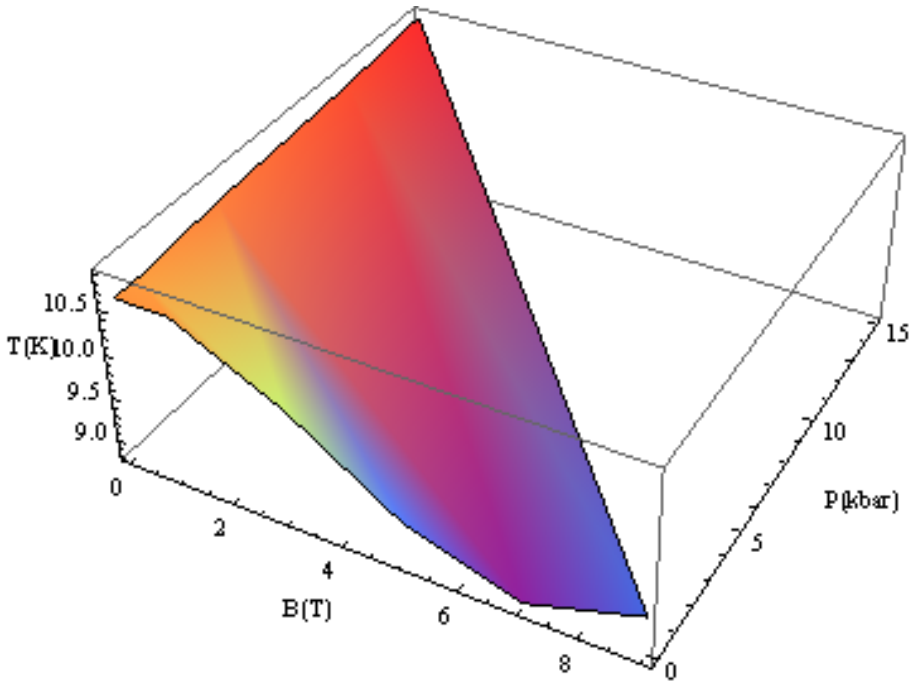

Figure 5.6: The Néel temperature has been found to be significantly diminished by applied field but only slightly enhanced by the application of pressure. The relationship is that $\mathrm{d}T_N/\mathrm{d}P \sim 0.02Kbar^{-1}$. Whilst this change is only very small, it is comparable to other heavy fermion magnets (48). The effect of applied pressure on the form of the resistivity is marked. The peak height and residual resistivity are substantially lowered and raised respectively.

6

$NiPS_3$ and $FePS_3$

6.1 Introduction

$NiPS_3$ belongs to a group of compounds: MPX_3 where X is sulphur or selenium and M is a divalent transition metal, ie Fe^{2+}, Mn^{2+}, Co^{2+} or Zn^{2+}. This family of compounds has received interest primarily for their potential as cathodes in batteries based on Li^+ transport. Atoms and molecules will generally intercalate very easily and at high densities. The structure is unaffected by the intercalation (49).

The crystal structures of these compounds are well known. They have a monoclinic unit cell with space group C2/m (50) and lattice parameters for $NiPS_3$ of $a_0 = 5.811$, $b_0 = 10.076$, $c_0 = 6.628$ and $\beta = 106.94°$ (51).

The magnetism in this family of materials is characterised by three exchange constants: that of the nearest, next-nearest and next-next-nearest neighbors. In $NiPS_3$ this results in an antiferromagnetic state with a transition temperature of 150K. The Ni ions form ferromagnetically coupled chains within the basal plane (52). These chains are coupled antiferromagnetically to adjacent chains within the plane and ferromagnetically between the planes.

Neutron diffraction studies of the magnetic structures of this family of compounds have been carried out by Wiedenmann et. al. (53), Le Flem et. al. (52) and Kurosawa et. al. (54). The experiments of Wiedenmann et. al. were on powdered polycrystalline samples of $MnPSe_3$ and $FePSe_3$. The crystal structure

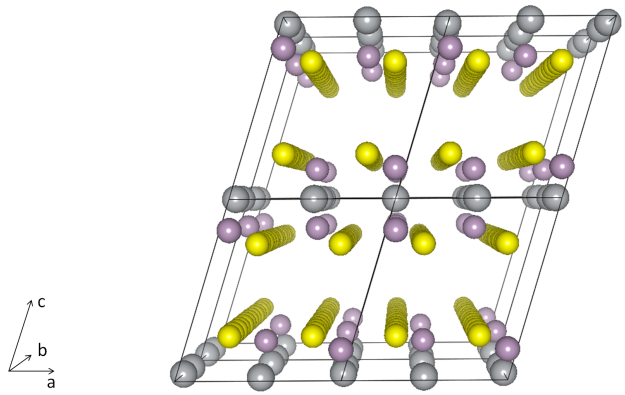

Figure 6.1: The structure is viewed down the b-axis. Yellow spheres are sulphur, purple phosphorous and grey are Nickel.

obtained in earlier x-ray experiments (55) was confirmed. The magnetic structures, deduced from the extra scattering peaks, although antiferromagnetic in both cases, are quite different. For $MnPSe_3$ the moments were found to lie within the basal plane and to be quite close in magnitude to the $5\mu_B$ for a spin, S = 5/2, system. The magnetic unit cell was found to be the same as the crystallographic unit cell. However, for $FePSe_3$, the moment was found to be perpendicular to the basal plane and enhanced over that expected for a spin, S = 1/2 system. The magnetic unit cell in this case is doubled along the c-axis and b-axis. The spin configuration that corresponds to this is one of chains of ferromagnetically coupled Fe ions. The chains are coupled antiferromagnetically within a plane, and ferromagnetically between planes.

Le Flem et. al. combined anisotropic susceptibility measurements with neutron diffraction on a wide range of MPX_3 compounds including $NiPS_3$. The magnetism is characterised by the exchange interactions between the M^{2+} ions. The metal ions lie on a honeycomb lattice and therefore have 3 first neighbours, 6 second and 3 third neighbours. They also have either 2 or 1 nearest interplanar neighbours on each of the 2 adjacent planes if they have monoclinic or rhombohedral symmetry respectively. All the MPS_3 as well as the $NiPSe_3$ compounds are monoclinic with the $FePSe_3$ and $MnPSe_3$ having a slight distortion of the oc-

tahedra and therefore, a rhombohedral structure. The distances between nearest interplanar neighbours is roughly equal to that of the third intraplanar neighbours. The distance spans a Van de Waals gap which leads to the assumption that any exchange coupling between planes is relatively weak compared to the intraplanar couplings. Le Flem et. al. suggest that the moments for $NiPS_3$ form an angle smaller than 30° with the c-axis. The magnetic interactions are either direct exchange or super-exchange. Direct exchange is due to the overlap of the t_{2g} orbitals. Super-exchange in this case will involve the mediation of the S or Se atom. In the case of $NiPS_3$ there can be no direct exchange as the t_{2g} orbitals are filled so the only exchange mechanism is super-exchange. The super-exchange couplings can be antiferromagnetic or ferromagnetic depending on the details of which orbitals are involved. This can lead to different couplings with the three first neighbours. The coupling to the three third neighbours is strongly dependent on the P_2S_6 octahedra. By analogy with other two-dimensional magnets, it is suggested that the third neighbour coupling is strongly antiferromagnetic, leading to an antiferromagnetic structure similar to that of $FePSe_3$; antiferromagnetically coupled chains of ferromagnetically coupled metal ions. They also suggest 2 possible structures for $FePS_3$: the same chain structure as $FePSe_3$ or antiferromagnetically coupled ferromagnetic planes. Kurosawa et. al. measured stacks of single crystalline $MnPS_3$ and $FePS_3$ by means of neutron diffraction. Their study favoured the ferromagnetic chains structure for $FePS_3$ and confirmed that the moments point out of the plane in both materials.

Joy and Vasudevan (56) measured the directional dependence of the magnetic susceptibility of MPS_3, M = Mn, Fe and Ni. These measurements were carried out on single crystal samples. These measurements show the anisotropy present in all of the systems.

There have been three calculations of the electronic band structure by Whangbo et. al. in 1985 (57), Kurita et. al. in 1989 (58) (59) and Zhukov et. el. in 1996 (60) as well as an empirical model by Piacentini et. al. in 1982 (61). The calculation of the band structure in this family of materials is computationally demanding and only partially successful at describing the experimental data. This is primarily due to the complexity of the unit cell. Each unit cell consists of 4 $M_2P_2X_6$ molecules that each contribute 48 electrons to filling the crystal bands.

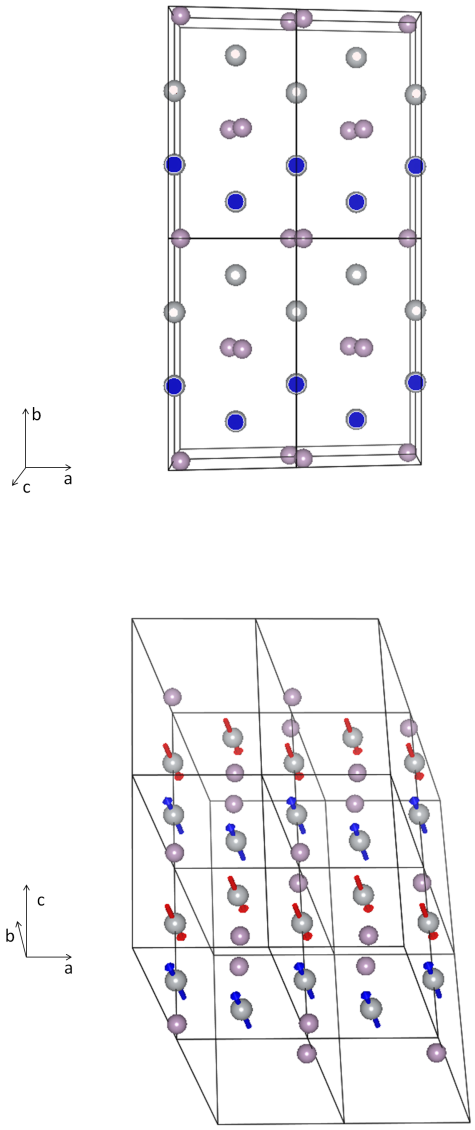

Figure 6.2: The sulphur atoms have been removed for clarity. Grey atoms are nickel and purple are phosphorous. In the top figure, looking down the c-axis, the white centred nickel atoms have their moment pointing into the page and the blue centred pointing out of the page. The bottom figure is the same as the top but rotated around the a-axis.

In the earlier works by Piacentini and Whangbo, this led to the assumption that either the metal ion or phosphorous atom, respectively, interacts weakly with the sulphur atoms. The calculation by Kurita was more complete but still lacked the sophistication necessary to deal with the magnetism in the system, being effectively a 1 electron model. Zhukov's work is more sophisticated again and reproduces the experimental data reasonably but by no means perfectly. The energy gap is systematically underestimated in all of the calculations, as is the size of the magnetic moment. The optical and x-ray data is in partial agreement with the calculated density of states, with the energies of the states or narrow bands associated with the metal ions being correct to a factor of 2 or so.

Previous measurements of the resistivity of the MPS_3 compounds have shown a wide range of values. For $FePS_3$ the room temperature values reported (62) are of the order of $10^5 \Omega cm$. Whereas, for $NiPS_3$ and $MnPS_3$ they are more like 10^{10} or $10^{11} \Omega cm$.

Raman studies have shown a broad peak at $530 cm^{-1}$ which is attributed to two-magnon (2M) scattering. In the study reported by S.S. Rosenblum and R. Merlin in Ref. (63) resonance raman scattering shows features that have only previously been observed in the cuprate superconductors and their parent compounds. The application of pressure moves the 2M peak to higher energies. Above 14.3GPa the peak no longer seems distinguishable from the background any longer.

6.2 Results and Discussion

Ambient pressure magnetisation data were recorded in a SQUID magnetometer (Fig. 6.3). Field cooled data were taken when cooling and zero-field cooled data when warming. The measurements were carried out in applied fields of 500, 1000, 5000 and 50000Oe. The expected transition at 150K corresponding to the Néel temperature was indeed observed. However, an unexpected upturn is also clearly visible. This upturn was observed in all 4 samples and at all applied fields. Upon closer inspection (see Fig. 6.4), not only is the upturn confirmed but a sharp peak is also observed in the zero-field cooled runs.

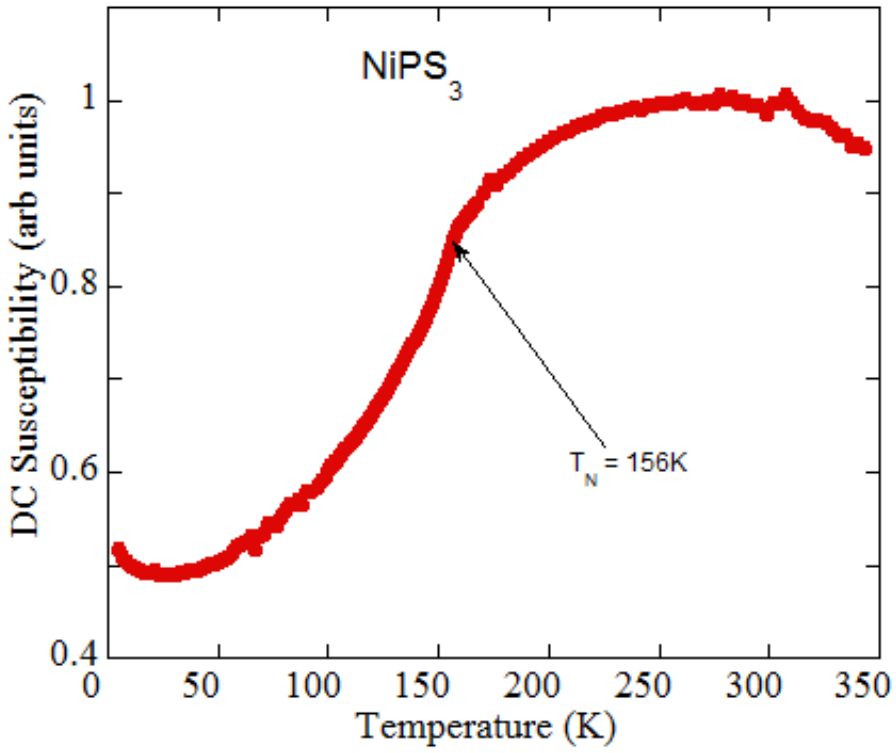

Figure 6.3: DC susceptibility for $NiPS_3$ under an applied magnetic field of 500Oe. The broad peak is clearly visible. The Transition temperature is defined to be the point with the largest gradient and can be seen just below a kink or shoulder at 156K.

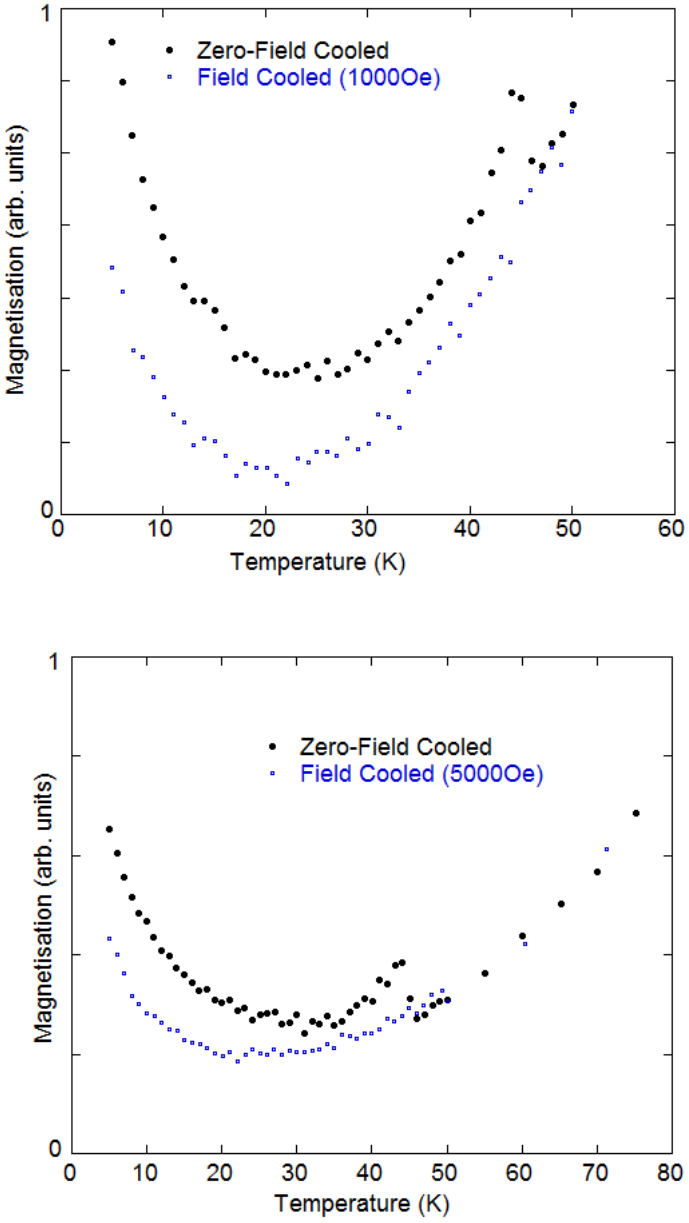

Figure 6.4: DC susceptibility measurements of two samples $NiPS_3$, one in an applied field of 1000Oe (top) and the other in a field of 5000Oe (bottom). In two separate samples the upturn is visible at temperatures below 20K. A sharp peak at 45K is also visible on the zero-field cooled measurements.

Using a Bridgmann cell and a Fluke Digital Multi-Meter(DMM), 2-point resistance measurements were made on $NiPS_3$ in ambient conditions as well as under pressure. The results obtained with the DMM were confirmed with a Lakeshore resistance bridge. The Lakeshore measurements were on the Heliox set-up and were intended to be temperature sweeps. However, as the temperature was decreased the resistance of the sample exceeded the limits of the experimental sensitivity.

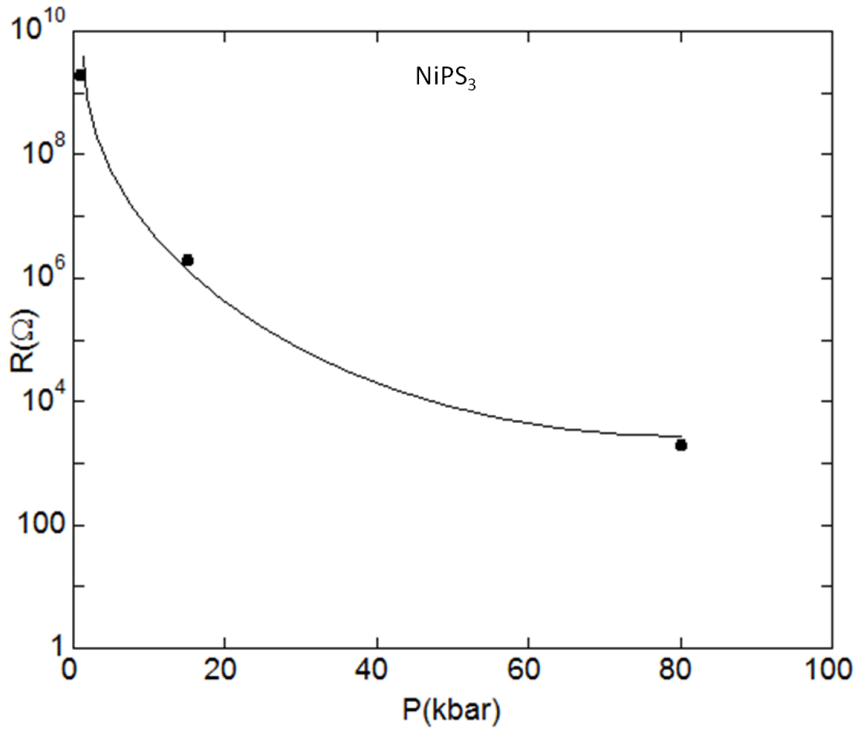

Figure 6.5: Room temperature resistivity of $NiPS_3$ under pressure. Even with only a few data points it is possible to see that the application of pressure drastically reduces the in-plane resistivity of $NiPS_3$

The results shown in Fig.6.5 are most certainly incomplete. The ambient pressure point is in fact a minimum resistance; this is the highest value that could be measured with the equipment at the time. However, even if the ambient pressure resistivity is no higher than this minimum value it can be seen that the application of 80kbar results in a reduction of the resistivity by 6 orders of

magnitude. This leads one to wonder whether the system is metallising. Work done in collaboration within my group on $FePS_3$ shows a similar drastic drop in the resistivity with applied pressure.

The temperature dependence of the resistance of these systems under pressure has not been previously measured. As has been discussed in Chapter 3, the measurement was not possible in $NiPS_3$ at ambient pressure due to the very high resistivity. However, at 80Kbar the measurement could be made (see Fig.6.6). The temperature dependence of the resistance is consistent with that of a semiconductor; the resistance increases with decreasing temperature. It should be noted now that the pressure estimate is inexact to say the least. No lead was used as a manometer, therefore, the pressure is estimated only from the applied load. This provides an upper limit. The actual pressure is, from past experience, some value between 80% and 90% of this value. The discrepancy is primarily because some of the applied load is dissipated in deforming the pressure cell and some is lost in friction. In this case the load applied would suggest a pressure of 90Kbar, therefore, the pressure used is 80Kbar. This is a best estimate but may be wrong by about 10Kbar either way. This, however, has no real significance for the discussion in this thesis.

As the system is semi conducting it is possible to estimate the energy gap from the thermal activation of the conduction. Using the Arrhenius equation for a thermally activated process:

$$\frac{1}{R} = \frac{1}{R_0} Exp\left(\frac{-E_g}{2K_B T}\right), \tag{6.1}$$

it is possible to estimate the energy gap by plotting the natural logarithm of the conductance against the inverse temperature, see Fig. 6.7. The value for E_g obtained from the gradient of the straight line in Fig. 6.7 is $E_g \sim 50meV$. Given that the energy gap at ambient pressure is 1.6eV (64) this represents a significant narrowing of the gap.

Measurements of $FePS_3$(65) show a much faster suppression of the energy gap.

As can be seen, the application of pressure reduces the band gap and the resistivity markedly leading eventually to metallic behaviour. The features of

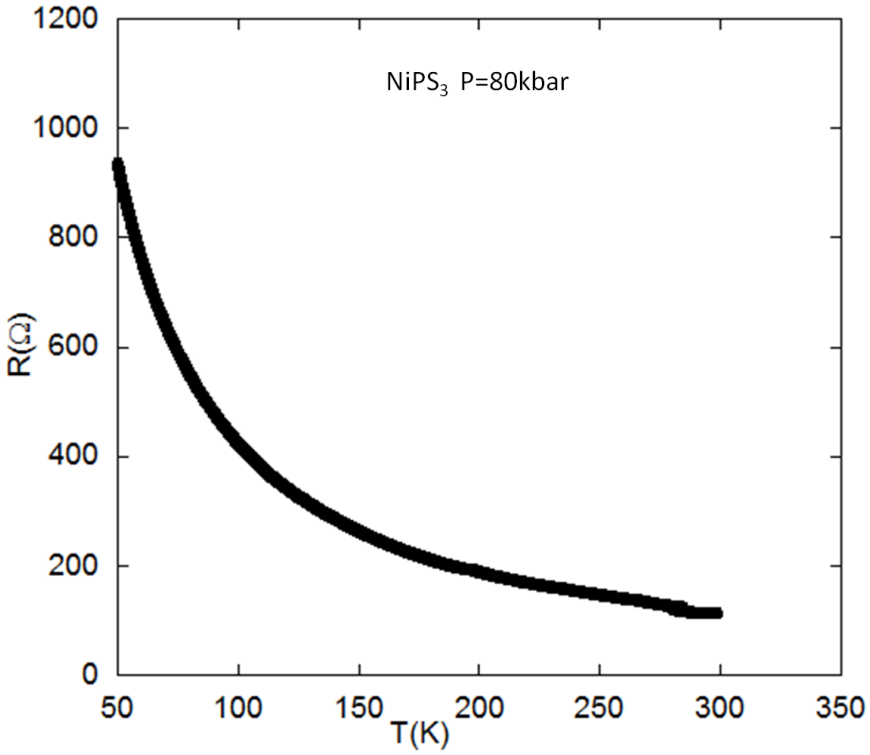

Figure 6.6: The high temperature resistance shows the expected form for a semiconductor. The lowering of temperature results in an increased resistance.

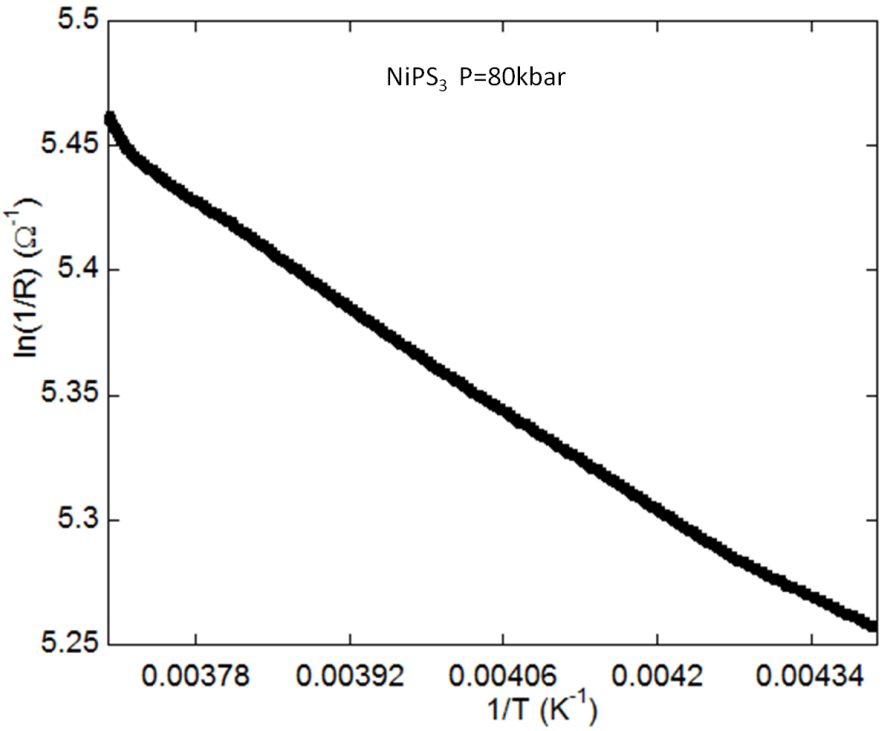

Figure 6.7: The straight line section of the resistance when plotted assuming an Arrhenius form can be used to estimate the energy gap, E_g.

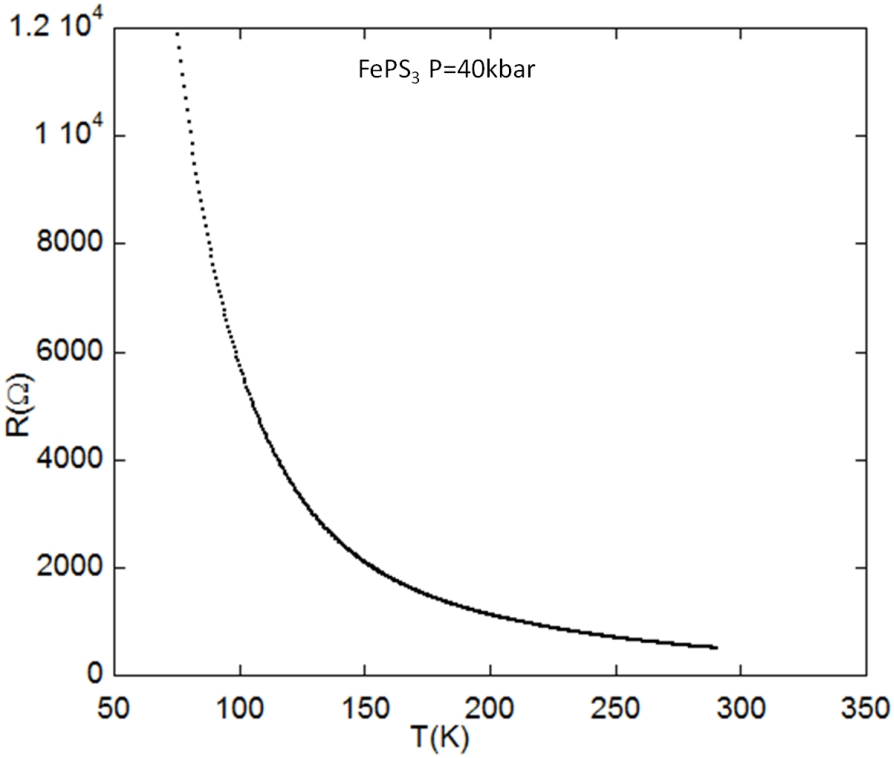

Figure 6.8: At around 40Kbar the resistivity increases with decreasing temperature - indicating insulating behaviour.

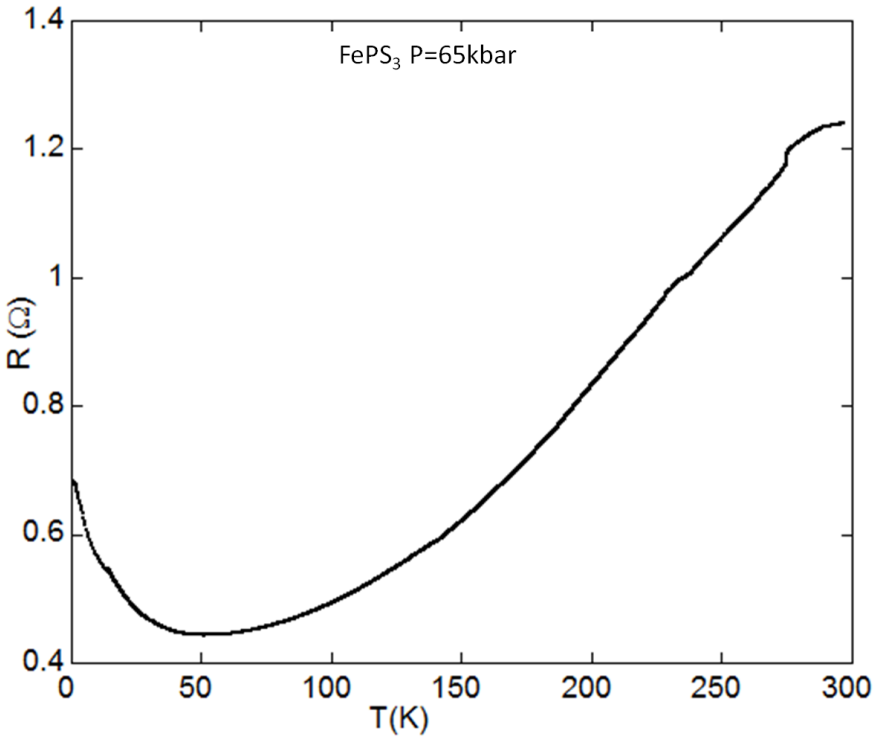

Figure 6.9: At around 65Kbar the resistivity decreases with decreasing temperature - indicating metallic behaviour.

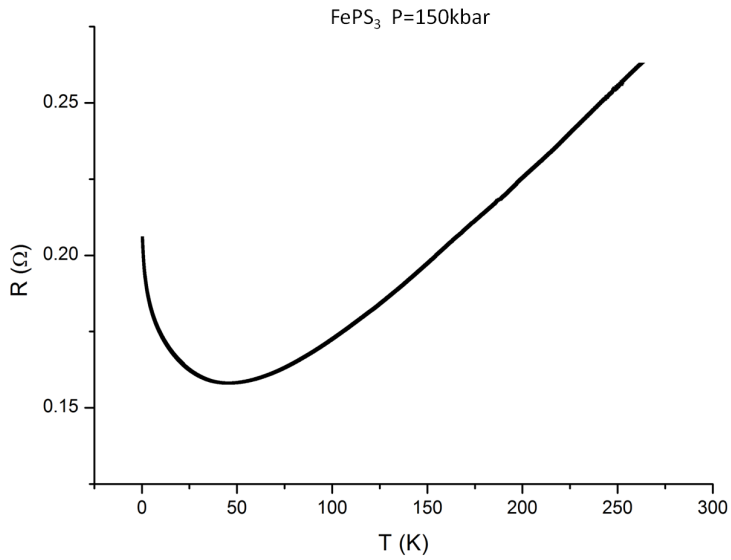

Figure 6.10: Increasing the pressure to around 150Kbar reduces the resistance further and moves the resistance minimum to a lower temperature.

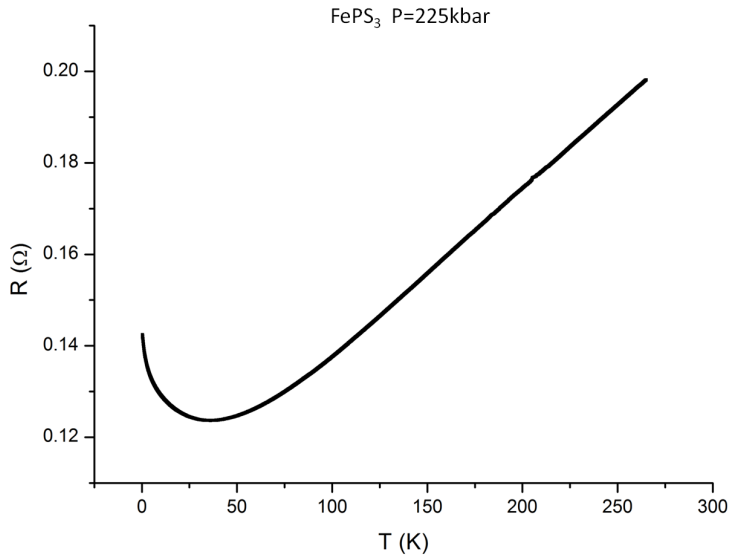

Figure 6.11: At around 225Kbar the resistance is still further reduced and the minimum is pushed to a lower temperature.

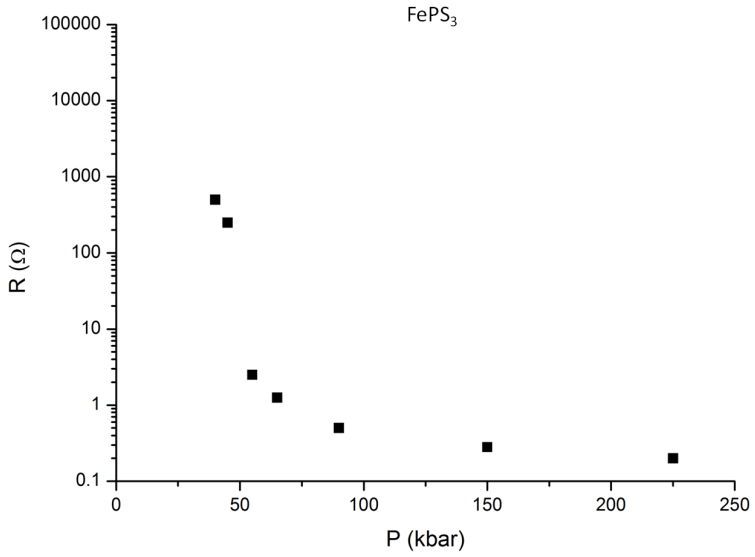

Figure 6.12: The resistance was measured in a 2-point configuration below the metallisation pressure (50kbar) and in a 4-point configuration above. The drastic suppression of the resistance can be seen to be mostly completed by 60Kbar.

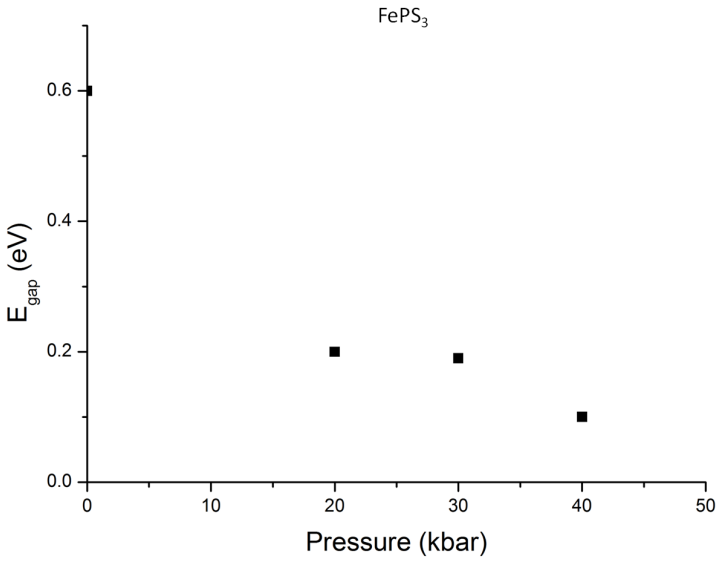

Figure 6.13: The energy gap narrows as the resistivity is suppressed under applied pressure.

the results obtained in the work on $NiPS_3$ seem to follow a very similar course to those seen in $FePS_3$. The shape of the resistivity dependence on temperature is very similar in the two materials below the metallisation pressure in $FePS_3$. The suppression of the room temperature resistivity and the energy gap are qualitatively similar. The resistivity of $NiPS_3$ is significantly higher at room temperature than that of $FePS_3$ and it is therefore reasonably unsurprising that the system would appear to require more pressure to metallise.

The question of induced metallicity has been posed in these compounds before, specifically in $FePS_3$ after chemical intercalation. This was shown not to be the case. However, there is good reason to suspect that application of pressure may induce metallicity. In the simplest picture, the squashing of the lattice will lead to greater overlap of the electronic states of the constituent atoms. This, one may conclude, will lead to a greater freedom for the electrons and then to metallic behaviour. The more the states overlap the wider the bands and the smaller the gaps can be expected to become. It is also to be noted that increased metallic behaviour could possibly be behind the disappearance of the 2M peak. Itinerant

electrons would dampen the mode and reduce its intensity. It is also possible that the magnetic correlations disappear at around 14.3GPa. However, $NiPS_3$ shows very robust magnetic correlations. This is seen in the very broad peak in the susceptibility that extends way above the magnetic transition temperature.

6.3 Proposals for Future Work

The MPS_3 compounds offer much to the field of low dimensional magnetism as well as to that of the QPT at metal-insulator transition. They certainly pose an experimental as well as theoretical challenge with a combination of very high resistances and potentially very high required pressures added to the complex unit cell and band structure.

In terms of detecting the proposed metal-insulator transition, one of the most desirable measurements is that of the temperature dependence of the resistivity. This is now possible and in the process of being done using the method outlined in the Experimental Methods chapter. Measurements on $FePS_3$ have shown reproducible metallic behaviour. These measurements are still waiting to be done on $NiPS_3$. These two of the family of compounds seem most likely to metallise due to them having the smallest band gaps and lowest resistivity, with $FePS_3$ the best candidate of these two.

7

Discussion

7.1 Fe_2P

Using a combination of magnetisation and resistivity measurements under hydrostatic pressure, it has been possible to observe the suppression of T_C from 210K to 7K. An anti-ferromagnetic state at temperatures above the FM transition temperature is induced above a pressure of about 5kbar. The P-T phase diagram constructed using this data is in good qualitative and quantitative agreement with previous measurements. Using this phase diagram, a critical pressure of 20Kbar is proposed for the complete suppression of the ferromagnetic state. A novel FM-AFM QPT is therefore suggested at low temperatures and at pressures around the critical pressure.

A significant enhancement of the 'A-coefficient' associated with the quasi-particle scattering cross-section provides evidence for the emergence of a new scattering mechanism. This extra scattering is understood, using the language of spin fluctuation theory, as being due to a quantum mechanical population of fluctuations in the magnetisation. These fluctuations are destructive to the Fermi liquid and therefore modify the temperature dependence of the resistivity as well as many other physical quantities. A departure from the quadratic Fermi liquid behaviour is indeed observed over a large temperature range at pressures above the critical pressure.

The residual resistivity of the samples studied was such that the very lowest

temperature data could not be analysed for the exponent. Samples with lower residual resistivity are necessary to investigate how low in T this behaviour extends.

No full spin fluctuation calculation has been done for this material or for this exact kind of transition. The counter-intuitive broadening of the magnetic hysteresis leading up to the FM-AFM QPT may well be a crucial clue as to the nature of the model needed to understand this phase transition. Any spin fluctuation model would have to take account of the interplay between the FM and the AFM interactions.

7.2 CeGe

The power of simple models like that of the Doniach phase diagram is in their ability to provide a familiar framework within which to consider the observations one makes. However, it is easy to forget quite how much complexity is being averaged out. In the case of CeGe it is not enough to consider just the competition between the Kondo interaction and that of the RKKY. To explain the observed behaviour it is necessary to look at the details of the electron correlations. The various ways in which the shape of the Fermi surface and the form of the density of states affect both the scattering rates and the resistive effect of the scattering processes could well lead to the sort of features seen in the resistivity. The Fermi surface and density of states will be dependent on applied pressure and field in different ways and it is therefore possible to use these two tuning parameters to determine the physics relevant to the anomalous resistivity. However, to do this will require calculations of the Fermi surface and density of states and their pressure and field dependence.

Monthoux and Lonzarich (see Refs. (66) and (46)) consider the case of a 2-D oxide assuming a dominant single band. Within these assumptions and a realistic Fermi surface, it is possible to show the possibility of both d-wave and p-wave superconductivity on the border of antiferromagnetism and ferromagnetism respectively. This is from a completely different field but demonstrates the need for detailed calculations as well as simple models.

7.3 $NiPS_3$

A reduction of the resistivity of $NiPS_3$ by a factor of six orders of magnitude is seen with the application of around 80kbar of pressure. The resistivity can be analysed using the Arrhenius equation and the band gap extracted. This shows that the gap is being closed by applied pressure and suggests an evolution towards metallisation as seen in the closely related system, $FePS_3$.

The fact that sulphur is in the same group as oxygen means that there are many possible analogies and comparisons to be drawn with the transition metal oxides. It is reasonable to assume that the 2-D Sulphur-based systems will display at least the level of complexity observed in the oxides. The P_2S_6 clusters demonstrate the numerous possibilities in these systems for band mixing that could then lead to novel physics. Sulphur has more potential for hybridisation and then band mixing than Oxygen. The P-S orbitals can, and do, mix to form a very complex range of molecular type orbitals in these clusters in the MPX_3 compounds. These are then the principal bands in the semi-conducting state. These P-S states can mediate exchange interactions between the transition metal ions sitting on a hexagonal lattice. The magnetic states of the MPX_3 are still yet to be definitively determined, especially at low temperatures and under pressure. Work presented in this thesis shows that at low temperature the magnetisation of $NiPS_3$ has previously unobserved and unexplained features. It seems highly likely that the anticipated metallisation under pressure will be accompanied by changes in the magnetic ordering of the system as the transition metal 3-d states are mixed in to the P-S bands.

The MPX_3 systems specifically and transition metal sulphides in general would appear to offer a huge amount to the fields of low dimensional magnetism and quantum critical phenomena.

References

[1] G. G. Lonzarich. *Electron.* Cambridge University Press, 1997. 9, 12

[2] S. S. Saxena, P. Agarwal, K. Ahilan, F. M. Grosche, R. K. W. Haselwimmer, M. J. Steiner, E. Pugh, I. R. Walker, S. R. Julian, P. Monthoux, G. G. Lonzarich, A. Huxley, I. Sheikin, D. Braithwaite, and J. Flouquet. Superconductivity on the border of itinerant-electron ferromagnetism in UGe_2. *Nature*, 406:587–592, 2000. 12, 39

[3] A. J. Schofield. Non-fermi liquids. *Contemporary Physics*, 40:95–115, 1999. 12

[4] G. G. Lonzarich and L. Taillefer. Effect of spin fluctuations on the magnetic equation of state of ferromagnatic or nearly ferromagnetic metals. *J. Phys. C: Solid State Phys.*, 18:4339–4371, 1985. 12

[5] F.M. Grosche, S.R. Julian, N.D. Mathur, F.V. Carter, and G.G. Lonzarich. Quantum-phase transitions in $CePd_2Si_2$ and $CeRh_2Si_2$. *Physica B: Condensed Matter*, 237-238:197 – 201, 1997. Proceedings of the Yamada Conference XLV, the International Conference on the Physics of Transition Metals. 13, 16

[6] F. M. Grosche, S. J. S. Lister, F. V. Carter, S. S. Saxena, R. K. W. Haselwimmer, N. D. Mathur, S. R. Julian, and G. G. Lonzarich. Superconductivity and anomalous normal state in the $CePd_2Si_2/CeNi_2Ge_2$ system. *Physica B: Condensed Matter*, 239(1-2):62 – 66, 1997. Proceedings of the Workshop on Transition Metals and Compounds under Multiextreme Conditions. 13, 39

[7] I. R. Walker, F. M. Grosche, D. M. Freye, and G. G. Lonzarich. The normal and superconducting states of $CeIn_3$ near the border of antiferromagnetic order. *Physica C: Superconductivity*, 282-287(Part 1):303 – 306, 1997. Materials and Mechanisms of Superconductivity High Temperature Superconductors V. 13, 16, 39

[8] ND Mathur, FM Grosche, SR Julian, IR Walker, DM Freye, RKW Haselwimmer, and GG Lonzarich. Magnetically mediated superconductivity in heavy fermion compounds. *Nature*, 394(6688):39–43, JUL 2 1998. 13

[9] F M Grosche, I R Walker, S R Julian, N D Mathur, D M Freye, M J Steiner, and G G Lonzarich. Superconductivity on the threshold of magnetism in $CePd_2Si_2$ and $CeIn_3$. *Journal of Physics: Condensed Matter*, 13(12):2845, 2001. 13

[10] C Pfleiderer, GJ McMullan, SR Julian, and GG Lonzarich. Magnetic quantum phase transition in MnSi under hydrostatic pressure. *Physical Review B*, 55(13):8330–8338, APR 1 1997. 13, 84

[11] C Thessieu, C Pfleiderer, AN Stepanov, and J Flouquet. Field dependence of the magnetic quantum phase transition in MnSi. *Journal Of Physics-condensed Matter*, 9(31):6677–6687, AUG 4 1997. 13

[12] R. P. Smith, M. Sutherland, G. G. Lonzarich, S. S. Saxena, N. Kimura, S. Takashima, M. Nohara, and H. Takagi. Marginal breakdown of the Fermi-liquid state on the border of metallic ferromagnetism. *Nature*, 455(7217):1220–1223, OCT 30 2008. 13

[13] J. R. Schrieffer and P. A. Wolff. Relation between the anderson and kondo hamiltonians. *Phys. Rev.*, 149(2):491–492, Sep 1966. 14

[14] C. Panagopoulos, J. L. Tallon, B. D. Rainford, T. Xiang, J. R. Cooper, and C. A. Scott. Evidence for a generic novel quantum transition in high-T_c cuprates. *Physical Review B*, 66:064501, 2002. 16

[15] Stephen Rowley, Robert Smith, Mark Dean, Leszek Spalek, Michael Sutherland, Montu Saxena, Patricia Alireza, Chris Ko, Cheng Liu, Emma Pugh, Suchitra Sebastian, and Gilbert Lonzarich. Ferromagnetic and ferroelectric quantum phase transitions. *Physica Status Solidi (b)*, 247(3):469–475, 2010. 16

[16] Kenji Ishida, Yusuke Nakai, and Hideo Hosono. To what extent iron-pnictide new superconductors have been clarified: A progress report. *Journal of the Physical Society of Japan*, 78(6):062001, 2009. 16

[17] Patricia L. Alireza, Y. T. Chris Ko, Jack Gillett, Chiara M. Petrone, Jacqueline M. Cole, Gilbert G. Lonzarich, and Suchitra E. Sebastian. Superconductivity up to 29 K in $SrFe_2As_2$ and $BaFe_2As_2$ at high pressures. *Journal Of Physics-condensed Matter*, 21(1):012208, JAN 7 2009. 17

[18] C. Hess, A. Kondrat, A. Narduzzo, J. E. Hamann-Borrero, R. Klingeler, J. Werner, G. Behr, and B. Buechner. The intrinsic electronic phase diagram of iron-oxypnictide superconductors. *EPL*, 87(1):17005, JUL 2009. 18

[19] IR Walker and CJ Moss. Spot welder for making small electrical contacts. *Review Of Scientific Instruments*, 69(7):2747–2756, JUL 1998. 22

[20] S. S. Saxena. *Magnetic and Superconducting Phases of Heavy Fermion Compounds*. PhD thesis, University of Cambridge, 1998. 25

[21] W. J. Nellis. Dynamic compression of materials: metallization of fluid hydrogen at high pressures. *Reports on Progress in Physics*, 69:1479–1580, 2006. 27

[22] W. F. Giauque. A thermodynamic treatment of certain magnetic effects. a proposed method of producing temperatures considerably below 1ř absolute. *Journal of the American Chemical Society*, 49(8):1864–1870, 1927. 29

[23] S Chiba. Magnetic properties of iron phosphide Fe_2P. *Journal Of The Physical Society Of Japan*, 15(4):581–585, 1960. 38

[24] H. Fujjiwara, H. Kadomatsu, K.Tohma, H. Fujii, and T. Okamoto. Pressure-induced magnetic transition in Fe_2P. *J. Magn. & Magn. Mater.*, 21:262–268, 1980. 38, 39, 41, 42, 57

[25] D. A. Yablonskii and L. I. Medvedeva. Classification of magnetic structures in compounds with the Fe_2P-structure. *Physica B*, 167:125–132, 1990. 38

[26] Ekkes Brück. Developments in magnetocaloric refrigeration. *Journal of Physics D: Applied Physics*, 38(23):R381, 2005. 38

[27] Leif Lundgren, Gulzar Tarmohamed, Olof Beckman, Bertil Carlsson, and Stig Rundqvist. First order magnetic phase transition in Fe_2P. *Physica Scripta*, 17(1):39, 1978. 38

[28] R. Wäppling, L. Häggström, T. Ericsson, S. Devanarayanan, E. Karlsson, B. Carlsson, and S. Rundqvist. First order magnetic transition, magnetic structure, and vacancy distribution in Fe_2P. *Journal of Solid State Chemistry*, 13(3):258 – 271, 1975. 38

[29] Cheol Woo Kim, Jong Suk Park, and Kyung Sub Lee. Effect of Fe_2P on the electron conductivity and electrochemical performance of $LiFePO_4$4 synthesized by mechanical alloying using Fe3+ raw material. *Journal of Power Sources*, 163(1):144 – 150, 2006. Special issue including selected papers presented at the Second International Conference on Polymer Batteries and Fuel Cells together with regular papers. 39

[30] L. Chen, N.Kurita, T. Fujiwara, M. Abliz, M. Hedo, I. Oguro, A. Matsuo, K. Kindo, Uwatoko, and H. Fujii. Effect of pressure on the magnetization measurements of Fe_2P. *J. Magn. Magn. Mat.*, 310:e219–e221, 2006. 39, 41

[31] A Huxley, I Sheikin, E Ressouche, N Kernavanois, D Braithwaite, R Calemczuk, and J Flouquet. UGe_2: A ferromagnetic spin-triplet superconductor. *Physical Review B*, 63(14):144519, APR 1 2001. 39

[32] Katsuya Shimizu, Tomohiro Kimura, Shigeyuki Furomoto, Keiki Takeda, Kazuyoshi Kontani, Yoshichika Onuki, and Kiichi Amaya. Superconductivity

in the non-magnetic state of iron under pressure. *Nature*, 412:316–318, 2001. 39, 40

[33] A. Huxley, I. Sheikin, and D. Braithwaite. Metamagnetic behavior near the quantum critical point in UGe_2. *Physica B: Condensed Matter*, 284-288(Part 2):1277 – 1278, 2000. 39

[34] E. A. Zavadskii, L. I. Medvedeva, and A. E. Filippov. Specific character of metamagnetic transitions in Fe_2P. *Journal of Magnetism and Magnetic Materials*, 43(1):53 – 58, 1984. 42

[35] Hideoki Kadomatsu, Makoto Isoda, Kiyokazu Tohma, Hironobu Fujii, Tetsuhiko Okamoto, and Hiroshi Fujiwara. Pressure-Induced Antiferromagnetism of Fe_2P. *Journal of the Physical Society of Japan*, 54(7):2690–2699, 1985. 42, 61

[36] Hironobu Fujii, Yoshiya Uwatoko, Kiyoichiro Motoya, Yuji Ito, and Tetsuhiko Okamoto. Neutron Scattering Investigation of Itinerant Electron System Fe_2P. *Journal of the Physical Society of Japan*, 57(6):2143–2153, 1988. 43

[37] H. Kadomatsu, M. Isoda, K. Tohma, H. Fujii, T. Okamoto, and H. Fujiwara. Pressure-Induced Antiferromagnetism of Fe_2P. *Jour. Phys. Soc. Japan*, 54 No.7:2690–2699, 1985. 43

[38] A Eiling and J S Schilling. Pressure and temperature dependence of electrical resistivity of Pb and Sn from 1-300K and 0-10 GPa-use as continuous resistive pressure monitor accurate over wide temperature range; superconductivity under pressure in Pb, Sn and In. *Journal of Physics F: Metal Physics*, 11(3):623–639, 1981. 43

[39] K. H. J. Buschow and J. F. Fast. Magnetic and structural characteristics of some equiatomic rare-earth germanides. *physica status solidi (b)*, 16:467–473, 1966. 74

[40] N. Marcano, J. I. Espeso, and J. C. Gomez Sal. Complex magnetism in CeGe binary alloy. *Journal Of Magnetism And Magnetic Materials*, 310(2, Part 1):E35–E37, MAR 2007. 17th International Conference on Magnetism (ICM 2006), Kyoto, JAPAN, AUG 20-25, 2006. 74, 75, 76, 77

[41] J.I. Espeso, N. Marcano, D.R. Noakes, G.M. Kalvius, and J.C.G. Sal. Electrical transport and magnetic properties of CeGe. *Physica B*, 359-361:269–71, 30 April 2005. 75

[42] Mark Ellerby, Keith A. McEwen, and Jens Jensen. Magnetoresistance and magnetization study of thulium. *Phys. Rev. B*, 57(14):8416–8423, Apr 1998. 75, 85

[43] M. Kurisu, T. Takahashi, Y. Maeda, H. Iwasaki, T. Takabatake, and H. Fujii. Effect of pressure on the magnetic superzone gap in antiferromagnetic uranium compounds UCu_2Sn and UCu_3Ga_2. *Physica B*, 186-188:766–768, May 1993. International Conference on Strongly Correlated Electron Systems, 7-11 September 1992, Sendai, Japan. 75

[44] P Schobinger-Papamantellos, M Kenzelmann, A Schenck, FN Gygax, KHJ Buschow, and C Ritter. Magnetic properties of the $CeGe_{1-x}Si_x$ series studied by powder neutron diffraction and μSR-measurements. *Physica B-condensed Matter*, 349(1-4):100–114, JUN 15 2004. 75, 84

[45] B. Coqblin, J. R. Iglesias, N. B. Perkins, S. G. Magalhaes, and F. M. Zimmer. Doniach diagram for ordered, disordered and underscreened Kondo lattices. *Journal of Magnetism And Magnetic Materials*, 320(14):1989–1994, JUL 2008. 8th Latin American Workshop on Magnetism, Magnetic Materials and Their Applications, Rio de Janeiro, BRAZIL, AUG 12-16, 2007. 82

[46] P. Monthoux and G. G. Lonzarich. Magnetic interactions in a single-band model for the cuprates and ruthenates. *Phys. Rev. B*, 71(5):054504, Feb 2005. 85, 106

[47] R.J Elliott and F.A Wedgwood. Theory of the resistance of the rare earth metals. *Proc. Phys. Soc.*, 81:846–855, 1963. 85

[48] JD Thompson. High-pressure experiments on heavy fermion mixed-valence compounds. *Journal Of Magnetism And Magnetic Materials*, 63-4:358–364, JAN 1987. 87

[49] Jean Rouxel, P. Molinie, and L.H. Top. Mechanistic studies of reversible layer-type electrodes. *Journal of Power Sources*, 9(3):345 – 357, 1983. 88

[50] W. Klingen, G. Eulenberger, and H. Hahn. Über hexachalkogeno-hypodiphosphate vom typ m₂p₂x₆. *Naturwissenschaften*, 57:88–88, 1970. 10.1007/BF00590690. 88

[51] Barry E. Taylor, John Steger, and Aaron Wold. Preparation and properties of some transition metal phosphorus trisulfide compounds. *Journal of Solid State Chemistry*, 7(4):461 – 467, 1973. 88

[52] G Leflem, R Brec, G Ouvard, A Louisy, and P Segransan. Magnetic-interactions in the layer compounds MPX_3 (M = Mn, Fe, Ni; X = S, Se). *Journal Of Physics And Chemistry Of Solids*, 43(5):455–461, 1982. 88

[53] A Wiedenmann, J Rossatmignod, A Louisy, R Brec, and J Rouxel. Neutron-diffraction study of the layered compounds $MnPSe_3$ and $FePSe_3$. *Solid State Communications*, 40(12):1067–1072, 1981. 88

[54] K Kurosawa, S Saito, and Y Yamaguchi. Neutron-diffraction study on $MnPS_3$ and $FePS_3$. *Journal Of The Physical Society Of Japan*, 52(11):3919–3926, 1983. 88

[55] W Klingen, R Ott, and H Hahn. Preparation and properties of hexathiohypodiphosphates and hexaselenohypodiphosphates. *Zeitschrift Fur Anorganische Und Allgemeine Chemie*, 396(3):271–278, 1973. 89

[56] P A Joy and S Vasudevan. Magnetism in the layered transition-metal thiophosphates MPS_3 (M = Mn, Fe, and Ni). *Physical Review B*, 46(9):5425–5433, SEP 1 1992. 90

[57] M. H. Whangbo, R. Brec, G. Ouvrard, and J. Rouxel. Reduction sites of transition-metal phosphorus trichalcogenides MPX_3. *Inorganic Chemistry*, 24(15):2459–2461, 1985. 90

[58] Noriyuki Kurita and Kenji Nakao. Band Structure of Magnetic Layered Semiconductor $NiPS_3$. *Journal of the Physical Society of Japan*, 58(1):232–243, 1989. 90

[59] Noriyuki Kurita and Kenji Nakao. Band Structures and Physical Properties of Magnetic Layered Semiconductors MPS_3. *Journal of the Physical Society of Japan*, 58(2):610–621, 1989. 90

[60] V Zhukov, S Alvarez, and D Novikov. Electronic band structure of the magnetic layered semiconductors MPS_3 (M=Mn, Fe and Ni). *Journal Of Physics And Chemistry Of Solids*, 57(5):647–652, MAY 1996. 90

[61] M Piacentini, FS Khumalo, CG Olson, JW Anderegg, and DW Lynch. Optical-transitions, XPS, and electronic states in $NiPS_3$. *Chemical Physics*, 65(3):289–304, 1982. 90

[62] P.J.S. Foot, J Suradi, and P.A. Lee. Optical and electronic properties of the layered semiconductors $NiPS_3$ and $FePS_3$. *Materials Research Bulletin*, 15(2):189 – 193, 1980. 92

[63] S. S. Rosenblum and R. Merlin. Resonant two-magnon Raman scattering at high pressures in the layered antiferromagnetic $NiPS_3$. *Phys. Rev. B*, 59(9):6317–6320, Mar 1999. 92

[64] R Brec, DM Schleich, G Ouvrard, A Louisy, and J Rouxel. Physical-properties of Lithium intercalation compounds of the layered transition chalcogenophosphates. *Inorganic Chemistry*, 18(7):1814–1818, 1979. 96

[65] P. Nahai-Williamson. *Tuning ordered states in transition metal chalcogenide systems*. PhD thesis, University of Cambridge, 2011. 96

[66] P. Monthoux and G. G. Lonzarich. p-wave and d-wave superconductivity in quasi-two-dimensional metals. *Phys. Rev. B*, 59(22):14598–14605, Jun 1999. 106